Studies on the influence of platelets on vascular integrity in primary tumors and the role of BIN2 in platelet calcium signaling

• • •

Studien zum Einfluss von Thrombozyten auf die Gefäßintegrität im Primärtumor und zur Rolle von BIN2 im Calcium-Signalweg von Thrombozyten

Doctoral thesis for a doctoral degree
at the Graduate School of Life Sciences,
Julius-Maximilians-Universität Würzburg,
Section Biomedicine
submitted by

Julia Volz
from Rastatt, Germany

Würzburg, 2020

Submitted on:

Members of the Promotionskomitee:

Chairperson: Prof. Dr. Manfred Gessler

Primary Supervisor: Prof. Dr. Bernhard Nieswandt

Supervisor (Second):   Prof. Dr. Süleyman Ergün

Supervisor (Third):   Prof. Dr. Guido Stoll

Date of Public Defense: _____

Date of Receipt of Certificates: _____

Nothing in life is to be feared, it is only to be understood.

Now is the time to understand more, so that we may fear less.

Marie Curie

Summary

Maintenance of tumor vasculature integrity is indispensable for tumor growth and thus affects tumor progression. Previous studies have identified platelets as major regulators of tumor vascular integrity, as their depletion selectively renders tumor vessels highly permeable, causing massive intratumoral hemorrhage. While these results establish platelets as potential targets for anti-tumor therapy, depletion is not a treatment option due to the essential role of platelets for hemostasis. This thesis demonstrates for the first time that functional inhibition of *glycoprotein* (GP) VI on the platelet surface rapidly induces tumor hemorrhage and diminishes tumor growth similar to complete platelet depletion but without inducing systemic bleeding complications. Both, the intratumoral bleeding and tumor growth arrest could be reverted by depletion of Ly6G$^+$ cells confirming them to be responsible for the induction of bleeding and necrosis within the tumor. In addition, GPVI inhibition increased intra-tumoral accumulation of co-administered chemotherapeutic agents, thereby resulting in a profound anti-tumor effect. In summary, this thesis manifests platelet GPVI as a key regulator of vascular integrity specifically in growing tumors, serving as a potential basis for the development of anti-tumor strategies.

In the second part of this thesis, light is shed on the modulating role of *bridging integrator 2* (BIN2) in platelet Ca^{2+} signaling. *Stromal interaction molecule 1* (STIM1) mediated *store-operated calcium entry* (SOCE) is the major route of Ca^{2+} influx in platelets, triggered by *inositol trisphosphate receptor* (IP$_3$R)-dependent Ca^{2+} store release. In this thesis, the BAR domain superfamily member BIN2 was identified as the first Ca^{2+} signaling modulator, interacting with both, STIM1 and IP$_3$R in platelets. Deletion of BIN2 resulted in reduced Ca^{2+} store release and Ca^{2+} influx in response to all tested platelet agonists. These defects were a consequence of impaired IP$_3$R function in combination with defective STIM1-mediated SOC channel activation, while Ca^{2+} store content and agonist-induced IP$_3$ production were unaltered. These results establish BIN2 as a central regulator of platelet Ca^{2+} signaling.

The third part of this thesis focuses on the effect of the soluble neuronal guidance protein Sema7A on platelet function. Rosenberger *et al.* discovered that Sema7A cleavage from red blood cells increases the formation of platelet-neutrophil complexes, thereby reinforcing thrombo-inflammation in myocardial ischemia-reperfusion injury (MIRI). This thesis establishes soluble Sema7A as a stimulator of platelet thrombus formation via its interaction with platelet GPIbα, thereby reinforcing PNC formation. Thus, interfering with the GPIb-Sema7A interaction during MIRI represents a potential strategy to reduce cardiac damage and improve clinical outcome following MI.

Zusammenfassung

Die Aufrechterhaltung einer intakten Gefäßstruktur im Primärtumor ist unerlässlich für dessen Wachstum und beeinflusst dadurch die Tumorentwicklung. Es wurde bereits gezeigt, dass Thrombozyten bei diesem Prozess eine große Rolle spielen, da ihre experimentelle Depletion in Mäusen zu extrem durchlässigen Gefäßen und in Folge dessen zu starken Blutungen im Tumor führt. Diese Ergebnisse machen Thrombozyten zu potentiellen Angriffspunkten in der Krebstherapie, eine komplette Depletion ist dabei jedoch auf Grund ihrer essentiellen Funktion bei der Hämostase nicht denkbar. In dieser Thesis wurde zum ersten Mal gezeigt, dass auch die Blockade des *Glykoproteins* (GP) VI auf der Thrombozytenoberfläche zu vergleichbaren Blutungen im Tumor und zur Hemmung des Tumorwachstums führt, ohne jedoch das generelle Blutungsrisiko zu beeinflussen. Die durch die GPVI Blockade induzierten Effekte können durch eine gleichzeitige Depletion von Ly6G$^+$ Zellen verhindert werden, was zeigt, dass dieser Zelltyp ursächlich an der Entstehung der Blutung beteiligt ist. Des Weiteren führt die Blockade von GPVI in Kombination mit einem Chemotherapeutikum zu einer Erhöhung dessen Konzentration im Tumorgewebe und damit zu einer verstärkten antitumoralen Wirkung. Zusammenfassend konnte gezeigt werden, dass GPVI ein wichtiger Regulator der Gefäßintegrität im wachsenden Tumor ist, was als Grundlage für die Entwicklung von Krebstherapien genutzt werden könnte.

Im zweiten Teil dieser Thesis wurde die Rolle des *bridging integrator 2* (BIN2) im Ca^{2+} Signalweg von Thrombozyten untersucht. Der STIM1 abhängige „store operated calcium entry" (SOCE) vermittelt den größten Ca^{2+}-Einstrom in Thrombozyten. SOCE wird durch den *inositol trisphosphate receptor* (IP$_3$R)-abhängigen Ca^{2+} Ausstrom aus dem zelleigenen Ca^{2+} Reservoir aktiviert. In dieser Thesis wurde BIN2 als erstes Adapterprotein im Ca^{2+} Signalweg von Thrombozyten identifiziert, das sowohl mit STIM1 als auch mit IP$_3$R interagiert. Das Fehlen von BIN2 führt zu einer Reduktion des Ca^{2+} Ausstroms aus dem zelleigenen Ca^{2+} Reservoir und eine Verminderung des Einstroms von extrazellulärem Ca^{2+}. Diesen Defekten liegen die Beeinträchtigungen der Funktion sowohl des IP$_3$R als auch von STIM1 zugrunde, während die Ca^{2+} Menge im Reservoir und die Agonisten-induzierte IP$_3$ Produktion unverändert bleiben. Zusammenfassend konnte BIN2 als zentrales Molekül im Ca^{2+} Signalweg von Thrombozyten etabliert werden.

Der dritte Teil der Thesis befasst sich mit dem Effekt des löslichen „neuronal guidance protein" Sema7A auf Thrombozyten. Die Arbeitsgruppe um Prof. Rosenberger konnte bereits zeigen, dass das von Erythrozyten abgespaltene Sema7A die Bildung von *Komplexen aus Thrombozyten und Neutrophilen* (PNC) fördert und damit die Thrombo-Inflammation während

des *Ischämie/Reperfusionsschadens des Myokards* (MIRI) begünstigt. In dieser Thesis konnte gezeigt werden, dass die Interaktion des löslichen Sema7A mit GPIbα auf der Thrombozytenoberfläche die Thrombenbildung fördert und über diesen Mechanismus auch die PNC Bildung und somit Thrombo-Inflammation verstärkt. Aufgrund dessen stellt der Eingriff in die GPIbα-Sema7a Interaktion eine potentielle Strategie dar, den Gewebeschaden während des MIRI zu reduzieren und damit den Schaden nach einem Myokardinfarkt einzugrenzen.

Table of Contents

1 Introduction

Giulio Bizzozero performed the first microscopic description of platelets in 1882: "*In addition to the red and white blood corpuscles, a third sort of morphological element circulates in the blood vessels. In form, they are very thin platelets, disc-shaped, with parallel surfaces or rarely lens-shaped structures, round or oval and with a diameter 2–3 times smaller than the diameter of the red cells*".[1] He found these cells to be the first ones present at a damaged blood vessel and honored their outstanding capacity to change from single circulating cells to a viscous white thrombus mass upon specific stimuli.[1] These observations formed the basis for decades of research revealing very detailed molecular insights into this unique cell type. Platelets are essential for thrombus formation at sites of vascular injury to prevent bleeding, but also have a critical role in pathophysiological conditions, such as myocardial infarction and ischemic stroke.[2,3] In recent years more and more areas of research have emerged, where platelets exert functions beyond classical hemostasis and thrombosis.[4] Platelets have been demonstrate to be important players in angiogenesis, inflammation, host defense, tumor progression and metastasis.[5-8] However, the detailed mechanisms underlying these novel functions are still incompletely understood. Targeting platelets may serve as novel therapeutic strategy for a plethora of related diseases in these fields underlining the importance of platelet research in hemostasis, thrombosis and far beyond.

1.1 Platelets

Platelets are the smallest cells in the bloodstream, with a size of 2-4 micrometer (µm) in humans and 1-2 µm in mice.[9,10] The constant equilibrium of platelet production and the clearance of aged, pre-activated or dysfunctional platelets leads to an average platelet count of 150-400 x10^3 per microliter (µl) in humans and 1,000 x10^3 per µl in mice.[11,12] The lifespan of a human platelet is 7-10 days, whereas a mouse platelet circulates on average for 5 days.[13]

Platelets are primarily produced in the bone marrow by *megakaryocytes* (MKs), which originate from a renewable pool of hematopoietic stem cells. MK maturation involves endomitosis, resulting in a polyploid cell which increases in size to fit all the essential components for platelet production, such as the *demarcation membrane system* (DMS), platelet-specific granules and cytoskeletal components.[14] Each mature MK extends long cytoplasmic protrusions, so called proplatelets, into the bone marrow sinusoids,[15] thereby producing in total ~10^3 platelets.[13] Once released into the blood stream, proplatelets form barbell-shaped structures with platelet-sized bulbs at the end and are separated into platelets presumably by the shear force generated in the flowing blood.[15] This process of platelet production is called thrombopoiesis and is

regulated by several transcription factors, as well as by the hormone *thrombopoietin* (TPO) and the MK environment.[9,16]

A prominent feature of platelets is the absence of a nucleus, limiting the *de novo* protein biosynthesis to the MK-derived mRNA. Furthermore, they contain numerous organelles, including mitochondria, glycosomes, peroxisomes and three different types of granules. The highly abundant α-granules contain more than 300 proteins involved in a variety of different processes, such as platelet adhesion, coagulation and wound healing, but also in inflammation and angiogenesis. Examples are *von Willebrand factor* (vWF), fibrinogen, *platelet factor* 4 (PF4), plasminogen, *platelet derived growth factor* (PDGF) and P-selectin. In contrast, dense granules are smaller, present in lower numbers and mainly contain non-proteinacious compounds important for platelet aggregation, such as *adenosine diphosphate* (ADP), *adenosine triphosphate* (ATP), serotonin and *calcium* (Ca^{2+}). The third type of granules are lysosomes, a pool of proteolytic enzymes. The cytoskeleton, characterized by highly organized actin microfilaments and a circumferential band of microtubule coils, stabilizes the discoid shape of the cell and undergoes massive rearrangements upon activation. Apart from the outer membrane, platelets harbor two further membrane systems, the *open canalicular system* (OCS), a membrane reservoir for the shape change during activation, and the *dense tubular system* (DTS), the equivalent of the endoplasmic reticulum and internal Ca^{2+} store.[17-19]

Platelets survey the vessel integrity throughout their lifetime but most get removed from the bloodstream without undergoing activation. Platelet senescence is characterized by desialylation, i.e. removal of terminal sialic acid residues from membrane glycoproteins leading to clearance. Damaged cells are recognized and removed by splenic macrophages and liver Kupffer cells.[14] However, in the case of vascular damage, platelets come into direct contact with components of the *extracellular matrix* (ECM), initiating a tightly regulated sequence of events including adhesion, activation and aggregation. Thus, a stable hemostatic plug is formed to further prevent blood loss and infection of the wound site.[2] This process is called primary hemostasis. In contrast, platelet aggregation can also occur under pathological conditions, leading to irreversible vessel occlusions. As a result, the obstruction of blood flow and loss of oxygen supply can damage vital organs such as the heart (myocardial infarction) and the brain (ischemic stroke), making occlusive thrombus formation one of the leading causes of death worldwide.[3,20] The process of platelet activation is characterized by a tightly regulated equilibrium between activatory and inhibitory mechanisms which ensure appropriate spatial and temporal responses upon different stimuli.[21] In recent years, more and more areas of research have emerged, identifying platelets as key players in angiogenesis, inflammation,

host defense, tumor progression and metastasis, processes that are mechanistically distinct from normal hemostasis.[5-8]

1.2 Platelet activation and thrombus formation

Platelet adhesion, activation and subsequent thrombus formation upon ECM exposure at sites of vascular injury is a tightly regulated sequence of events, which can be divided into three main steps (Figure 1-1): (i) platelet tethering and adhesion, (ii) platelet activation accompanied by granule release and (iii) platelet firm adhesion and aggregation, enabling thrombus growth.[2]
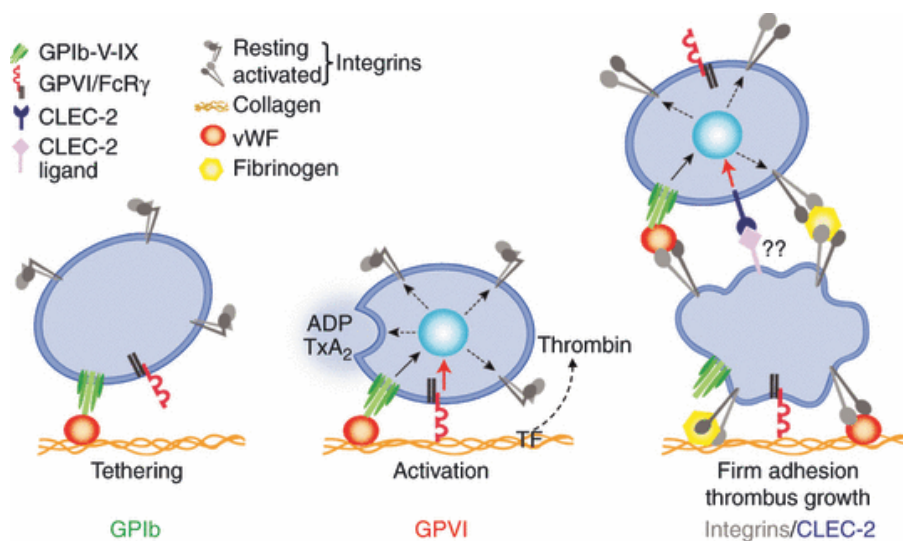
Figure 1-1: Simplified model of platelet adhesion, activation and thrombus formation upon contact with the ECM. First contact and tethering of the platelets on the exposed ECM of the wounded vessel is mediated by the interaction of collagen-bound vWF with the *glycoprotein* (GP) Ib. This enables the binding of GPVI to collagen, initiating activation by intracellular signaling events and granule release. The released second wave mediators, such as *adenosine diphosphate* (ADP) and *thromboxane A2* (TxA$_2$) in combination with thrombin generation mediated by exposed *tissue factor* (TF) further enhances activation and leads to *phosphatidylserine* (PS) exposure. In the final step, cellular events mediate the conformational shift of integrins into a high-affinity state to establish firm platelet adhesion. The growing thrombus is stabilized by *C-type lectin-like receptor 2* (CLEC-2) signaling and integrin binding to free vWF and fibrinogen. (Taken from Nieswandt *et al. J Thromb Haemost,* 2011)[2]

In arterioles and stenosed arteries, high shear rates between 1,000 and 10,000 s^{-1} require platelet deceleration to enable firm contact with exposed ECM. Therefore, initial platelet tethering is essential and mediated by the interaction of the platelet receptor complex *glycoprotein* (GP) Ib/V/IX with collagen-bound vWF. This transient and weak interaction facilitates platelet "rolling" along the side of injury in a stop-and-go manner and thus enables closer contact to the macromolecules of the ECM, such as collagens, laminins and fibronectin.[21-24] Hence, the central activating collagen receptor GPVI binds to its ligand, which induces an intracellular signaling cascade via an *immunoreceptor tyrosine-based activation*

motif (ITAM) in the associated *Fc receptor* (FcR) γ-chain (see 1.3.1).[25,26] As a result, intracellular Ca^{2+} levels increase and the platelet gets activated.[2] Scramblase-mediated *phosphatidylserine* (PS) exposure on the platelet surface enables thrombin production by interaction with the coagulation cascade. Thrombin production is further amplified through *tissue factor* (TF) locally exposed at the side of injury.[27] Additionally, second wave mediators such as ADP are released from platelet granules and platelet *cyclooxygenase-1* (COX-1) synthesizes *thromboxane A2* (TxA$_2$) which is directly released. Together with thrombin, these soluble agonists activate *G-protein coupled receptors* (GPCRs) to reinforce and sustain firm platelet activation via different downstream signaling pathways (see 1.3.2) and recruit additional platelets from the blood stream.[28] *C-type lectin-like receptor 2* (CLEC-2) is the second (Hem) ITAM-coupled receptor on the platelet surface responsible for platelet activation and stabilization of the growing thrombus by interacting with a yet unknown intravascular ligand.[29]

The last step of firm adhesion and thrombus growth is induced by the conformational change of integrins from an inactive to an active state through inside-out signaling, enabling high affinity binding of their respective ligands. Platelets express three β1 integrins (α2β1 binding to collagen; α5β1 binding to fibronectin; α6β1 binding to laminin) and two β3 integrins (αvβ3 binding to vitronectin; αIIbβ3).[30,31] αIIbβ3 is the most abundant integrin on platelets and the dominant receptor mediating aggregation. Its ability to bind different divalent or multivalent ligands, most importantly fibrinogen, fibrin and vWF, bridges adjacent platelets and incorporates further activated platelets into the growing thrombus. Furthermore, ligand binding induces outside-in signaling through the integrin, resulting in cytoskeletal rearrangements, spreading and clot retraction.[32,33]

1.3   Platelet signaling

Two major signaling pathways contribute to platelet activation. Based on the initial stimulus and the thereby activated receptors they are grouped in (i) (hem)ITAM-bearing receptor signaling (1.3.1) and (ii) GPCR signaling (1.3.2). Both signaling pathways share the activation of different *phospholipase C* (PLC) isoforms, mediating the hydrolysis of *phosphatidylinositol-4,5-bisphosphate* (PIP$_2$) to *inositol-3,4,5-trisphosphate* (IP$_3$) and *diacylglycerol* (DAG).[34] IP$_3$ and DAG increase the Ca^{2+} concentration in the cytoplasm by different mechanisms (see 1.3.3). Ca^{2+} is an important second messenger in platelets and essential for granule release, integrin activation and procoagulant activity.[35] Another important step of platelet activation is the rearrangement of the actin and tubulin cytoskeleton, mainly

initiated by integrins, enabling the formation of membrane protrusions, so-called filopodia and lamellipodia.[36]

1.3.1 (hem)ITAM receptor signaling

The ITAM signaling motif is a well conserved sequence in a variety of different hematopoietic immunoglobulin receptors expressed for example on dendritic cells, T and B cells.[37] On mouse platelets, two receptors contain an ITAM or a (hem)ITAM: the GPVI-FcRγ-chain complex and CLEC-2 (Figure 1-2). The physiological ligand for GPVI is collagen.[26] The only known ligand for CLEC-2 is podoplanin, which is not expressed in the vasculature under healthy conditions and therefore unlikely to be involved in thrombus growth.[38,39] For investigations of CLEC-2-dependent platelet activation the snake venom *rhodocytin* (RC) is used as non-physiological agonist.[40] Of note, in humans a third ITAM receptor, FcγRIIA, is expressed on platelets.[41]
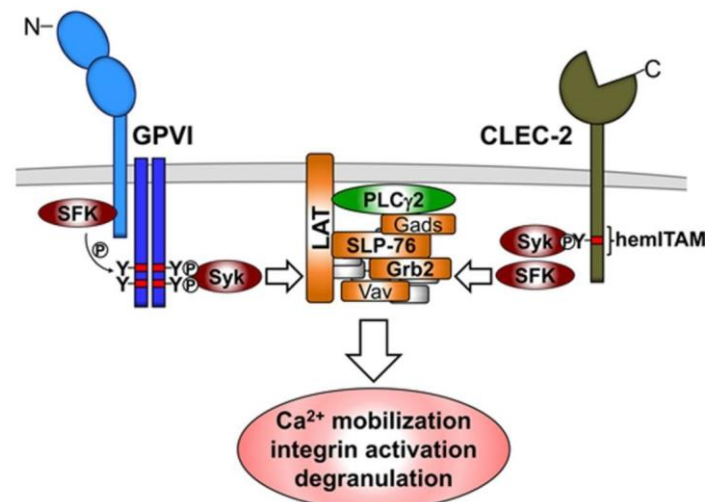
Figure 1-2: (hem)ITAM signaling in platelets. Phosphorylation of the (hem)ITAM of the GPVI-FcRγ-chain complex by *Src family kinases* (SFK) or CLEC-2 by *spleen tyrosine kinase* (Syk) initiates a downstream signaling cascade, involving, among others, the *linker for activation of T cells* (LAT), the *SH2 domain containing leukocyte protein of 76 kDa* (SLP-76) and the *growth factor receptor bound protein 2* (Grb2). This culminates in the activation of the major effector enzyme in the ITAM signaling cascade, *phospholipase C* (PLC)γ2, inducing Ca^{2+} mobilization, integrin activation and degranulation. (Modified from Stegner *et al. Arterioscler Thromb Vasc Biol*, 2014)[42]

The hemITAM consists of a sequence of 4 *amino acids* (aa) (YxxL/I; x denotes an unspecific aa). The ITAM contains two of these sequences separated by 6-12 aa (YxxL/I(x)$_{6-12}$YxxL/I). Upon ligand binding to GPVI, the tyrosine residues within the ITAM of the non-covalently linked FcRγ-chain get phosphorylated by the *Src family kinases* (SFK) Fyn and Lyn. This phosphorylation is recognized by the *Src homology 2* (SH2) domain of the *spleen tyrosine kinase* (Syk). Syk in turn gets activated and initiates a signaling cascade involving a large number of adaptor and effector proteins, such as the *linker for activation of T* cells (LAT), the

SH2 domain-containing leukocyte protein of 76 kDa (SLP-76) and the *growth factor receptor-bound protein 2* (Grb2). This culminates in the activation of the major effector enzyme downstream of GPVI signaling, PLCγ2, leading to Ca^{2+} mobilization, integrin activation and degranulation (Figure 1-2).[42,43] Except for slight differences, the activation of CLEC-2 orchestrates a similar intracellular signaling cascade, including the phosphorylation of Syk, SFKs, LAT and PLCγ2 (Figure 1-2).[44,45]

1.3.2 G protein-coupled receptor signaling

Soluble agonists like TxA_2, thrombin and ADP exert their activating effect on platelets through GPCRs on the cell surface. TxA_2 stimulates the *TxA_2 receptor* (TP). Thrombin binds to *protease-activated receptors* (PARs) 1/4 on humans or PAR 3/4 on mouse platelets. All of these receptors are linked to the heterotrimeric G proteins $G_{12/13}$ and G_q. ADP signals through $P2Y_1$ and $P2Y_{12}$, coupled to G_q and G_i (Figure 1-3).[28]

Activation of $G_{12/13}$ leads to the activation of GTPases of the Rho family, initiated by Rho *guanine nucleotide-exchange factors* (GEFs). Subsequently, *myosin light chain* (MLC) is
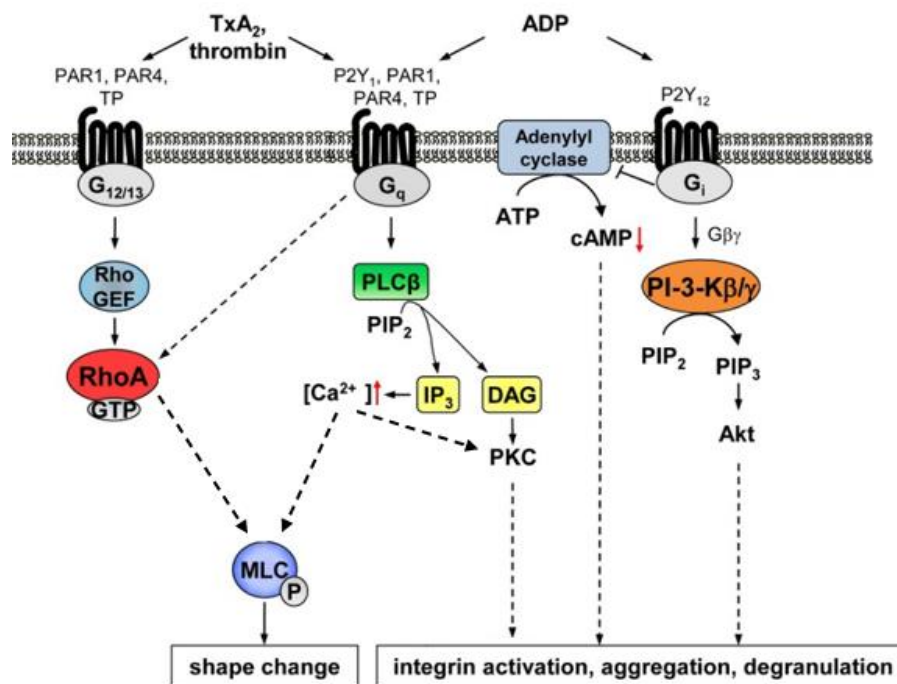
Figure 1-3: GPCR signaling in platelets. *Thromboxane A_2* (TxA_2), thrombin and *adenosine dihosphate* (ADP) signal through *G-protein coupled receptors* (GPCRs) on the platelet surface mediated by by G_i, G_q and G_{13}. The resulting downstream signaling induces platelet shape change, aggregation, degranulation, as well as integrin activation. RhoGEF: Rho-specific guanine nucleotide exchange factor; RhoA: Ras homolog family member A; MLC: myosin light chain; PLC: phospholipase C; PIP_2: phosphatidylinositol-4,5-bisphosphate; IP_3: inositol 3,4,5 trisphosphate; DAG: diacyl glycerol; PKC: protein kinase C; cAMP: cyclic adenosine monophosphate; PI-3-K: phosphoinositide-3-kinase; PIP_3: phosphatidylinositol-3,4,5-trisphosphate; (Taken from Offermanns *et al. Circ Res,* 2006,[28] modified and kindly provided by Ina Hagedorn).

phosphorylated in a Rho/Rho-kinase-dependent manner, mediating platelet shape change (Figure 1-3).[28] Another way to induce platelet shape change is the activation of RhoA, as well as the Ca^{2+}-dependent phosphorylation of MLC downstream of G_q. In addition, the activation of G_q mediates the hydrolysis of PIP_2 into IP_3 and DAG through the PLCβ isoform. This leads to an increased Ca^{2+} concentration in the cytoplasm, activation of *protein kinase C* (PKC) and consequently to platelet activation, aggregation and degranulation (Figure 1-3).[46] Downstream effects of G_i are the reduction of *cyclic adenosine monophosphate* (cAMP) by inhibition of the adenylyl cyclase and the production of PIP_3 through the activation of *phosphatidylinositide-3-kinase* (PI-3-K) isoforms. Both induce integrin activation, aggregation and degranulation (Figure 1-3).[47]

Of note, the activation of GPCRs in turn leads to the release of more soluble factors like TxA_2, ADP and ATP, inducing further amplification of platelet activation.[28]

1.3.3   Calcium signaling

Ca^{2+} is a second messenger, which is essential for signaling processes in virtually all cells.[48] In platelets, the increase in cytoplasmic Ca^{2+} level is the central step in platelet activation, mediating degranulation, integrin activation, aggregation and shape change. While different receptors on the platelet surface trigger different signaling pathways, virtually all activate PLC isoforms and thus the production of DAG and IP_3 (1.3.1; 1.3.2). Both molecules contribute in different ways to Ca^{2+} influx (Figure 1-4).[35]

IP_3 binds to IP_3Rs, thereby inducing the release of Ca^{2+} from the DTS, which is the platelet equivalent of the *endoplasmic reticulum* (ER) and the internal Ca^{2+} store. The store depletion triggers a large Ca^{2+} influx across the *plasma membrane* (PM). This mechanism is called *store-operated Ca^{2+} entry* (SOCE) and is the major route of Ca^{2+} influx in platelets.[34,49] *Stromal interaction molecule 1* (STIM1) has been identified as the essential Ca^{2+} sensor localized in the DTS membrane. Its EF-hand motif senses the reduced Ca^{2+} in the DTS upon store release and consequently STIM1 activates the *Ca^{2+} release-activated Ca^{2+}* (CRAC) channel Orai1. This channel is localized in the PM of platelets and allows the entry of extracellular Ca^{2+} (Figure 1-4).[50-53] Mouse models deficient in STIM1 or Orai1 exhibit severely defective Ca^{2+} responses upon all tested agonists and are protected from arterial thrombosis and ischemic stroke. Interestingly, bleeding times were only mildly prolonged.[52,53]
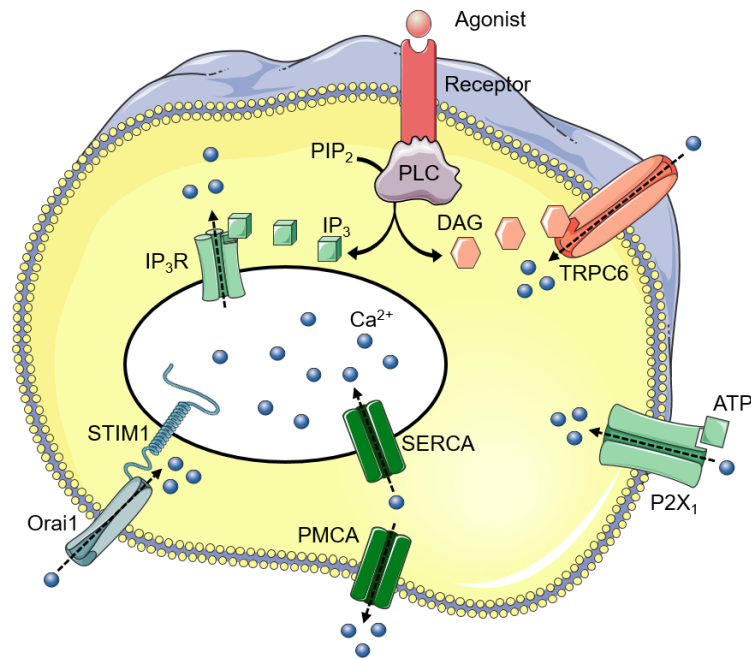
Figure 1-4: Simplified model of Ca^{2+} signaling in platelets. Agonist induced receptor activation leads to phosphorylation of *phospholipase C* (PLC) isoforms, mediating the hydrolysis of *phosphatidylinositol-4,5-bisphosphate* (PIP$_2$) to *inositol-1,4,5triphosphate* (IP$_3$) and *diacyl-glycerol* (DAG). SOCE: IP$_3$ activates its receptor (IP$_3$R) in the DTS membrane, inducing Ca^{2+} store release. The reduced Ca^{2+} concentration in the store is sensed by *stromal interaction molecule 1* (STIM1), which opens the *Ca^{2+} release-activated Ca^{2+}* (CRAC) channel Orai1 in the plasma membrane. Non-SOCE: DAG activates the canonical *transient receptor potential channel 6* (TRPC6) in the plasma membrane. ROCE: the *receptor-operated calcium* (ROC) channel P2X$_1$ is directly activated by ATP. *Sarcoplasmatic/endoplasmatic reticulum Ca^{2+} ATPases* (SERCAs) and *plasma membrane Ca^{2+} ATPases* (PMCAs) pump Ca^{2+} back into the DTS or out of the cell, respectively. (Graphic design: Julia Volz using Servier Medical Art: https://smart.servier.com/)

The functional coupling model, developed in other cells than platelets, suggests that STIM1, Orai1 and IP$_3$R form puncta structures at the ER-PM junctions, where the actual SOCE may then occur.[54-60] While this process forms the essential framework for SOCE in virtually all non-excitable cells, several enzymes and adaptor proteins have been identified to be critical regulator of this process,[60-63] thereby allowing a cell-specific assembly of Ca^{2+} signaling systems with very different spatial and temporal dynamics.[48,64] To date, STIM1 adaptors in platelets remain to be identified.

DAG initiates the so called *non-store-operated calcium entry* (non-SOCE) by directly activating Ca^{2+} channels in the PM, such as the *transient receptor potential channel 6* (TRPC6) (Figure 1-4). Studies in TRPC6-deficient mice revealed an abolished DAG-induced Ca^{2+} influx, but found no functional influence on hemostasis and thrombosis.[65]

A third way of Ca^{2+} influx is the *receptor-operated calcium entry* (ROCE), mediated by the purinoreceptor P2X$_1$ in the PM and its agonist ATP (Figure 1-4). This mechanism amplifies platelet activation, especially at low agonist concentrations and at higher arterial shear rates.[66,67]

Platelets also express Ca^{2+} ATPases that counteract SOCE, non-SOCE and ROCE. *Sarcoplasmatic/endoplasmatic reticulum Ca^{2+} ATPases* (SERCAs) and *plasma membrane Ca^{2+} ATPases* (PMCAs) pump the Ca^{2+} back into the DTS or out of the cell, respectively (Figure 1-4). Thapsigargin is a SERCA pump inhibitor, which enables the agonist-independent analysis of platelet function by slowly emptying the intracellular Ca^{2+} store.[35]

1.4 The ITAM receptor GPVI

GPVI is the main activating receptor for collagen on platelets. It is a 58-60 kDa type I transmembrane protein belonging to the *immunoglobulin* (Ig) superfamily of surface receptors.[68] It is only expressed on platelets and MKs and recognizes the *glycin-prolin-hydroxyproline* (GPO) repeats of collagen. Therefore, the GPO-rich non-physiological ligand *collagen-related peptide* (CRP) is also a powerful activator of this receptor. Furthermore, *convulxin* (CVX), a C-type lectin from the venom of the rattlesnake triggers GPVI activation.[26,69] More recently, two novel ligands, fibrin and laminin, were discovered to promote thrombin generation and stimulate spreading in a GPVI-dependent manner.[70-72] GPVI signals through the ITAM of the non-covalently associated FcRγ-chain as described in 1.3.1. Upon collagen binding, GPVI dimer clustering is induced, resulting in a higher avidity for its ligand and representing a crucial step to initiate and maintain signaling.[73] GPVI can be shed from the surface by metalloproteinases, resulting in a transmembrane remnant and a soluble GPVI fragment.[74]

Irreversible downregulation of GPVI from the platelet surface can be achieved in mice by the injection of monoclonal rat anti-GPVI antibodies, called JAQ1, JAQ2 and JAQ3. This immunodepletion allows the induction of a "knock-out like" phenotype in wild-type mice for up to two weeks, associated with a short thrombocytopenia at the beginning of the treatment.[75,76] FcγRIIb on liver sinusoidal endothelial cells interacting with the Fc portion of the anti-GPVI antibodies was shown to be crucial for the immunodepletion, but the exact mechanism of this downregulation is still incompletely understood.[77] To functionally block GPVI without inducing thrombocytopenia, Fab or F(ab)$_2$ fragments of these antibodies can be used.[78]

Loss or functional inhibition of GPVI provides profound protection in models of arterial thrombosis, ischemia reperfusion injury after myocardial infarction and ischemic stroke, while having only very limited effects on hemostasis.[79-81] Therefore, GPVI is considered as a potentially safe anti-thrombotic target.[82]

Furthermore, besides its central role in thrombosis, GPVI is increasingly recognized to be critically involved in platelet function during inflammation, a process that is mechanistically

distinct from normal hemostasis. Important roles for GPVI were demonstrated in the recruitment of platelets and leukocytes to the inflamed vessel, the regulation of vascular permeability and leukocyte activation.[83] Moreover, GPVI also contributes to the maintenance of vascular integrity during inflammation and its absence induces inflammatory bleeding.[84-86] Interestingly, this mechanism seems to be highly organ and stimulus-dependent. A current model of inflammatory bleeding in immune complex–mediated dermatitis is depicted in Figure 1-5.[87,88]
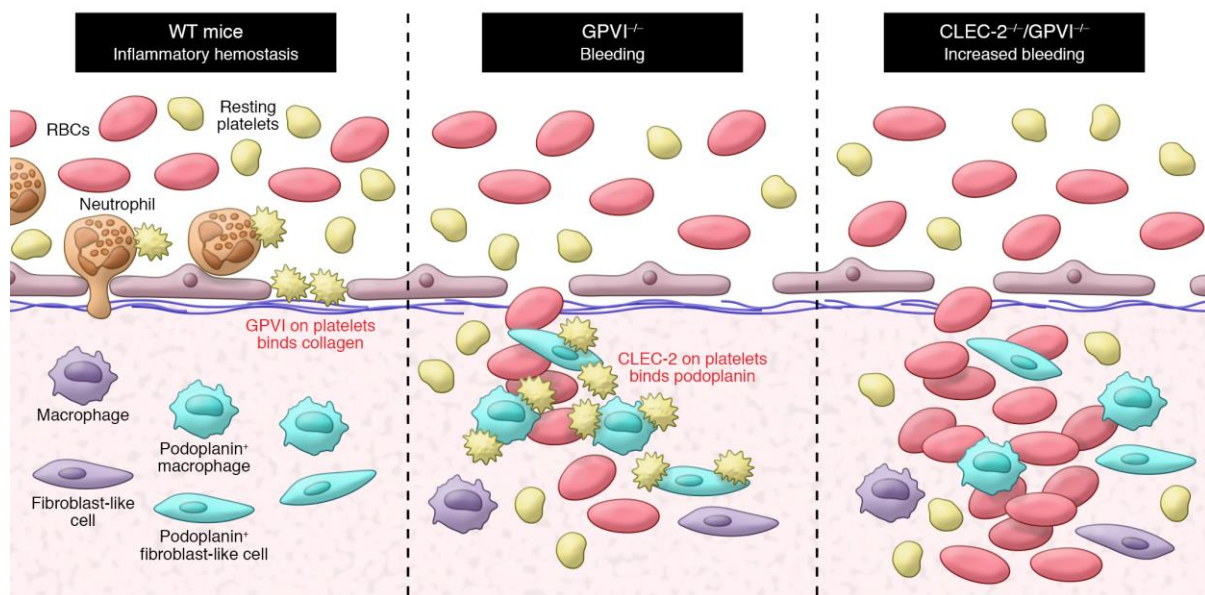
Figure 1-5: Model of inflammatory bleeding in immune complex–mediated dermatitis. At sites of inflammation, platelets prevent bleeding by a process which is mechanistically distinct from classical hemostasis. Single platelets were shown to seal neutrophil-induced vascular breaches via GPVI. Genetic deficiency or blockade of GPVI signaling induced bleeding, which was more pronounced with concomitant deficiency of CLEC-2. (Taken from Rayes *et al. J Clin Invest*, 2019)[88]

Recruitment and activation of neutrophils to the inflamed tissue and their transmigration through the vessel wall induces vascular damage, which is sealed by platelets in a GPVI-dependent manner. In GPVI-deficient mice bleeding can be observed, which is, however, limited by the interaction of CLEC-2 with podoplanin on cells in the ECM. Thus, the concomitant deficiency of GPVI and CLEC-2 leads to a more severe bleeding and loss of vascular integrity.[88]

1.5 Cancer

Cancer belongs to the leading causes of death worldwide. According to Cancer Research UK (https://www.cancerresearchuk.org/health-professional/cancer-statistics), 9.6 million people

died worldwide in 2018 from this very diverse disease, resulting from abnormal cell growth. Cancer is a generic term for a variety of pathologies with different symptoms and disease courses, depending on the initially affected cell type. However, carcinogenesis and tumor progression do not exclusively rely on cell-autonomous processes but are also influenced by the cellular and molecular environment of the tumor location. This surrounding is called *tumor microenvironment* (TME) and includes blood vessels, pericytes, immune cells, bone-marrow derived cells, growth factors, cytokines and ECM molecules.[89] Tissue damage, an innate danger signal elicited by the growing tumor, induces the recruitment of immune cells. Consequently, cancer is accompanied by sustained inflammation. This emphasizes the concept of "tumors as chronic, non-healing wounds", highlighting a potential role of classical players of wound healing, such as platelets, in the underlying pathophysiological mechanisms.[90,91]

1.5.1 The role of platelets in cancer

First evidence of a relation between cancer and platelets has been provided by Armand Trousseau in 1865, who has described the formation of venous thrombi in cancer patients. Thromboembolic diseases in cancer patients are nowadays a well-characterized problem in the clinics, associated with worse prognosis and survival.[8,92] The reason for the higher thrombotic risk is the ability of cancer cells to activate platelets in a direct or indirect manner by several mechanisms. The so-called *tumor-cell induced platelet aggregation* (TCIPA) can be induced by cancer cell secretion of soluble platelet activators, such as thrombin, TxA_2 and ADP.[93-95] Moreover, several cancer types express podoplanin, mediating platelet activation through CLEC-2 binding. Colon, prostate and breast cancer cells are able to bind platelet $Fc\gamma RIIa$, thereby triggering dense granule release.[8] An indirect mechanism for TCIPA is the expression of TF on cancer cells, which is the principal activator of the extrinsic coagulation cascade.[93] The expression of mucins on cancer cells oblige platelets to interact with granulocytes, which consequently release cathepsin G. Cathepsin G in turn mediates the cleavage of the platelet PAR4 receptor, resulting in the activation of G protein signaling pathways.[96,97] The activation of platelets has several beneficial effects for cancer cells, such as the stimulation of tumor growth and angiogenesis, as well as the promotion of cancer metastasis.

A newly formed tumor, which grows beyond a size of a few millimeters, depends on the establishment of an own blood vascular system to ensure nutrition and oxygen supply as well as waste removal. This angiogenic switch is initiated by growth factors, released from tumor cells and the TME.[98] The thereby activated endothelium increases the expression of vWF, P-

selectin, αvβ3 integrins and TF, leading to local platelet recruitment.[90,99-101] Once recruited and activated, platelets release molecules such as *vascular endothelial growth factor* (VEGF), PDGF, *basic fibroblast growth factor* (bFGF), *transforming growth factor-β* (TGFβ) and angiopoietin to promote tumor growth and angiogenesis.[102-107] Of note, platelets also contain anti-angiogenic factors such as PF4, endostatin and the microRNA miR-24,[108,109] suggesting a stage and context-dependent effect of platelet function on cancer progression.[8]

Metastasis is the spread of single cells of the primary tumor throughout the body. The process of tumor metastasis, including ECM degradation, invasion of the vasculature, tumor cell survival in the blood stream and the establishment of malignancies in distant tissues is highly supported by activated platelets.[110] *Epithelial-mesenchymal transition* (EMT), a process in which individual tumor cells lose their adhesive properties and acquire a migratory and invasive phenotype, is mediated by platelet-derived TGFβ, *prostaglandin E2* (PGE$_2$) and *lysophosphatidic acid* (LPA).[107,111,112] Upon entering the blood stream, the tumor cell is exposed to high shear rates and numerous immune cells, such as *natural killer* (NK) cells. Via αvβ3 interactions and TCIPA, platelet aggregates cover the tumor cell, forming a protective shield ("cloaking") (Figure 1-6).[113,114]
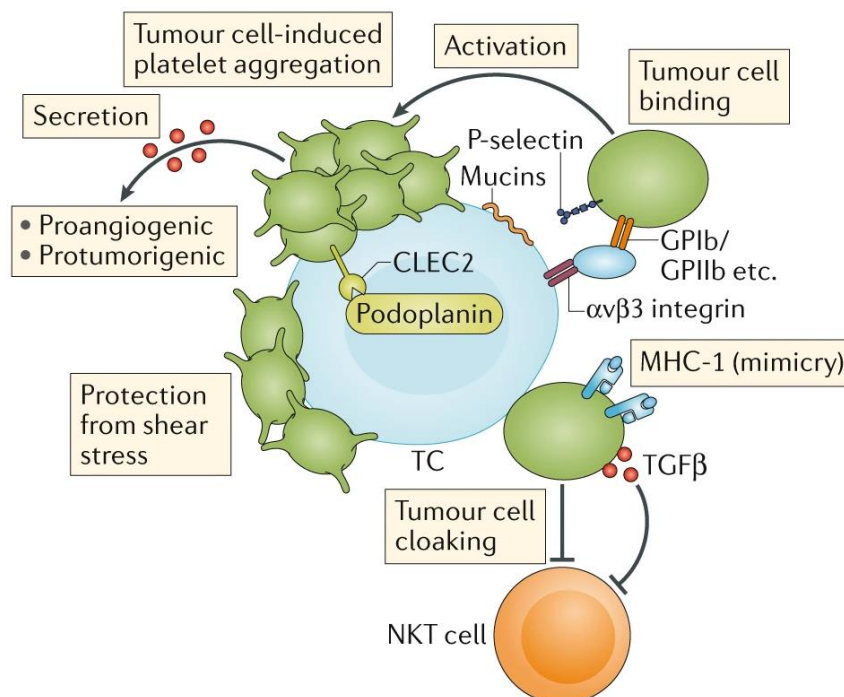
Figure 1-6: Platelet-cancer cell interactions during metastasis. Platelets bind to *tumor cells* (TCs) through interaction with the αvβ3 integrin on the tumor cell surface and via P-selectin. Upon activation and *tumor cell-induced platelet aggregation* (TCIPA), platelets secret proangiogenic and protumorigenic factors and protect the TC from shear stress (cloaking). Furthermore, TC cloaking inhibits *natural killer* (NK) and T-cell function by spatial distancing, TGFβ secretion and MHC1 transfer onto tumor cells. (Modified from Gärtner et al. *Nat Rev Immunol,* 2019[90]).

However, platelets do not only passively shield the tumor cell, they also actively suppress NK cell cytotoxicity. The secretion of TGFβ induces downregulation of the major recognition receptor for tumor cells on NK cells, NKG2D.[115] Moreover, platelets transfer MHC class I onto the tumor cell surface, allowing them to suppress NK cell function (Figure 1-6).[116] In order to initiate tumor cell extravasation, platelet P-selectin, GPIb and integrin αIIbβ3 are used to mediate rolling and firm adhesion of the tumor cells at the endothelium. Once attached to the endothelium, platelets promote coagulation and weaken the endothelial barrier.[8,90] Platelet derived *C-X-C motif chemokine ligand* (CXCL) 5 and CXCL7 induce the recruitment of granulocytes and the formation of the early metastatic niche.[117] Furthermore, platelet *glycoprotein A repetition predominant* (GARP) reinforces TGFβ activity, thereby dampening T-cell function.[118]

Taken together, platelets play a tremendous role in carcinogenesis and tumor progression by supporting tumor growth, angiogenesis and metastasis. The option to interfere with platelet function to achieve an anti-cancerogenic effect has been controversially discussed in literature for decades. First evidence has been provided in the 1970s by several animal studies using adenocarcinoma and B16 melanoma which demonstated anti-metastatic effects of aspirin, which irreversibly inactivates COX-1 and COX-2.[119,120] However, this has not been observed in other tumor models, emphasizing tumor type specificity.[121] More recently, retrospective analysis from large patient datasets indicates a protective role of aspirin to develop cancer, as well as a reduced mortality and decreased metastasis in cancer patients.[122-125] However, it is not clarified whether this effect is induced by aspirin-mediated inhibition of platelet COX-1, by inhibition of COX-2 on other cell types or tumor cells, by COX-independent mechanisms or a combination of all.[89] Blockade of the ADP receptor $P2Y_{12}$ on platelets by clopidogrel or ticagrelor dampens tumor growth and metastasis rate in mouse models of pancreatic and melanoma cancer.[126,127] In contrast to aspirin, no patient data was collected to confirm this effect in humans. Furthermore, it is important to mention that $P2Y_{12}$ is also expressed on other cells than platelets, such as osteoclasts. The inhibition of $P2Y_{12}$ in these cells is protective for pathologic bone loss associated with tumor growth.[128] A drawback of platelet inhibition by these mechanisms is the bleeding risk, especially in patients who are thrombocytopenic due to their anti-cancer therapy.[129] Therefore, further research on the role of platelets in cancer is mandatory to predict potential risks and benefits of anti-platelet therapies.

1.5.2 The role of platelets in maintaining tumor vascular integrity

As described above, a growing tumor is dependent on a blood vascular system due to its constant need for nutrients and oxygen and to ensure waste removal.[98] Amongst other specific

features, tumor vascularization is characterized by a high angiogenic potential and a constant level of inflammation.[98,130] Interestingly, platelets prevent hemorrhage at sites of angiogenesis and inflammation,[84,131] emphasizing their potential impact on tumor vessel integrity.

Indeed, depletion of platelets in tumor-bearing mice induces loss of vascular integrity and thus profound bleeding in the tumor, while leaving vessels in non-tumor tissue largely unaffected.[132] This process seems to be mechanistically distinct from normal hemostasis, since no aggregate formation in the tumor microcirculation has been observed by intravital microscopy or in tumor sections.[132,133] Consistently, the ability of platelets to maintain tumor vascular integrity is not altered by the absence of the vWF/GPIb interaction, as demonstrated by the use of GPG290, a GPIb inhibitor, and in vWF-deficient mice. In line with this, mice being deficient for P-selectin, β3 integrins or incapable of proper integrin inside-out signaling do not show spontaneous hemorrhage in the tumor tissue.[132,134]

During inflammation, immune cells are thought to contribute to the damage of the vascularization, which is then repaired by platelets.[135] In line with this, reducing the numbers of tumor infiltrating neutrophils and macrophages in CD18- and β3-deficient mice was protective for thrombocytopenia-induced hemorrhage.[136] Of note, platelet depletion had no influence on the amount of infiltrating immune cells in *WT* animals.[136]

Interestingly, it has been shown that platelet depletion promotes the intratumoral accumulation of chemotherapeutic agents in mice, thereby enhancing the anti-tumoral effect without affecting its overall toxicity.[134] These studies revealed a critical tumor-supporting role of platelets and indicated that targeting platelets might be a valid strategy to limit tumor progression and to potentiate the efficacy of chemotherapy. While effective in experimental animals, the induction of acute thrombocytopenia in cancer patients is not a therapeutic option due to severe side effects on hemostasis. Thus, it is imperative to identify the molecular mechanisms how platelets safeguard vascular integrity in tumors in order to develop anti-platelet agents allowing selective destabilization of the tumor vasculature during chemotherapy in patients without triggering unwanted systemic bleeding complications. A promising target is the platelet-specific receptor GPVI, which is involved in maintaining vascular integrity during angiogenesis and inflammation and is considered to be a potentially safe anti-thrombotic target.

1.6 Bridging integrator 2 (BIN2)

Bridging integrator (BIN) proteins belong to the superfamily of adapter proteins characterized by a common N-terminal *Bin-Amphiphysin-Rvs* (BAR) domain. The BAR domain consists of

three long bent α-helices, typically forming homodimers with a positively charged concave interface. This enables the binding to negatively-charged phospholipids of membranes and favors its curvature.[137] The degree of membrane curvature varies depending on the BAR domain subfamilies: N-BAR (n-terminal amphipathic helix), F-BAR (extended Fes-CIP4 homology) or I-BAR (IRSp53-MIM homology).[138] Diverse cellular functions of BAR domain protein family members have been described, including membrane dynamics,[139] organization of the actin cytoskeleton,[140] cell cycle control,[141] as well as tumor suppression.[141,142]

Three different BIN isoforms are known: BIN1, BIN2, and BIN3, which belong to the N-BAR proteins. BIN1 is ubiquitously expressed, but exists in a variation of differently spliced isoforms, depending on the cell type.[143] The most prominent splice variant, containing a Myc-binding domain and a C-terminal *Src-homology 3* (SH3) domain, is depicted in Figure 1-7. BIN1 has been shown to fold cardiac T-tubules, thereby facilitating cytoskeleton-based Ca^{2+} channel trafficking to the T-tubule membranes and refraining free diffusion of local Ca^{2+} and K^+ ions.[144,145] Furthermore, BIN1 was identified as an important risk locus for late onset Alzheimer's disease and acts as a tumor suppressor.[143,146] BIN3 only consists of the N-BAR domain (Figure 1-7) and is expressed in all tissues excluding the brain. The role of BIN3 in cellular processes is barely understood, except for its involvement in the regulation of Rac1- and Cdc42-dependent processes in myogenesis.[147]

BIN2 consists of an N-BAR domain and an unstructured C-terminal part with proline rich regions (Figure 1-7). Only very limited information is available about the function of BIN2, which is predominantly found in hematopoietic cells.[148] Previous studies have shown that BIN2 is present at podosomes of adherent leukocytes, indicating a functional role in cell adhesion and possibly integrin activation.[149] In addition, siRNA knockdown of BIN2 in macrophages led to enhanced phagocytosis and reduced cell movement of monocytes and mast cells.[149]
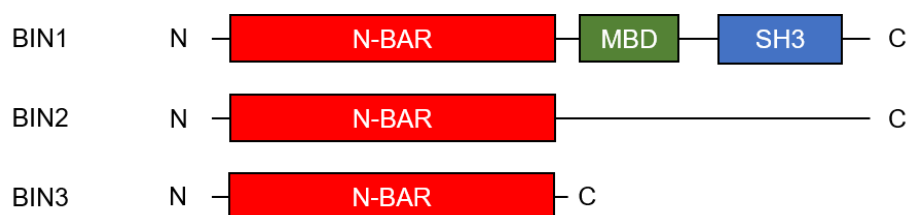
Figure 1-7: Schematic representation of the BIN protein family. The simplified domain structures of the N-BAR domain proteins BIN1 (most prominent splice variant), BIN2 and BIN3. N-BAR: n-terminal amphipathic helix BAR domain; MBD: Myc-binding domain; SH3: Src-homology 3 domain.

1.7 Semaphorins

The first members of the semaphorin family were discovered in the 1990s as regulators of axon growth and guidance.[150-152] Since then, the family grew to 30 membrane-bound, *glycosylphosphatidylinositol* (GPI)-membrane linked or secreted proteins, all sharing the sema domain. Semaphorins are grouped into 8 classes according to different structural features and their occurrence in invertebrates (class 1-2), vertebrates (class 3-7) and viruses (class V).[153] Semaphorins interact with a plethora of receptors and co-receptors, amongst which the plexins are the most prominent group.[154] Other important receptors and co-receptors for semaphorins are neurophilins, receptor tyrosine kinases and integrins.[155]

Semaphorin-initiated signaling translates into cytoskeletal rearrangements to modulate cellular adhesion and cell shape and effects cell differentiation, motility and survival in a wide range of physiological processes.[153,156-158] Their extensively studied roles in the nervous system, the immune system and the circulatory system are complemented by emerging roles in organs such as lung, kidney and bone.[159-164] Furthermore, semaphorins are associated with cancer progression and tumor angiogenesis.[165,166]

1.7.1 Semaphorins and platelets

In platelets three different semaphorins are expressed (Sema4B, Sema4D and Sema7A) (Figure 1-8).[167,168] Sema4D expression is increased upon platelet activation and it can be shed from the cell surface by *a disintegrin and metalloproteinase* (ADAM) 17.
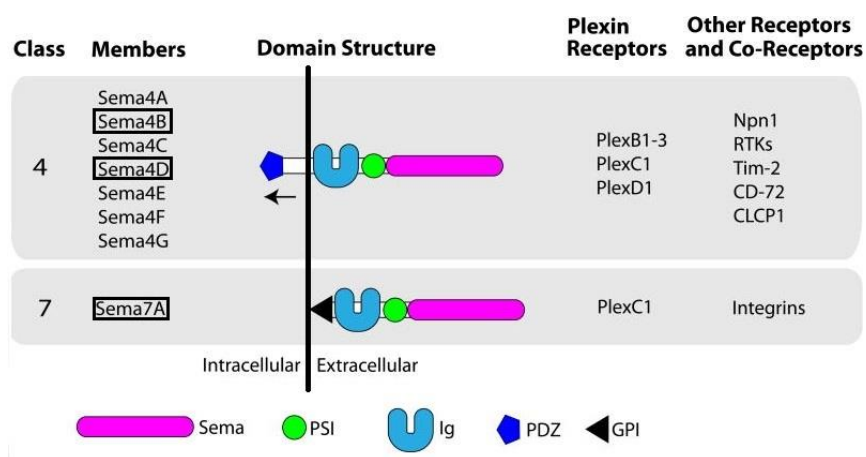
Figure 1-8: Schematic representation of semaphorin protein classes expressed in platelets. The semaphorins are grouped into 8 classes according to different structural features and their occurrence in invertebrates (class 1-2), vertebrates (class 3-7) and viruses (class V). Two Semaphorins from class 4 (Sema4B and Sema4D) and Sema7A are expressed on platelets. PSI: plexin-semaphorin-integrin domain; Ig: immunoglobulin domain; PDZ: PDZ domain; GPI: glycosylphosphatidylinositol linkage (Modified from Alto *et al. Methods Mol Biol,* 2017.[153]).

The soluble/shed Sema4D in turn can accelerate platelet activation and thrombus formation. Sema4D-deficient mice show impaired arterial thrombus formation *in vivo.*[167] Their platelets exhibit a reduced aggregation potential in response to collagen and decreased Syk phosphorylation, resulting in reduced Ca^{2+} influx.[167,169] The role of Sema4B and the GPI-membrane bound Sema7A in platelets still remains elusive. Besides the presence of semaphorins, 8 plexins were detected in platelets so far,[170] emphasizing the potential role of this signaling axis in platelets.

There are also semaphorins described, which are expressed on other cell types and can influence platelet function. Sema3A, produced by endothelial cells, was shown to bind to platelets and alter platelet function through inhibition of αIIbβ3 signaling and altered agonist-induced Rac1-dependent actin rearrangements.[171]

1.7.2 Soluble Sema7A

Sema7A was detected on the platelet surface and in α-granules, but the functional role of membrane-bound Sema7A remains elusive so far.[168] Moreover, Sema7A is further expressed on a variety of other cell types, such as endothelial cells and *red blood cells* (RBC) and is sensitive to ADAM17-mediated cleavage, resulting in a soluble protein.[153,168] Soluble Sema7A negatively influences megakaryocyte differentiation from CD34+ progenitor cells and alters immune cell function via interaction with integrin α1β1.[155,172] It enhances autoimmune encephalitis in a T-cell-dependent manner and increases the infiltration of neutrophils into sites of tissue hypoxia.[173-175] Furthermore, increased levels of Sema7A were associated with atherosclerosis and atherothrombotic stroke.[176,177] Apart from this, only little is known about the function of soluble Sema7A and its interaction with platelets in (patho-)physiological conditions.

Our collaboration partners Prof. Peter Rosenberger and Dr. David Köhler from the University Hospital in Tübingen (Department of Anesthesiology and Intensive Care Medicine) investigated the role of Sema7A in the process of thrombo-inflammatory *myocardial ischemia (MI)-reperfusion injury* (MIRI).[178] Soluble Sema7A was found to be elevated in MI patient blood and levels correlate with the extent of MIRI. The injection of commercially available recombinant Sema7A (Gln45-Ala646)-mouse IgG2A Fc fusion protein (referred to as rSema7A) into *WT* mice increased the infarct size upon MIRI dramatically, whereas Sema7A KO mice depicted smaller infarcts compared to littermate controls. This underlines a functional role of soluble Sema7A in MIRI progression. Using cell type-specific Sema7A knockout animals, RBCs were identified as major source for soluble Sema7A. Furthermore, *platelet-neutrophil*

complex (PNC) formation was observed in the presence of Sema7A. However, nothing is known about a potential effect of soluble Sema7A on platelets so far. Therefore, an initial characterization of the effect of rSema7A on platelet function was performed in this thesis as a collaboration in the framework of this project.

1.8 Aim of the study

Maintenance of tumor vascular integrity is indispensable for tumor growth and thus affects tumor progression. Previous studies have identified platelets as major regulators of tumor vascular integrity. However, the exact mechanism has remained elusive. Platelet GPVI is involved in preventing hemorrhage at sites of angiogenesis and inflammation and is therefore a promising candidate to play a role in this process in primary tumors as well. Therefore, the fist aim of this thesis was to investigate the role of platelet GPVI in maintaining tumor vascular integrity. Furthermore, the potentially beneficial effect of GPVI inhibition on tumor growth and concomitant chemotherapy was evaluated in mice.

In the second part of this thesis, the role of BIN2 in platelet Ca^{2+} signaling was analyzed. BIN2 has been previously discovered by our group as a potential interaction partner of the Ca^{2+} sensor protein STIM1. Therefore, two mouse strains deficient for BIN2 (a constitutive and a platelet/megakaryocyte specific knockout mouse line) were generated and used to study the role of BIN2 in platelet function with special focus on its role in Ca^{2+} signaling.

The role of the neuronal guidance protein Sema7A in thrombo-inflammation in myocardial ischemia-reperfusion injury was investigated by our collaboration partners Prof. Peter Rosenberger and Dr. David Köhler. PNCs were increased upon rSema7A treatment in this model, indicating a potential effect of rSema7a on platelets and neutrophils. Therefore, the third aim of this thesis was to shed light on the effect of soluble Sema7A on platelet function in the framework of this project.

2 Materials and Methods

2.1 Materials

2.1.1 Reagents, kits and cell culture material

Reagent	Company
β-mercaptoethanol	Roth (Karlsruhe, Germany)
[3H]-paclitaxel	Moravec (Brea, USA)
3,3',5,5'-tetramethylbenzidine (TMB)	EUROPA (Cambridge, UK)
Adenosine diphosphate (ADP)	Sigma-Aldrich (Steinheim, Germany)
Agarose	Roth (Karlsruhe, Germany)
Albumin Fraction V, endotoxin tested (bovine serum albumin, BSA)	Roth (Karlsruhe, Germany)
Ammonium chloride	Sigma-Aldrich (Schnelldorf, Germany)
Ammonium persulfate (APS)	Roth (Karlsruhe, Germany)
Apyrase (grade III)	Sigma-Aldrich (Schnelldorf, Germany)
Avidin-Biotin (AB)-Complex	ThermoFisher Scientific (Waltham, USA)
BioScint Cocktail	National Diagnostics (Waltham, USA)
Biosol	National Diagnostics (Waltham, USA)
BlueBlockPF (10x)	SERVA Electrophoresis (Heidelberg, Germany)
BlueStar Plus Prestained protein marker	Nippon Genetics (Düren, Germany)
BlueStar Prestained protein marker	Nippon Genetics (Düren, Germany)
$CaCl_2$	Roth (Karlsruhe, Germany)
Cacodylate	AppliChem (Darmstadt, Germany)
Collagen related peptide (CRP)	kindly provided by Paul Bray (Baylor Collage, USA)
Collagenase I	Merck Millipore (Darmstadt, Germany)
Convulxin	Axxora (Lörrach, Germany)

Reagent	Company
DePeX mounting medium	VWR Int. GmbH (Vienna, Austria)
DirectPCR-tail lysis buffer	VWR Int. GmbH (Vienna, Austria)
Doxil (liposomal doxorubicin)	Ortho Biotech (Horsham, USA)
DreamTaq Green DNA Polymerase	Life Technologies (Darmstadt, Germany)
Dulbecco's modified Eagle's medium (DMEM)	Gibco (Karlsruhe, Germany)
Dulbecco's phosphate buffered saline (PBS)	Sigma-Aldrich (Schnelldorf, Germany)
Eosin	Roth (Karlsruhe, Germany)
Epon 812	Roth (Karlsruhe, Germany)
Ethylene glycol tetraacetic acid (EGTA)	Roth (Karlsruhe, Germany)
Ethylenediaminetetraacetic acid (EDTA)	AppliChem (Darmstadt, Germany)
Eukitt	VWR (Darmstadt, Germany)
Fetal calf serum (FCS)	Perbio (Bonn, Germany)
Fibrinogen	Sigma-Aldrich (Schnelldorf, Germany)
Fluoroshield containing DAPI	Sigma-Aldrich (Schnelldorf, Germany)
Freund's Adjuvant, complete	Sigma-Aldrich (Schnelldorf, Germany)
Freund's Adjuvant, incomplete	Sigma-Aldrich (Schnelldorf, Germany)
Fura-2-acetoxymethyl ester (AM)	ThermoFisher Scientific (Waltham, USA)
GeneRuler DNA Ladder Mix	Life Technologies (Darmstadt, Germany)
Glucose	Roth (Karlsruhe, Germany)
Glucose oxidase	Sigma-Aldrich (Schnelldorf, Germany)
Glutaraldehyde	EMS (Hatfield, USA)
Glycine	AppliChem (Darmstadt, Germany)
Glyoxal solution stock	Sigma-Aldrich (Schnelldorf, Germany)
Hank's balanced salt solution (HBSS)	GE Healthcare (Chicago, USA)
Hematoxylin	Sigma-Aldrich (Steinheim, Germany)
High molecular weight heparin	Ratiopharm (Ulm, Germany)

Reagent	Company
Horm Collagen type I	Takeda (Linz, Austria)
hypoxanthine-aminopterin-thymidine (HAT) Supplement	ThermoFisher Scientific (Waltham, USA)
IGEPAL CA-630	Sigma-Aldrich (Schnelldorf, Germany)
IgG2A-Fc (control)	R&D Systems (Minneapolis, USA)
Imidazole	AppliChem (Darmstadt, Germany)
Indomethacin	Sigma-Aldrich (Schnelldorf, Germany)
Ionomycin	Merck Millipore (Darmstadt, Germany)
IP1 ELISA KIT	Cisbio (Codelet, France)
Iso-Ins(1,4,5)P3/PM (caged IP3)	Enzo Life Sciences (Lörrach, Germany)
Isopropanol	Roth (Karlsruhe, Germany)
Kernechtrot	Roth (Karlsruhe, Germany)
KH2PO4	Roth (Karlsruhe, Germany)
Lead citrate	EMS (Hatfield, USA)
LIVE/DEADTM fixable dye	ThermoFisher Scientific (Waltham, USA)
Membrane amersham hybond 0.45 µM polyvinylidene difluoride (PVDF)	VWR (Darmstadt, Germany)
Mercaptoethylamine	Sigma-Aldrich (Schnelldorf, Germany)
Midori GreenTM Advanced DNA stain	Nippon Genetics Europe (Düren, Germany)
N-2-Hydroxyethylpiperazine-N'-2-ethanesulfonic acid (HEPES)	Roth (Karlsruhe, Germany)
Na3VO4	Sigma-Aldrich (Schnelldorf, Germany)
NaBH4	ICN Biomedicals (Costa Mesa, USA)
Nickel sulfate	Merck Millipore (Darmstadt, Germany)
Ni-NTA agarose	Qiagen (Hilden, Germany)
Paraformaldehyde (PFA)	Roth (Karlsruhe, Germany)
Penicillin/Streptomycin	Gibco (Karlsruhe, Germany)

Reagent	Company
Pluronic F-127	ThermoFisher Scientific (Waltham, USA)
Polyethylene glycol (PEG) 1500	Sigma-Aldrich (Schnelldorf, Germany)
Powdered milk, blotting grade, fat free	Roth (Karlsruhe, Germany)
Propylenoxide	Merck Millipore (Darmstadt, Germany)
Prostacyclin (PGI2)	Sigma-Aldrich (Schnelldorf, Germany)
recombinant mouse Sema7A (rSema7A)	R&D Systems (Minneapolis, USA)
Rhodocytin	kindly provided by J. Eble (University of Münster, Germany)
Roswell Park Memorial Institute (RPMI) 1640 medium	Gibco (Karlsruhe, Germany)
Rotiphorese® Gel 30 acrylamide	Roth (Karlsruhe, Germany)
Sodium chloride	AppliChem (Darmstadt, Germany)
Sodium dodecyl sulphate (SDS)	Roth (Karlsruhe, Germany)
Tetramethylethylendiamine (TEMED)	Roth (Karlsruhe, Germany)
Thapsigargin (TG)	Life Technologies (Darmstadt, Germany)
Thrombin	Roche Diagnostics (Mannheim, Germany)
Tissue-Tek (O.C.T. compound)	Sakura (Alphen aan den Rijn, Netherlands)
Triton X-100	Sigma-Aldrich (Schnelldorf, Germany)
Tween 20®	Roth (Karlsruhe, Germany)
U46619	Alexis Biochemicals (San Diego, USA)
Uranyl acetate	EMS (Hatfield, USA)
Western Lightning Plus-ECL, enhanced chemiluminescence substrate	PerkinElmer (Waltham, USA)
Xylol	Roth (Karlsruhe, Germany)

All non-listed standard reagents were purchased from AppliChem (Darmstadt, Germany), Roth (Karlsruhe, Germany) or Sigma-Aldrich (Schnelldorf, Germany).

2.1.2 Cell lines

Cell line	Source
AT3	Kindly provided by Scott Abrams (Roswell Park Comprehensive Cancer Center, USA)
SP2/0 AG14 myeloma cells	DMSZ (Braunschweig, Germany)
TrampC1	Kindly provided by Erik Henke (University of Würzburg, Germany)

2.1.3 Antibodies

2.1.3.1 Purchased primary and secondary antibodies

Antibody (anti-)	Origin	Company
BIN2 (14245-1-AP)	rabbit	Proteintech (Manchester, UK)
BIN2 n-terminal domain (ab175482)	rabbit	Abcam (Cambridge, UK)
CD105 (clone MJ7/18)	rat	BioLegend (San Diego, USA)
CD115 (clone AFS98)	rat	ThermoFisher Scientific (Waltham, USA)
CD31 (#sc-28188)	rabbit	SantaCruz (Dallas, USA)
CD34 (# ab8158)	rat	Abcam (Cambridge, UK)
CD45 (clone 30-F11)	rat	BD Biosciences (Heidelberg, Germany)
Cleaved-Cas3 (#9668)	mouse	Cell Signaling Technology (Danvers, USA)
Collagen-I (#ab34710)	rabbit	Abcam (Cambridge, UK)
Collagen-IV (#2150-1470)	rabbit	Bio-Rad AbD Serotec (Puchheim, Germany)
GAPDH (G9545)	rabbit	Sigma-Aldrich (Schnelldorf, Germany)
hIL-4Rα (G077F6)	mouse	BioLegend (San Diego, USA)
IP3R (07-1210)	rabbit	Merck Millipore (Darmstadt, Germany)
LAT (#9166)	rabbit	Cell Signaling Technology (Danvers, USA)
Ly6G (clone 1A8)	rat	BD Biosciences (Heidelberg, Germany)
NG2 (#AB5320)	rabbit	Merck Millipore (Darmstadt, Germany)

Antibody (anti-)	Origin	Company
Phospho-histone-3 (PH3) (#06-570)	rabbit	Merck Millipore (Darmstadt, Germany)
phospho-LAT (Y132; ab4476)	rabbit	Abcam (Cambridge, UK)
phospho-PLCγ2 (Y759; #3874)	rabbit	Cell Signaling Technology (Danvers, USA)
phospho-Syk (Y525/526; #2711)	rabbit	Cell Signaling Technology (Danvers, USA)
PLCγ2 (Q-20)	rabbit	Santa Cruz (Heidelberg, Germany)
R300 (anti-GPIb)	rat	Emfret Analytics (Eibelstadt, Germany)
STIM1 (D88E10)	rabbit	Cell Signaling Technology (Danvers, USA)
Syk (D1I5Q)	rabbit	Cell Signaling Technology F(Danvers, USA)
Ter119 (#116202)	rat	BioLegend (San Diego, USA)
α-tubulin (B-5-1-2)	mouse	Sigma-Aldrich (Schnelldorf, Germany)
β1 integrin	hamster	BD Biosciences (Heidelberg, Germany)

2.1.3.2 In-house generated antibodies

Antibody	Clone	Isotype	Antigen	Described in
DOM1	89H11	IgG1	GPV	[179]
DOM2	89F12	IgG2a	GPV	[179]
JAQ1	98A3	IgG2a	GPVI	[75]
JON/A	4H5	IgG2b	αIIbβ3	[180]
JON6	14A3	IgG2b	αIIbβ3	unpublished
LEN1	12C6	IgG1	α2 integrin	[181]
p0p/B	57E12	IgG2b	GPIbα	[78]
p0p4	15E2	IgG2b	GPIb	[179]
p0p6	56F8	IgG1	GPIX	[179]
ULF3	96H10	IgG2b	CD9	unpublished
WUG1.9	5C8	IgG1	P-selectin	unpublished

2.1.3.3 Provided antibodies

Antibody	Provider
anti-GR-1 (clone RB6-8C5)	RB6-8C5 hybridoma182 kindly provided by Ulrich E. Schaible (Research Center Borstel, Germany)
anti-Laminin α4	kindly provided by Lydia Sorokin (University of Münster, Germany),

2.1.4 Buffers, Media and Solutions

All stock solutions and buffers were prepared in deionized water (MilliQ Water Purification System, Millipore, Schwalbach, Germany) if not stated differently and the pH was adjusted with HCL or NaOH.

ACK buffer

NH_4Cl	155 mM
$KHCO_3$	10 mM
Na_2EDTA	110 µM

Cacodylate buffer, pH 7.2 (TEM)

Sodium cacodylate	0.1 M

Carbonate buffer, pH 9.0 (ELISA)

$NaHCO_3$	50 mM

DAB development buffer

Phosphate buffer	0.1M (pH 7.4)
Nickel sulfate	0.05%
Glucose	0.2%
Ammonium chloride	0.25 mg/ml
DAB	0.5 mg/ml
Glucose oxidase	9.2 µg/ml

ELISA wash buffer

PBS	
NaCl	300 mM
Tween	0.05%

Freezing medium (TrampC1 and AT-3)

DMEM	40%
FCS	50%
DMSO	10%

Feeder cell medium

RPMI	
FCS	10%

Glyoxal fixation solution, pH 5,0

Ethanol	20%
Glyoxal solution stock	3%
Acetic acid	0.75%

Growth medium (TrampC1 and AT-3)

DMEM	89%
FCS	10%
Pen/Strep	1%

HAT medium (Fusion)

RPMI	
FCS	10%
HAT supplement (50x)	1x

***Immune fluorescence* (IF) blocking buffer**

PBS	
Tween-20	0.1%
BSA	3%
serum of the host of the 2. AB	3%

IF fixation buffer: *periodate-lysine- paraformaldehyd* **(PLP)**

Lysin	13.5 µg/ml
NaH_2PO_4	28 mM
Na_2HPO_4	9.5 mM
PFA	3%
NaIO	2.5 mg/ml

IF washing buffer

Tween-20	0.1%
in PBS	

Laemmli running buffer for SDS-PAGE

TRIS	0.25 M
Glycine	1.92 M
SDS	35 mM

Lysis buffer (2x for Tyrosine phosphorylation assay)

NaCl	300 mM
TRIS	20 mM
EGTA	2 mM
EDTA	2 mM
IGEPAL CA-630	2 %
Protease inhibitor cocktail	2 %
Na_3VO_4	0.01 %

Lysis buffer (1x for platelet lysates)

NaCl	150 mM
TRIS	15 mM
EDTA	1 mM
IGEPAL CA-630	1 %
Protease inhibitor cocktail	1 %
Na_3VO_4	0.005 %

Phosphate buffered saline (PBS), pH 7.14

NaCl	137 mM
KCl	2.7 mM
KH_2PO_4	1.5 mM
Na_2HPO_4 x 2 H_2O	8 mM

Photoswitching buffer, pH 7.4

PBS	
Mercaptoethylamine	100 mM

Pulldown buffer A, pH 7.6

HEPES	50 mM
NaCl	150 mM
Glycerol	5 %

Pulldown buffer B, pH 7.6

HEPES	50 mM
NaCl	150 mM
Glycerol	5 %
Imidazole	400 mM

***Red blood cell* (RBC) buffer, pH 7.4**

HEPES	10 mM
NaCl	140 mM
Glucose	5 mM

Separating gel buffer (Western Blot), pH 8.8

TRIS/HCl	1.5 M

***Sodium dodecyl sulfate* (SDS) sample buffer (4x)**

TRIS/HCl, pH 6.8	200 mM
Glycerol	40%
SDS	8%
Bromophenol blue (3',3",5',5"-	0.04%
β-mercaptoethanol (for reducing conditions)	20%

Stacking gel buffer (Western Blot), pH 6.8

TRIS/HCl	0.5 M

Stripping buffer ("mild"), pH 2.0

SDS	1%
Glycine	25 mM
in HCl/PBS	

TAE (gel electrophoresis) 50x, pH 8.0

TRIS	0.2 M
Acetic acid	5.7%
EDTA (0.5 M, pH 8.0)	10%

TBS-T (Wash buffer for Western Blot), pH 7.2

Tween 20	0.1%
in TBS	

Transfer buffer (semi-dry blot)

TRIS ultra	48 mM
Glycine	39 mM
Methanol	20%

***Tris-buffered saline* (TBS), pH 7.3**

NaCl	137 mM
TRIS/HCl	20 mM

Tyrode's buffer, pH 7.4

NaCl	137 mM
KCl	2.7 mM
$NaHCO_3$	12 mM
NaH_2PO_4	0.43 mM
$CaCl_2$	2 mM
$MgCl_2$	1 mM
HEPES	5 mM
BSA	0.35 %
Glucose	0.1 %

2.1.5 Mouse strains

C57BL/6J, NMRI ex-Breeder and rats were purchased from Charles River (Sulzfeld, Germany) or Janvier (Le Grenest-Saint-Isle, France). The genetically modified mice and knockout (KO) mice used for this work are listed below. All mice are on the genetic background of C57BL/6J and are used at an age of 8-15 weeks. All animal studies were approved by the District Government of Lower Franconia (Bezirksregierung Unterfranken, Würzburg, Germany).

Mouse strain	Publication	Comment
Gp6^{-/-}	[79]	generated by Markus Bender in our laboratory
Bin2^{f/lfl,CMV-Cre+/-}, referred to as Bin2^{-/-}	[183]	generated by David Stegner and Michael Popp in our laboratory
Bin2^{fl/fl,Pf4Cre+/-}	[183]	generated by David Stegner and Michael Popp in our laboratory
GPIbα-hIL-4r-tg	[184]	
vWF^{-/-}	[185]	

2.1.6 Software

Software	Company
Cell QuestTM	BD Biosciences, Heidelberg, Germany
FlowJo v7	TreeStar, Ashland, OR, USA
GraphPad Prism 6	GraphPad Software, San Diego, CA, USA
ImageJ	National Institutes of Health (NIH) (rsbweb.nih.gov/ij/)
rapidSTORM 3.3	kindly provided by M. Sauer [186]
WinLab	PerkinElmer, Waltham, USA

2.2 Methods

2.2.1 Production of monoclonal antibodies

2.2.1.1 Immunization of rats

Female WISTAR rats were immunized with 150 *microgram* (µg) BIN2 inclusion bodies (provided by Julia Preu in our laboratory) by subcutaneous injection under isoflurane anesthesia. For the first immunization, the protein was dissolved in complete Freund's adjuvant, followed by at least five further immunizations at an interval of 3-4 weeks, using the BIN2 inclusion bodies dissolved in incomplete adjuvant.

2.2.1.2 Preparation of feeder cells

NMRI ex-breeder mice were *intraperitoneally* (i.p.) injected with 1 ml of prewarmed sterile PBS. 10-16 *hours* (h) later, the mice were decapitated, the skin was removed, and the peritoneum was flushed with 12 ml ice cold feeder cell medium. This cell containing medium was diluted to 50 ml and 100 µl/well were seeded into 96-well plates. Plates were checked for contamination after two days.

2.2.1.3 Generation of hybridoma cells and antibody production

The spleen of the immunized rat was removed under sterile conditions and a single cell suspension was prepared using a 100 µm cell strainer. After two washing steps using feeder cell medium (900 rpm, 5 min), the spleen cell suspension was mixed with AG14 cells (mouse myeloma cells, 10^8 per fusion), washed twice and spun down (900 rpm 5 min) to get a mixed cell pellet. The supernatant was discarded, and the pellet was loosened. For the fusion, 1 ml of 37°C warm *polyethylene glycol* (PEG) 1500 was added dropwise over a time period of 2 min, followed by the addition of 10 ml feeder cell medium (37°C) within 10 min. The suspension was diluted to 50 ml using HAT medium, to ensure cell death of non-fused AG14 cells, which cannot survive since they do not express *hypoxanthine-guanine phosphoribosyl transferase* (HGPRT). 100 µl/well were seeded onto the feeder cells. The cells were grown at 37°C, 5% CO_2. Non-fused spleen cells die and only fused spleen/AG14 cells survive the next 7-10 days and form hybridoma clones. When the hybridoma clones were big enough, the supernatant was tested for the presence of antibodies against BIN2 (2.2.1.4). Positive clones were subcloned twice and expanded from 96 well platelet into tissue culture flasks (T175), using RPMI medium. 4 l of antibody containing hybridoma supernatant was collected and sterile filtered. The antibody was purified via affinity chromatography using an immobilized protein G

column. After elution, the antibody suspension was dialyzed against PBS *overnight* (o/N) at 4°C.

2.2.1.4 Screening of hybridoma clones by ELISA

96-well plates (MediSorp^{TM}; Nunc, Roskilde, Denmark) were coated with 5 µg per well recombinant BIN2 (provided by Julia Preu and Inga Scheller in our laboratory) diluted in carbonate buffer o/N at 4°C. Blocking was performed with 5% skim milk diluted in wash buffer for 1 h at 37°C. 50 µl hybridoma clone supernatant was incubated in the well for 2 h at *room temperature* (RT). After five washing steps, an HRP-coupled anti-rat IgG was added for 1 h at RT to detect bound BIN2 antibodies. After further extensive washing, 50 µl of TMB substrate was added to the wells. The blue color indicated the presence of an antibody in the hybridoma supernatant which can bind to the coated BIN2 protein.

2.2.2 Mouse genotyping

2.2.2.1 Lysis of mouse ear clips

To isolate the DNA from mouse ear biopsies, the samples were lysed using a tail lysis buffer for 2 h at 56°C followed by 30 min at 85°C. This suspension was directly used for *polymerase chain reaction* (PCR).

2.2.2.2 PCR

For genotyping, the lysed mouse ear biopsies were used for PCR with different primers and programs as indicated below.

Pipetting scheme used for all PCRs:

1 µl	genomic DNA
2.5 µl	DreamTaq Buffer (10x)
0.5 µl	$MgCl_2$ (25 mM)
1 µl	dNTPs (10 mM)
1 µl	fwd primer (100 pM)
1 µl	rev primer (100 pM)
0.25 µl	DreamTaq Green DNA Polymerase
to 25 µl	H_2O

Detection of the PF4-Cre transgene

<u>Primer:</u>

PF4-Cre_fwd: 5' CCC ATA CAG CAC ACC TTT G 3'
PF4-Cre_rev: 5' TGC ACA GTC AGC AGG TT 3'

<u>PCR program:</u>

95 °C	5:00 min	
95 °C	0:30 min	
58°C	0:30 min	35x
72°C	0:45 min	
72°C	5 min	
4°C	∞	

<u>Resulting band size:</u>

wt: no PCR product
PF4-cre[+]:   450 bp

Detection of the Bin2 floxed allele

<u>Primer:</u>

Bin2fl_fwd: 5' TGC AGT CAA AGG TGG GTG TAT TCG 3'
Bin2fl_rev: 5' GCA CAT CCC ATG GCT GTG TC 3'

<u>PCR program:</u>

95 °C	4:00 min	
95 °C	0:30 min	
58°C	0:30 min	35x
72°C	0:30 min	
72°C	5 min	
4°C	∞	

<u>Resulting band size:</u>

wt: 392 bp
floxed allele: 460 bp

Detection of the *CMV-Cre* allele

<u>Primer:</u>

Bin2KO_fwd: 5' GAG GGC ATC CAC CAT CTC AAT GC 3'
Bin2KO_rev: 5' GCA CAT CCC ATG GCT GTG TC 3'

<u>PCR program:</u>

95 °C	5:00 min	
95 °C	0:30 min	
62°C	0:30 min	35x
72°C	1:30 min	
72°C	5 min	
4°C	∞	

<u>Resulting band size:</u>

wt: 1085 bp
Bin2 KO   570 bp

Detection of the *vWF^-/-* allele

<u>Primer:</u>

vWF_fwd: 5' AGT GAG ACC TTT GGC TTT GC 3'
vWF_WT_rev: 5' CCC AAC TTT TGC CAA CAA ATA 3'
vWF_KO_rev: 5' CCT TCT ATC GCC TTC TTG ACG 3'

<u>PCR program:</u>

96 °C	5:00 min	
94 °C	0:45 min	
65°C	0:45 min	35x
72°C	1:00 min	
72°C	5 min	
4°C	∞	

<u>Resulting band size:</u>

wt: 965 bp
ko: 670 bp

2.2.2.3 Gel electrophoresis

Depending on the size of the PCR product, 1-2% of agarose was diluted in TAE buffer and heated up using a microwave until it was completely dissolved. When the solution was not evaporating anymore, 5 µl/100 ml Midori Green was added, and the solution was poured into a tray with a comb to polymerize. 20 µl of each PCR sample was loaded into the gel after it was positioned in an electrophoresis chamber containing TAE buffer. DNA was separated by size for 45 min at 140 – 160 V and the size was discriminated by comparing the bands to a 1 kb DNA ladder under UV light detection.

2.2.2.4 Genotyping using flow cytometry

Detection of the GPIbα-hIL-4r-tg on the platelet surface

Detection of hIL-4 receptor on the platelet surface was performed by flow cytometry as described in 2.2.4.3 with a specific antibody against the hIL-4 receptor.

Detection of the absence of GPVI on the platelet surface

The absence of GPVI on the platelet surface was detected by flow cytometry as described in 2.2.4.3 using a specific antibody against GPVI.

2.2.3 Biochemistry

2.2.3.1 Immunoblotting (Western Blotting)

Platelet lysates or pulldown samples were supplied with 4x SDS sample buffer and boiled for 5 min at 95°C before being loaded onto a 10 - 12% polyacrylamide gel immersed in Laemmli buffer to separate proteins according to their size. BlueStar Prestained or BlueStar Plus Prestained protein ladder was used for the determination of the respective protein sizes. Proteins were then transferred onto a *polyvinylidene difluoride* (PVDF) membrane for 1 h with 0.8 mA/cm^2 using a semi-dry transfer system. Non-specific antibody-binding was prevented by blocking membranes at RT using Blueblock, 5% BSA in TBS-T or 5% skim milk powder in TBS-T. The primary antibodies were diluted according to the manufacturer's instructions or to 5 µg/ml in the respective blocking solution and incubated with the membrane o/N at 4°C under gentle shaking. Following three washing steps with TBS-T for 10 min at RT, the membranes were incubated with HRP-labeled secondary antibodies for 1 h at RT. After three additional washing steps, proteins were visualized using ECL. Images were acquired at an Amersham Image 680 (GE Healthcare).

To re-probe the membranes, bound antibodies were removed using stripping buffer for 30 min at RT, followed by three washing steps with TBS-T for 10 min at RT. After blocking, the membranes were probed with new antibodies as described above.

2.2.3.2 Pulldown experiments using the BIN2-HIS protein

Platelet lysates (approx. $0.2x\ 10^9$ platelets) were mixed with 30 µg of BIN2-HIS (provided by Julia Preu and Inga Scheller) for 5 min at RT, followed by a protein purification step using Ni-NTA agarose. To this end, 40 µl of Ni-NTA Agarose was filled into a spin column and washed with Buffer A. The lysate was allowed to incubate on the beads for 10 min before it was slowly centrifuged through the column (500*g*). After two washing steps (1: 95% buffer A and 5% buffer B; 2: 88% buffer A and 12% buffer B), the bound protein was eluted using Buffer B. Each fraction was subsequently analyzed using SDS-PAGE and Western blot.

2.2.3.3 IP$_1$ ELISA

To determine IP$_1$ levels in platelets, a commercially available ELISA kit (Cisbio, France) was used. The platelets were purified from mouse blood as described in 2.2.4.2. However, the last washing step was performed with Tyrode's buffer without phosphate. After the last centrifugation step, the platelet count was adjusted to 700 000 plt/µl using Tyrode's buffer without phosphate, containing 2 mM Ca^{2+} and 50 mM Lithium chloride. After 5 min incubation with the second wave inhibitors indomethacin (10 micromolar (µM)), apyrase (2 U/ml) and EDTA (5 mM), the platelets were activated with the indicated agonist for 15 min, followed by lysis for 30 min at 37°C using the lysis reagent provided in the kit. The ELISA was performed as described in the manufacturer's manual.

2.2.4 *In vitro* analysis of platelet function

2.2.4.1 Determination of platelet count and size in whole blood

Platelet count in whole blood was measured using the ScilVet analyzer (scil animal care company GmbH, Viernheim, Germany) as described in [187]. In brief, one drop of blood was collected in EDTA-coated tubes and was inverted at least 10 times immediately before the measurement was performed.

2.2.4.2 Platelet purification from mouse blood and platelet lysis

To prepare washed platelets, 1 ml blood was taken from the retroorbital plexus of anesthetized mice, using heparinized capillaries. It was collected into reaction tubes containing 300 µl of a

heparin solution (20 U/ml in TBS). After a 6 min centrifugation step at 800 rpm (Eppendorf Centrifuge 5415C), the supernatant and the intermediate phase were transferred into a new tube containing 200 µl heparin. The centrifugation was repeated and the supernatant (referred to as *platelet rich plasma* (PRP)) was transferred into a new tube. To remove plasma components, platelets were pelleted by a centrifugation step (5 min, 2800 rpm) in the presence of apyrase (0.02 U/ml) and prostacyclin (PGI$_2$, 0.1 µg/ml) and the supernatant was dicarded. After two washing steps with 1 ml Tyrode's buffer without Ca^{2+} containing apyrase and PGI$_2$ (centrifugation: 5 min, 2800 rpm), the platelet count was measured using a Sysmex KX-21N Hematology Analyzer and the pellet was resuspended in Tyrode's buffer without Ca^{2+} at the desired final concentration for following experiments. Platelets were allowed to rest for 30 min at 37°C in the presence of apyrase prior to the respective experiment. For platelet lysis, the cells were resuspended in 1x lysis buffer after the second washing step in a concentration which is dependent on the following experiment.

2.2.4.3 Flow cytometric analysis of mouse platelets

To determine glycoprotein expression on the platelet surface, 50 µl of blood was taken from the retroorbital plexus of anesthetized mice using heparinized capillaries. It was collected in 1.5 ml reaction tubes containing 300 µl of heparin solution and filled up to 1 ml with Tyrode's buffer without Ca^{2+}. 50 µl were transferred to a FACS tube and incubated with saturating amounts of the respective fluorophore-conjugated antibodies for 7 min at 37°C, followed by 7 min at RT in the dark. The reaction was stopped by adding 500 µl of PBS and the samples were measured using a FACSCalibur (BD, Heidelberg, Germany) flow cytometer and the Cell Quest^{TM} software.

To analyze platelet activation responses, blood was taken as described above and filled up to 1 ml with Tyrode's buffer without Ca^{2+}. To remove the heparin, the blood was washed twice with 1 ml Tyrode's buffer without Ca^{2+} (centrifugation: 5 min, 2800 rpm) and finally resuspended in 750 µl Tyrode's buffer containing 2mM Ca^{2+}. 50 µl washed blood was added to a FACS tube containing the respective agonist for activation and 20 µl of a 1:1 mixture of the PE-labeled JON/A antibody (4H5-PE) against the activated form of αIIbβ3 and the FITC-labeled anti-P-selectin antibody (5C8-FITC) for 7 min at 37°C, followed by 7 min at RT in the dark. The reaction was stopped by adding 500 µl of PBS and the samples were measured as described above for platelet glycoprotein expression.

2.2.4.4 Aggregometry

PRP was prepared as described previously (2.2.4.2). 50 µl of PRP was diluted in 110 µl of Tyrode's buffer containing Ca^{2+} and treated with the indicated amount of rSema7a or buffer under stirring conditions. After 5 min, the indicated amount of ADP was added and the measurement continued for 6 min. Light transmission was recorded on a four-channel aggregometer (Fibrintimer; APACT, Hamburg, Germany) and is expressed in arbitrary units, with buffer representing 100% light transmission

2.2.4.5 Measurement of intracellular Ca^{2+} levels in platelets

Platelets were washed as described above and resuspended at a concentration of 200,000 plt/µl in Tyrode's buffer without Ca^{2+}. 100 µl platelet suspension was labeled with 5 µM Fura-2-AM for 20 min at 37°C in the presence of 0.2 µg/ml pluronic acid (F-127). After a washing step to remove the residual extracellular Fura-2-AM (2800 rpm, 2 min), the platelet pellet was resuspended in 500 µl HBSS supplemented with 1 mM $MgCl_2$. The fluorescent emission was measured at 509 nm with a PerkinElmer LS 55 fluorimeter (PerkinElmer, Waltham, USA) under stirring conditions for 50 s with an alternating excitation between 340 and 380 nm to determine the baseline. After adding the respective agonists, the emission was measured for another 250 s, followed by a calibration with 1% Triton X-100 and 0.5 M EGTA to determine total and zero emission values for the calculation of the absolute values. The measurements were performed in the presence of extracellular Ca^{2+} to measure Ca^{2+} influx and in the absence of Ca^{2+} to measure store release. The data was analyzed using the WinLab software.

For measurements with the UV-inducible caged IP_3, IP_3 was loaded to the platelets together with Fura-2-AM and the protocol was followed as described above. To induce IP_3 activity, UV light was applied to the sample for 1 s after the 50 s baseline measurement.

2.2.4.6 Tyrosine phosphorylation assay

Platelets were washed as described above except for the use of BSA- and Ca^{2+}-free Tyrode's buffer in the second washing step. Platelets were also resuspended therein to a final concentration of 700,000 platelets/µl. After incubation for 5 min at 37°C with EDTA (5 mM), apyrase (2 U/ml) and indomethacin (10 µM), 210 µl of the suspension was filled into a stirring cuvette. 50 µl of the sample was taken upon activation with the respective agonist at the indicated time points and lysed immediately using 50 µl 2x lysis buffer. Lysates were centrifuged at 14,000 rpm to remove cell debris and analyzed by immunoblotting (2.2.3.1). To

this end, phospho-specific antibodies and the respective antibody against the total protein were used for detection and visualized using HRP-labeled secondary antibodies.

2.2.4.7 Flow adhesion experiments of platelets on collagen

Platelet adhesion under flow was measured by perfusion of murine whole blood on collagen-coated cover slips (200 µg/ml fibrillar type I collagen o/N at 37°C) at 1000 s^{-1}. To this end, 700 µl blood was collected in 300 µl heparin and platelets were labelled with a DyLight 488-conjugated anti-GPIX Ig derivate (0.2 µg/ml) for 5 min on 37°C prior perfusion. Two parts of blood were diluted with one part Tyrode's buffer containing Ca^{2+} and filled into a 1 ml syringe. A pulse-free pump was connected to the syringe and perfused the blood over the collagen coated and BSA blocked (1% BSA/PBS for 1 h at RT) cover slips, which were previously placed in a transparent flow chamber with a slit depth of 50 µm. The 4 min run was monitored using a Leica DMI6000B inverted microscope (63x/1.3 glycerol HCX PL APO objective) equipped with a Leica DFC 360 FX camera. To remove the residual non-bound blood components, Tyrode's buffer with Ca^{2+} was perfused under the same flow conditions and perfusion time as the whole blood. For quantification, at least 8 bright field and fluorescent images were acquired and analyzed using ImageJ. Results were depicted as mean percentage of total area covered by platelets and mean integrated fluorescence intensity.

For reconstituted collagen flow chamber experiments, 700 µl of washed platelets (700,000 /µl) (see 2.2.4.2) and 500 µl washed red blood cells ($8x10^6$/µl) were mixed and supplemented with 250 µg/ml fibrinogen and 2 mM Ca^{2+} (f.c.). The flow chamber assay was performed as described above. Prior to use, the red blood cells had been washed at least five times with RBC buffer at 900 rpm for 5 min.

To block GPIb, 100 µg/mouse p0p/B Fab was injected *intravenously* (i.v.) into anesthetized mice 20 minutes before blood withdrawal. To study the effect of Sema7A on thrombus formation under flow, 1 µg/ml rSema7A, SL4cd or IgG_{2A} Fc (negative control) were incubated *in vitro* during the platelet labeling step for 5 minutes on 37°C prior perfusion.

2.2.5 Transmission electron microscopy (TEM)

PRP was supplemented with 5% glutaraldehyde (in PBS) in a 1:2 ratio and incubated for 10 min at 37°C, followed by 1 h at RT. After centrifugation (2,800 rpm, 5 min) and three washing steps in cacodylate buffer, the samples were incubated with 1% OsO_4, diluted in cacodylate buffer. After two washing steps with cacodylate buffer and H_2O, 2% uranyl acetate (in H_2O) was incubated for 1 h at 4°C and a graded ethanol series (3x 70% for 5 min, 3x 95%

for 15 min, 3x 100% for 15 min) was performed for dehydration. Samples were then incubated twice with propylenoxide for 10 minutes, one time for 1 h with a 1:1 mixture of propylenoxide and epon and finally with epon alone o/N at RT. Epon was hardened for 48 h at 60°C and cut into 50 nm slices. These sections were stained using 2 % uranyl acetate (in ethanol) and lead citrate (in H_2O) and examined at 80 kV using an EM900 (Zeiss, Jena, Germany).

2.2.6 Direct stochastic optical reconstruction microscopy (dSTORM)

This method was performed in close collaboration with Charly Kusch, Mara Meub and Prof. Dr. Markus Sauer.

Resting platelets were allowed to settle on glycine coated (200 µl 2M glycine solution, 10 min at RT) chamber slides (8 Chambered Cover Glass, #1.5, Cellvis). To visualize spread platelets, the cells were stimulated with thrombin (0.01U/ml) and allowed to spread on similar chamber slides, which were previously coated with 100 µg fibrinogen (o/N 4°C) and blocked with 1% BSA/PBS for 1h at RT. Both samples were fixed with 3% glyoxal solution[188] for 20 min, quenched with 0.1% $NaBH_4$ for 7 min, permeabilized with 0.25% Triton-X 100 for 15 min and washed 3 times with PBS for 10 min. After blocking in a 5% BSA solution in PBS for 1h, the samples were stained with Alexa Fluor 647 coupled anti-Bin2-antibody (12E1) before being washed another 3 times with PBS for 5 min.

One color dSTORM samples were imaged on a widefield setup, based on an inverted microscope (Olympus IX-71) equipped with an oil immersion objective (60×, NA 1.45; Olympus). The dye was excited with a diode laser at 641 nm at an irradiation intensity of ~ 5 kW/cm2 (Cube 640-100C, Coherent). Emission light was separated from the excitation light using a dichroic mirror (635rpc, Chroma) spectrally filtered by a bandpass filter (Em01-R442/514/647-25; Semrock) and projected onto an electron multiplying CCD camera chip (Ixon DU 897; Andor). Imaging was performed with an exposure time of 20 ms for at least 15000 frames in photoswitching buffer containing 100 mM ß-mercaptoethylamin, pH 7.4. Spread platelets were imaged by *total internal reflection fluorescence* (TIRF) illumination; resting platelets were measured by *epifluorescence* (EPI). dSTORM images were reconstructed using the open source software rapidSTORM 3.3.

2.2.7 Tumor cell lines and implantation

TrampC1 (prostate cancer) and AT-3 (breast cancer) cell lines were cultured at 37°C, 5% CO_2 in DMEM supplemented with 10% FCS and 1% Penicillin/Streptomycin. For the heterotopic prostate cancer model, 5×10^6 TrampC1 cells in 50 µl of PBS were injected subcutaneously

into the back of 8 week old male C57BL/6J mice. 0.5×10^6 AT-3 cells in 50 µl of PBS were injected dorsally of the inguinal mammary gland into the mammary fat pad of 8 week old female virgin C57BL/6J mice.

2.2.8 Treatment of tumor bearing mice

2.2.8.1 Platelet depletion, blockade of platelet glycoproteins and neutrophil depletion

Platelets were depleted by i.v. injection of 50 µg anti-GPIb IgG R300 (Emfret, Germany) per mouse. To block GPVI, GPIb and $\alpha IIb\beta 3$, 100 µg/mouse JAQ1 F(ab')$_2$, p0p/B Fab or JON/A F(ab')$_2$ were injected i.v., respectively. Control animals were injected with 100 µg non-immune rat IgG F(ab')$_2$. Neutrophils were depleted by i.p. injection of 500 µg anti-Ly6G antibody [RB6-8C5][182].

2.2.8.2 Treatment with chemotherapeutic agents

Mice were injected i.v. with 5 µg/g body weight of doxil or 20 µg/g paclitaxel immediately after platelet depletion or GPVI-blockade. Paclitaxel was diluted in sterile saline from a 2 mg/ml stock solution in EtOH/cremophor EL (1:1). Control substance for doxil was saline, while saline/EtOH/cremophor EL was used for paclitaxel.

2.2.9 Analysis of tumor tissue

2.2.9.1 Tumor volume

Tumor volumes were measured using a Vernier caliper and calculated using the following equation: Volume = $\pi/6 \times l \times w^2$. In treatment studies, where tumor growth was a critical outcome, assessment of tumor volume was performed blinded by a second experimenter.

2.2.9.2 Hemoglobin measurement in tumor tissue and organs

Organs and tumors of sacrificed mice were excised and homogenized in PBS (9x of the respective weight) and centrifuged (14000 rpm, 10 min). Hemoglobin content of the supernatant was measured as absorbance at 405 nm in the microplate reader Multiscan Ex device (Thermo Electron Corporation, Germany).

2.2.9.3 Bio-distribution of doxorubicin

For biodistribution studies, a bolus of doxil (100 µg free doxorubicin) in 0.9% NaCl was injected i.p. in doxorubicin-naïve wildtype mice bearing established tumors (average size > 50 mm^3).

Mice were sacrificed 2 h or 24 h post-injection, when doxorubicin was expected to be cleared from the blood stream.[189] Tissue samples were flash frozen and stored at -80°C until extraction. The protocol for doxorubicin extraction was described previously[190] and only slightly adapted to account for the respective experimental settings. Briefly, tissue samples were homogenized by sonification in 9 parts (v/w) H_2O. 200 µl homogenate were mixed with 50 µl 10% Triton X-100 (v/v) and 750 µl 0.75 HCl in 2-propanol. The mixture was vortexed briefly and doxorubicin was extracted for 12 h at -20°C. Samples were vortexed and cleared by centrifugation (20 min, 4°C, 20,000g). Fluorescence signal was read (Ex.: 470 nm, Em.: 590 nm) in a microplate reader and corrected against extracts from tissue samples of non-treated animals. A standard curve was established by adding defined amounts of doxorubicin/doxil to homogenates of non-treated tissue samples prior to extraction.

2.2.9.4 Bio-distribution of ³H-paclitaxel

1 µCi of tritium-labeled paclitaxel was injected into wildtype mice bearing established tumors (average size > 50 mm³). Animals were euthanized 2 h or 24 h later and major organs (heart, liver, spleen, kidney, intestine and lung) were harvested. Specific amounts of each organ (up to 200 mg) were dissolved in 1 mL Biosol at 37 °C. To decolorize, 80 µL 30% H_2O_2 were added to 400 µL aliquots of the dissolved tissue and the samples were again incubated at 37°C for 25 min. After addition of 4 mL BioScint Cocktail, samples were read on a LS 6000 β-scintillation counter (Beckman, Fullerton, CA).

2.2.9.5 Analysis of immune cells in tumor, blood and bone marrow by flow cytometry

For the isolation of leukocytes from whole blood, red blood cells were lysed using ACK lysis buffer. Bone marrow was obtained by flushing femurs of mice with PBS supplemented with 1% FCS. For the analysis of tumor-infiltrating leukocytes, tumors were carefully removed, minced and incubated for 1 h at 37°C with collagenase I. Cells were stained for 30 min on ice using a combination of specific antibodies (CD45, clone 30-F11; Ly6G, clone 1A8; CD115, clone AFS98). To exclude dead cells from the analysis, a LIVE/DEAD™ fixable dye dilution 1:1000 was added to the antibody cocktail. Probes were measured using a FACS Celesta (BD Biosciences) and analyzed with FlowJo.

2.2.10 Histology of tumor sections

2.2.10.1 *Hematoxylin and eosin* (HE) staining

Tumors were harvested, fixed in 4% paraformaldehyde o/N and embedded in paraffin. After cutting and mounting the sections onto glass slides, they were dried overnight, deparaffinized using xylol (2x 5 min) and rehydrated using an ethanol series (100%, 96%, 90%, 80% and 70% for 2 min) followed by a 2 min wash with H_2O. Staining was performed with hematoxylin (15 sec), followed by a washing step for approximately 10 min with tap water and by staining with 0.05% eosin. After one washing step with H_2O, dehydration was carried out, using the inverted alcohol series (see above) followed by incubation in xylol (2x 5 min). The slides were mounted using Eukitt. For quantification of necrotic areas and bleeding, whole tissue sections were imaged on a Keyence BD microscope with an automated stage. The whole virtual slide was used for quantification using the ImageJ software package.

2.2.10.2 Immunohistochemistry

Tumors were harvested, fixed in 4% paraformaldehyde o/N and embedded in paraffin. After sectioning onto glass slides, the sections were deparaffinized and rehydrated (see 2.2.10.1). To block the endogenous peroxidase, the slides were incubated in 3% H_2O_2 for 10 min at RT shaking in the dark. After two washing steps in H_2O (2 min), a heat-induced antigen retrieval was performed in 10 mM citrate buffer (pH 6.0). Therefore, the slides were cooked for 10 s in the microwave, followed by a 50 s break for 7 times before they were cooled down for 30 min to reach RT. The citrate buffer was replaced by H_2O and the slides were washed in PBS (3x 5 min). After blocking with 5%BSA/PBS for 2 h at RT, sections were incubated o/N at 4°C with an anti-CD31 antibody. On the following day, after extensive washing, the slides were incubated with the HRP labelled secondary antibody (rabbit) for 1 h at RT in the dark. After washing in PBS (3x 5 min), the slides were incubated with Avidin Biotin-Complex for 30 min in the dark. To prepare the slides for the development, they were washed two times with PBS (5 min) and two times with 0.1 M phosphate buffer (pH 7.4). The developing reaction was performed using DAB development buffer in the dark for 10 – 30 min and stopped with PBS. After washing with PBS (3x 5 min), a kernechtrot staining (0.1%) was performed for 3 min, followed by a dehydration step using an alcohol series (see above) and xylol. The slides were mounted using DePeX.

2.2.10.3 Immunofluorescent staining

Tumors were harvested, embedded into Tissue Tek and immediately frozen on dry ice. Tumors were cut into 10 µm sections using a cryostat (CM1900, Leica) and sections were immobilized on glass slides. Fixation was performed using 1% PLP buffer for 30 min at RT. After washing three times with IF washing buffer, sections were blocked for 1 h using blocking buffer. Primary or fluorescently-labeled antibodies were diluted in blocking buffer and incubated on the slides for 1 h at RT or overnight at 4°C in the dark, followed by washing (3x for 5 min). In case a secondary antibody was necessary, it was applied in washing buffer for 1 h at RT in the dark. After washing once in wash buffer and once in PBS, the slides were mounted using Fluoroshield containing DAPI.

2.2.11 Statistical Analysis

Data is presented as Mean ± SD if not stated otherwise (bar graphs). Growth curves are represented as Mean ± SEM. Data was analyzed by Mann-Whitney-test, Kruskal-Wallis with Dunn's multiple comparisons test or two-way ANOVA with Tukey's multiple comparison test using Graph-Pad Prism 6 Software. Asterisks indicate significances (* $p \leq 0.05$, ** $p \leq 0.01$, *** $p \leq 0.001$).

3 Results

3.1 Platelet GPVI is a major regulator of tumor vascular integrity

Platelets have been previously shown to maintain vascular integrity in the primary tumor in mice.[132] However, the exact mechanism how they exert this function has remained elusive. GPVI is known to prevent vascular leakage in several models of inflammatory bleeding, e.g. in the skin.[86] Since the tumor vascularization is characterized by signs of inflammation, we hypothesized that GPVI might be a promising candidate involved in the prevention of vascular leakage in the TME. Therefore, the effect of functional blockade of GPVI on the tumor vasculature was studied. The importance of the first step in classical thrombus formation, mediated by the GPIb-vWF-dependent platelet tethering, in the process of maintaining tumor vascular integrity was investigate by blocking GPIb. This blockade has been previously shown to ameliorate thrombo-inflammation in acute ischemic stroke without causing cerebral hemorrhage.[191] The effect of interfering with the last step in classical thrombus formation - firm adhesion and thrombus growth - was investigated by blocking integrin $\alpha IIb\beta 3$.

Two different tumor models were used in this study: the heterotopic TrampC1 as well as the orthotopic AT-3 tumor. The TrampC1 cell line was derived from a heterogeneous primary tumor (32 weeks) in the prostate of a C57BL/6 mouse, which was hemizygous for the TRAMP transgene and therefore developed progressive forms of prostate cancer.[192] In this heterotopic prostate cancer model, TrampC1 cells were injected subcutaneously at the back of male animals. The AT-3 cell line was derived from primary mammary tumor cells of a transgenic MTAG mouse, which expressed the polyoma virus middle T antigen under control of the MMTV-LTR promoter.[193] To obtain an orthotopic breast cancer model, the cells were implanted into the mammary fat pad of female animals.

3.1.1 The effect of functional inhibition of platelet glycoproteins on tumor vascular integrity

To study the effect of pharmacological inhibition of GPVI, GPIb and $\alpha IIb\beta 3$ on intratumoral vascular integrity, *WT* C57BL/6 mice were implanted with TrampC1 or AT-3 cells. When tumors reached an average size of 300 mm^3, the mice were divided into five groups. In group (1) platelet function remained unaffected upon treatment with a corresponding IgG F(ab')$_2$ control. In group (2) thrombocytopenia was induced, using the R300 platelet depletion antibody. In group (3), (4) and (5) GPVI (using JAQ1 F(ab')$_2$), GPIb (using p0p/B Fab) and $\alpha IIb\beta 3$ (using JON/A F(ab')$_2$) were functionally inhibited, respectively. In line with previous reports,[132] we

observed a drastic increase in hemoglobin concentration in the tumor upon platelet depletion within 18 h post-treatment, reflecting intratumoral hemorrhage (Figure 3-1). Remarkably, a comparable effect was observed upon administration of JAQ1 F(ab')$_2$ with the relative hemoglobin concentration in tumors being 2.5 – 4.2 times higher as compared to the IgG F(ab')$_2$-treated mice in both tested cancer models. In contrast, functional inhibition of GPIb or αIIbβ3 had no influence on hemoglobin concentrations, neither in the TampC1 nor in the AT-3 model. This demonstrates that GPVI rather than GPIb or αIIbβ3 is involved in the maintenance of tumor vascular integrity.
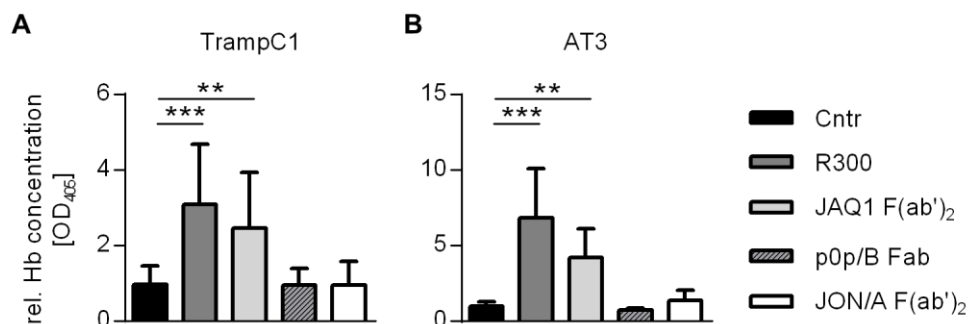
Figure 3-1: Increased bleeding in TrampC1 and AT-3 primary tumors upon GPVI-blockade. Effect of platelet depletion (R300) and blockade of GPVI (JAQ1 F(ab')$_2$), GPIb (p0p/B Fab) and αIIbβ3 (JON/A F(ab')$_2$) (100 µg/mouse each) on TrampC1 (A) and AT-3 (B) primary tumors grown in C57BL/6 animals 18 h after antibody treatment. The relative hemoglobin concentration (control is set to 1) was measured at OD405 nm and is depicted as mean ± SD, n=8.

3.1.2 Potential off-target effects of JAQ1 F(ab')$_2$ in tumor-bearing mice

Since JAQ1 F(ab')$_2$ treatment has not been evaluated in tumor-bearing mice before, its effects on platelet count, blocking efficacy at lower concentrations, as well as potential off-target effects were examined in more detail. To this end, platelet counts after R300 and JAQ1 F(ab')$_2$ treatment were investigated using flow cytometry and an automated cell counter (ScilVet). Treatment with R300 led to an almost complete removal of platelets from the circulation within minutes, while injection of JAQ1 F(ab')$_2$ had no effect on platelet count compared to the IgG control in naïve (Figure 3-2 A) and tumor-bearing mice (Figure 3-2 B). Of note, the platelet count in AT-3 tumor bearing mice treated with IgG F(ab')$_2$ or JAQ1 F(ab')$_2$ decreased throughout the time course of the experiment. This is in line with previous reports showing a progressive decrease in platelet counts during tumor progression.[194]
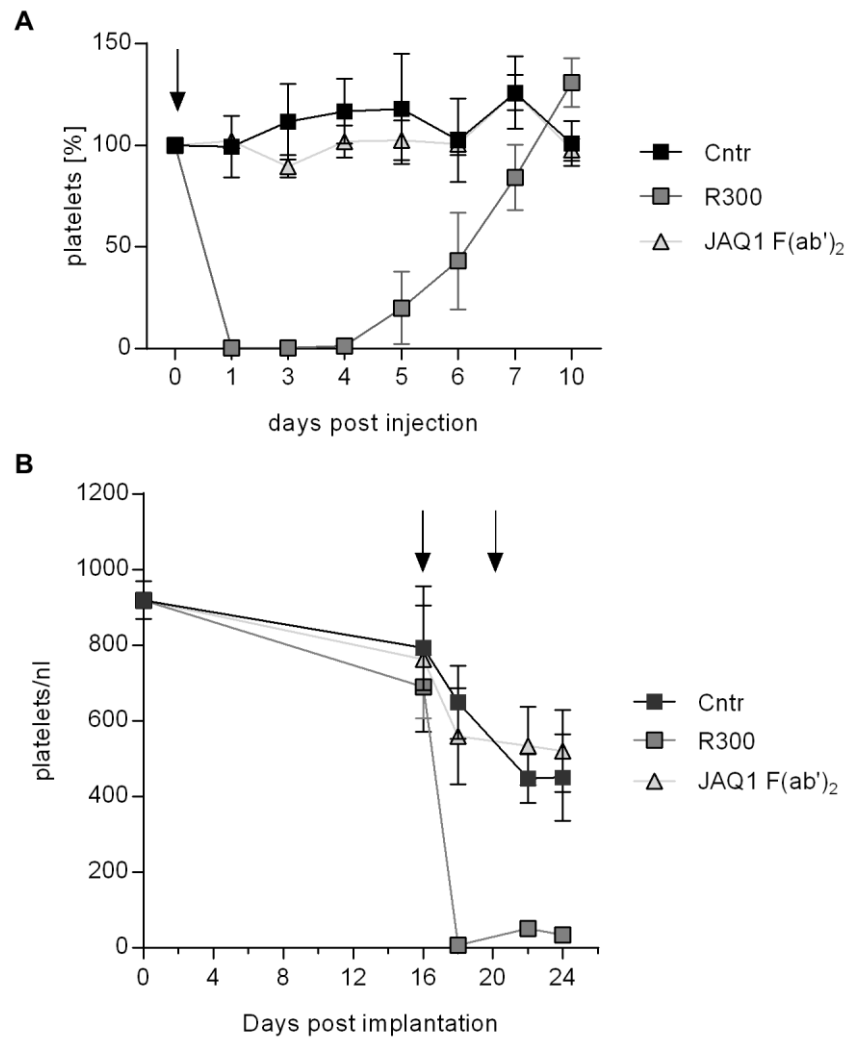
Figure 3-2: Effect of antibody-mediated blockade of GPVI on platelet count in naïve and AT-3 tumor-bearing mice (A) *WT* animals were treated with IgG control, R300 or JAQ1 F(ab')$_2$ (arrow) and circulating platelet count was measured using flow cytometry. The data is presented as % platelets of the respective genotype relative to day 0 and depicted as mean ± SD. n=4. (B) AT-3 tumor-bearing *WT* mice were treated with IgG control, R300 or JAQ1 F(ab')$_2$ from day 16 on after tumor implantation every 4 days (indicated by arrows). Platelet count over the time of the experiment was measured using an automated cell analyzer (SciIVet) and presented as mean ± SD. n=6. (Volz *et al. Blood*, 2019)[195]

So far, a rather high amount of 100 µg/mouse JAQ1 F(ab')$_2$ was used to ensure optimal blockade over the entire time course of the experiments. Nevertheless, the antibody fragment still mediated full blockade at doses of 0.1 – 0.5 µg/g body weight at day 1 post treatment (Figure 3-3 A). On day 2, a rapid decline of receptor blockade was observed in low-dose (0.1 µg/g and 0.5 µg/g) treated animals, whereas the inhibitory effect of 100 µg started to decline on day 3 and partially persisted until day 7. In tumor-bearing mice, the effect of 100 µg of JAQ1 F(ab')$_2$ started to decline on day 4 post injection (Figure 3-3 B).
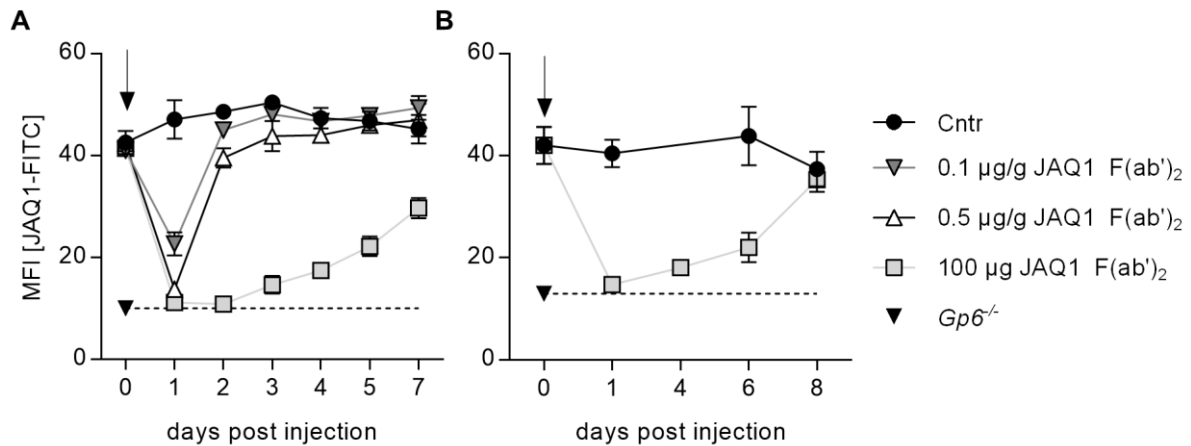
Figure 3-3: Titration and half-life of JAQ1 F(ab')$_2$. Flow cytometric measurement of JAQ1-FITC binding to circulating platelets in naïve (A) and AT-3 (B) tumor-bearing C57BL/6 animals treated with different doses of JAQ1 F(ab')$_2$ (arrow), n=4.

Potential off-target effects of JAQ1 F(ab')$_2$ were investigated in tumor-bearing *Gp6$^{-/-}$* mice. No inhibition of tumor growth or increase in hemoglobin concentrations and hemorrhage were detected, thereby confirming the specific inhibition of GPVI by JAQ1 F(ab')$_2$ in this experimental setting (Figure 3-4).

Taken together, JAQ1 F(ab')$_2$ treatment did not alter the platelet count and depicted no off-target effects in tumor-bearing mice, confirming that the functional blockade of the collagen binding site of GPVI is causative for the observed dramatic effects on tumor vascular integrity.
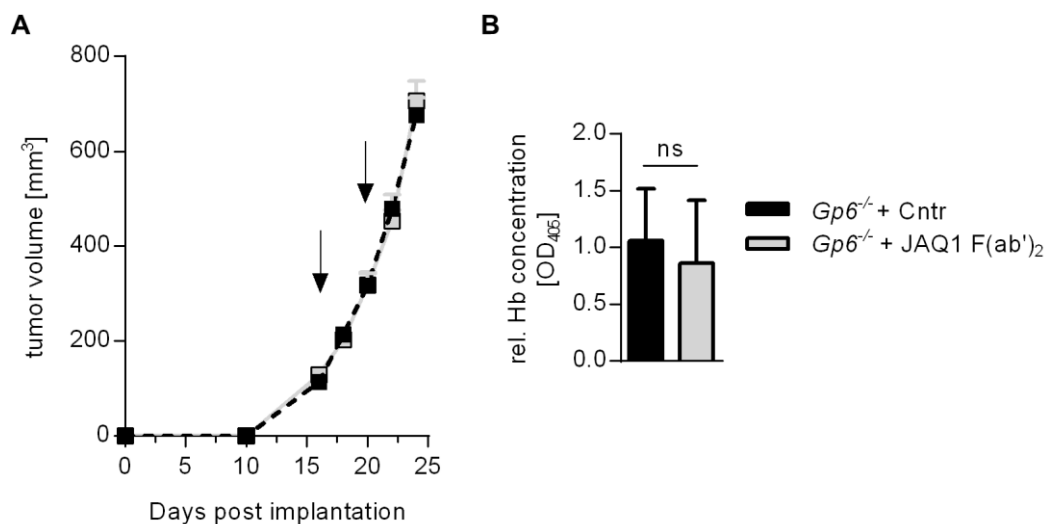
Figure 3-4: Effect of JAQ1 F(ab')$_2$ on tumor growth and intratumoral bleeding in *Gp6$^{-/-}$* mice. AT-3 breast cancer tumors were grown in GPVI-deficient animals and treated every 4 days with IgG F(ab')$_2$ or JAQ1 F(ab')$_2$ (arrow). Tumor growth was measured every second day for 24 days post implantation. n=8; mean ± SEM (B) 24 days post-implantation, the relative hemoglobin concentration relative to the Cntr was measured. n=8; mean ± SD. (Volz *et al. Blood*, 2019)[195]

3.1.3 Functional inhibition of GPVI induces profound hemorrhage specifically at the tumor site

To further clarify how GPVI exerts its role on tumor vascular integrity, the tumors were investigated in further detail. Confirming the macroscopically visible hemorrhage and the hemoglobin measurements in tumors isolated from mice 18 h after blockade of GPVI or depletion of platelets, histopathological analysis revealed extravasated red blood cells. In contrast, tumors from control IgG F(ab')$_2$ treated mice did not show these signs of bleeding (Figure 3-5).
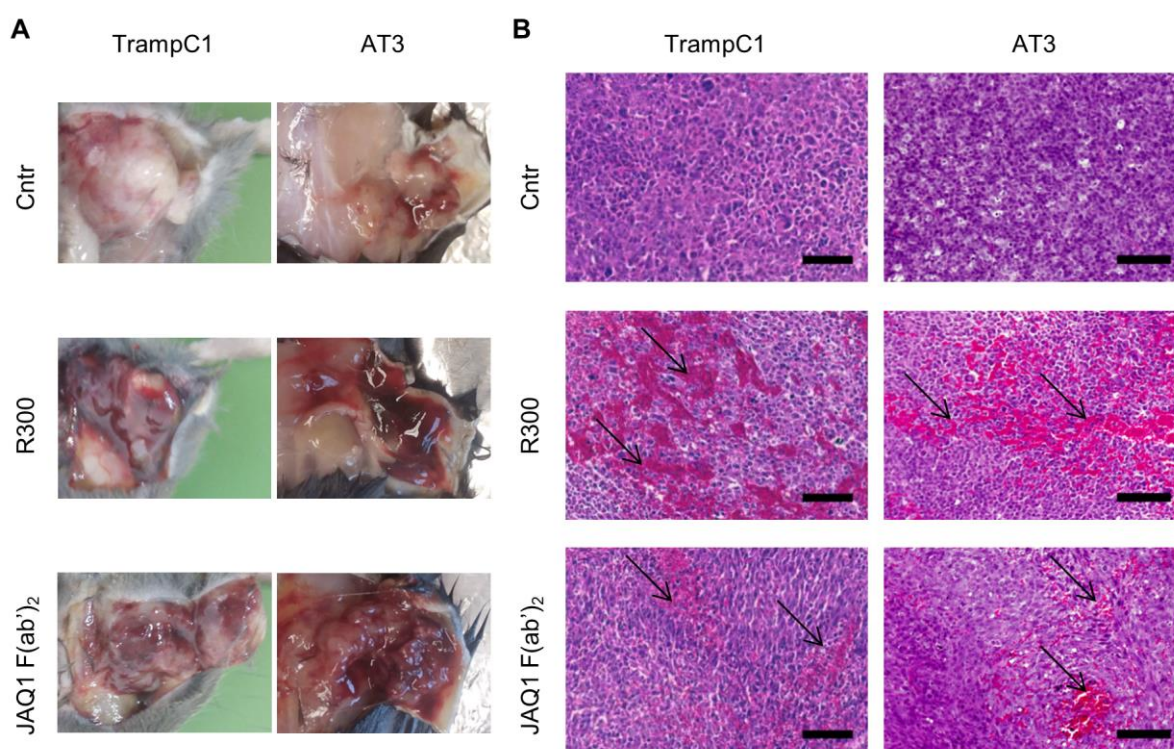
Figure 3-5: Increased bleeding in TrampC1 and AT-3 primary tumors upon GPVI-blockade. (A) Representative macroscopic pictures and (B) H&E staining of TrampC1 and AT-3 tumor sections 18 h post IgG F(ab')$_2$ (Cntr), R300 or JAQ1 F(ab')$_2$ treatment. Arrows indicate accumulation of RBCs in the tumor tissues. Scale bar: 100 µM. (Volz *et al. Blood*, 2019)[195]

To investigate the effect of GPVI blockade on intact non-tumor vasculature, different organs were examined. Interestingly, no hemorrhage was observed in H&E stained sections of remote organs, such as spleen, liver, intestine, kidney or lung of TrampC1 tumor-bearing animals treated with IgG F(ab')$_2$ control, R300 or JAQ1 F(ab')$_2$ (Figure 3-6 B). In line with this, no differences in the relative hemoglobin content of the tested organs could be detected among the different treatments (Figure 3-6 A). This emphasizes the unique effect of GPVI blockade on the tumor vasculature.
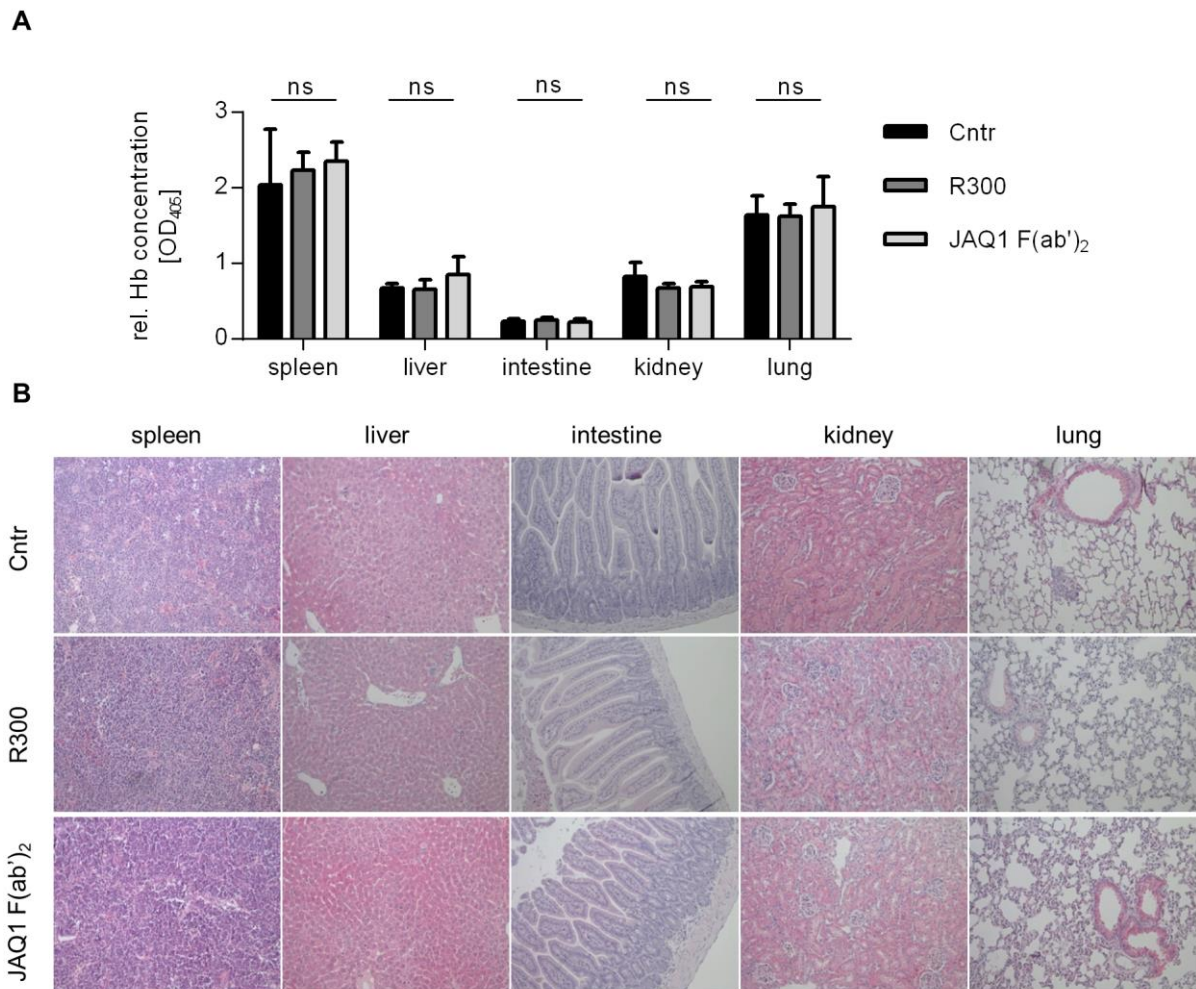
Figure 3-6: Antibody-mediated blockade of GPVI induces no hemorrhage in other organs. (A) TrampC1 tumor-bearing *WT* mice were treated with IgG control (Cntr), R300 or JAQ1 F(ab')$_2$ and 18 h after antibody treatment, spleen, liver, intestine, kidney and lung were harvested and relative hemoglobin concentrations were determined (B). Histopathological analysis of organs of mice treated with IgG control, R300 or JAQ1 F(ab')$_2$ antibody. Tissues were fixed and stained with hematoxylin and eosin. mean ± SD n=4; two-way ANOVA with Tukey's multiple comparison test. (Volz *et al. Blood*, 2019)[195]

To characterize the damage of tumor vascular integrity induced by platelet depletion or by GPVI inhibition, co-immunofluorescent staining for the endothelial marker CD31 and the basement membrane components of tumor vessels, laminin α4 and collagen IV was performed. Interestingly, the lumen size of the vessels was dramatically decreased in animals treated with R300 or JAQ1 F(ab')$_2$ compared to controls, indicating vascular collapse (Figure 3-7 A,B). However, the staining pattern of basement membrane components in non-collapsed vessels was comparable between all groups (Figure 3-7 C).
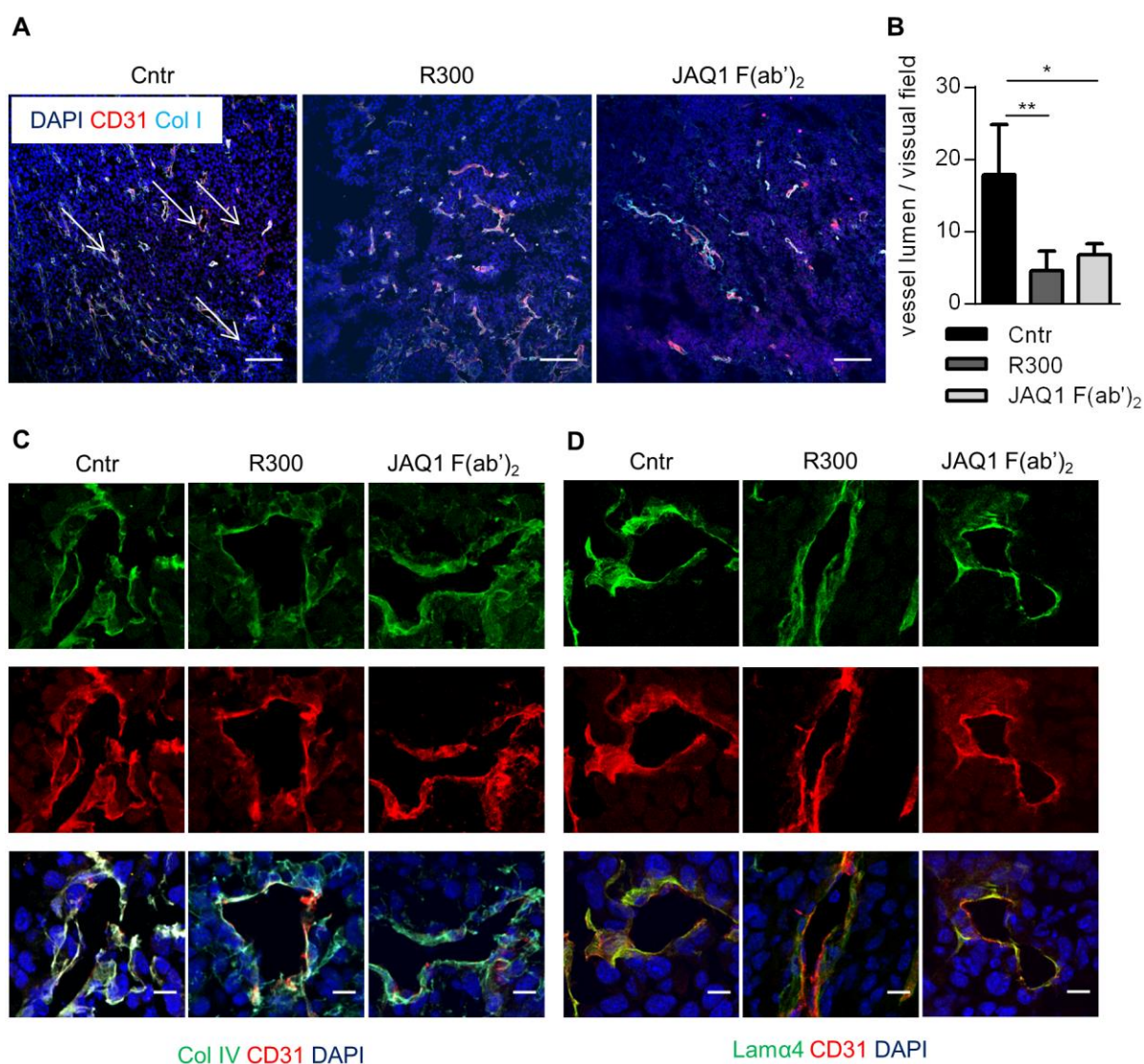
Figure 3-7: Tumor vasculature in mice after platelet depletion or GPVI blockade. (A) AT-3 primary tumors 18 h after antibody treatment stained for CD31 (red), *collagen I* (Col I; cyan) and DAPI (blue); Scale bar: 100 µm. Arrows indicate vessels with lumen. (B) For quantification of the number of vessels with lumen, the average of 10 visual fields per mouse was calculated, n>4; mean ± SD (C) AT-3 primary tumors 18 h after antibody treatment stained for CD31 (red), Col IV (green) and DAPI (blue). Scale bar: 10 µm. (D) AT-3 primary tumors 18 h after antibody treatment stained for CD31 (red), *laminin α4* (Lamα4; green) and DAPI (blue). Scale bar: 10 µm. (Volz *et al. Blood*, 2019)[195]

To investigate whether the increased hemorrhage induced by GPVI inhibition affects tumor cell viability, immunofluorescence staining was performed 18 h post JAQ1 F(ab')$_2$ treatment. In both cancer models, the number of apoptotic cells was increased upon GPVI inhibition compared to the control, as assessed by detection of *cleaved caspase 3* (Cas3). Furthermore, the amount of *phospho-histone H3* (PH3)-positive cells was significantly decreased in JAQ1 F(ab')$_2$-treated mice, demonstrating a decrease in cell proliferation (Figure 3-8). In line with previous results, R300-treated tumors depicted a comparable increase in apoptotic cells and decrease in proliferation within the tumor.
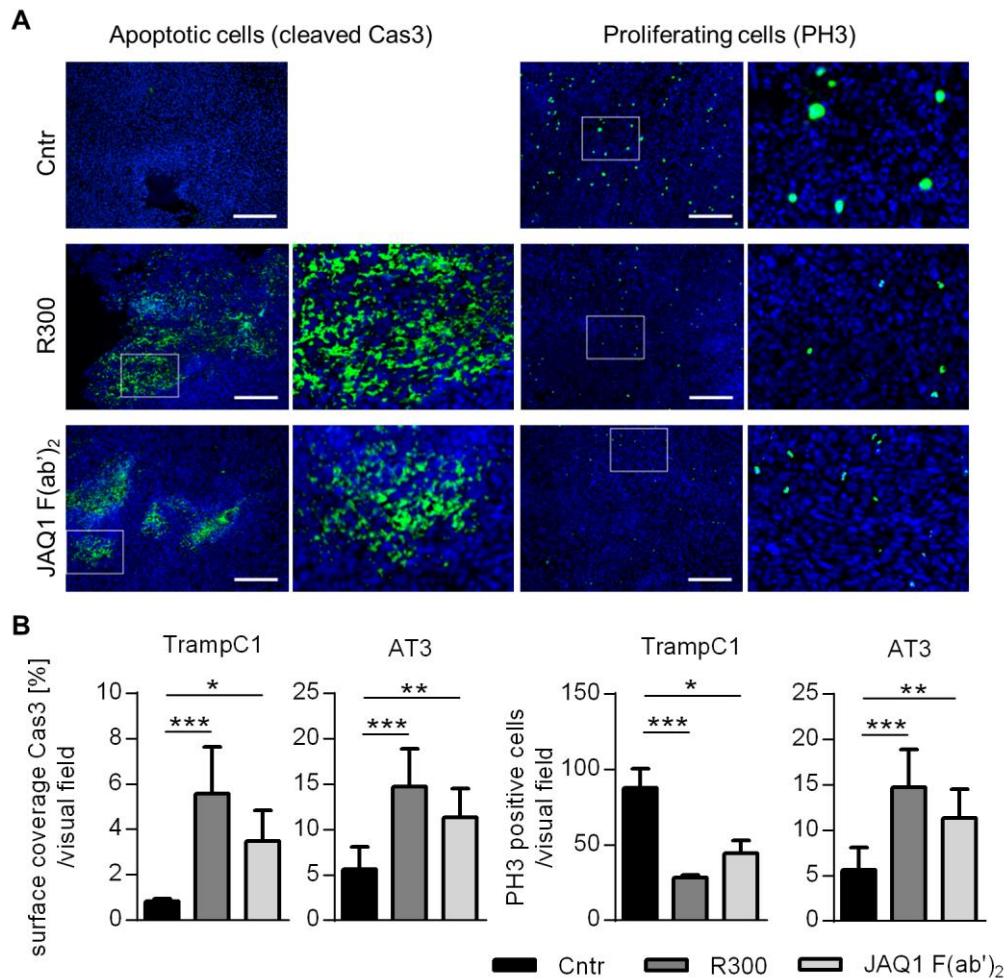
Figure 3-8: Increased apoptosis and decreased proliferation in TrampC1 and AT-3 primary tumors upon GPVI blockade. (A) TrampC1 primary tumors 18 h after antibody treatment stained for *cleaved caspase 3* (Cas3) and *phospho-histone H3 (*PH3). Scale bar: 250 μm. (B) For quantification in the TrampC1 model with n>5 and the AT-3 model with n>4 the average of 10 visual fields per mouse was calculated. Kruskal-Wallis with Dunn's multiple comparisons test. (Volz *et al. Blood*, 2019)[195]

Altogether, these results demonstrate that pharmacological inhibition of GPVI rapidly destabilizes vascular integrity in tumors leading to profound tumor hemorrhage and reduced tumor cell viability, while no such effect was observed in vessels of non-tumor tissue.

To better understand how platelets and in particular GPVI prevent tumor hemorrhage, we performed confocal fluorescence microscopy of tumor sections in *WT* mice with or without GPVI inhibition at two different time points. In IgG-control treated tumors, we detected numerous single platelets firmly adhering to the vessel wall. In GPVI-blocked animals, a slight tendency towards a lower amount of platelets was observed, but did not reach statistical significance (Figure 3-9). Therefore, the hypothesis that platelets may "seal" vascular leakages in the tumor by adhering to the exposed extracellular matrix (collagens and laminins), similar to their described function in a model of skin inflammation,[84] could not be confirmed.
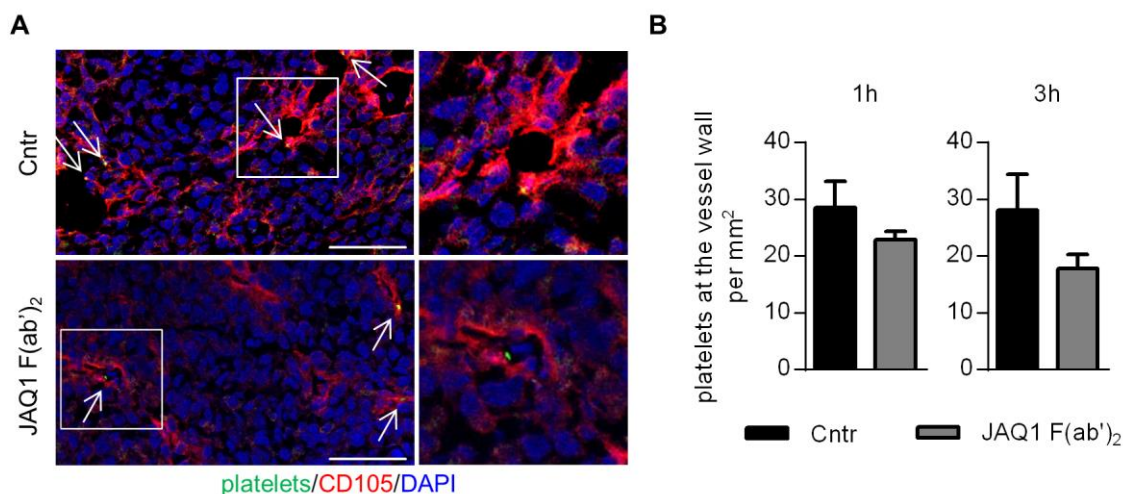
Figure 3-9: Platelets at the vessel wall in tumor tissue. AT-3 tumor-bearing *WT* mice were treated with IgG control or JAQ1 F(ab')$_2$ antibody. Tumors were harvested 1 h or 3 h post treatment and stained for the endothelial cell marker CD105 (red), the platelet marker GPIX (green) and nuclei were counterstained using DAPI (blue). (A) Representative images 3 h post-treatment are shown. Arrows indicate single platelets at the vessel wall. Scale bar: 50 µm (B) For quantification, the number of platelets adherent at the vessel wall was determined in a tile scan of 1.65 mm^2 and is depicted as mean ± SD. n=6; Mann-Whitney-test.

3.1.4 Antibody-mediated inhibition of GPVI improves delivery of chemotherapeutic agents into the tumor

It has been previously shown that platelet depletion in tumor-bearing mice increases the amount of chemotherapeutic agents in the tumor.[134] This result could be reproduced in the here tested tumor models using R300 for platelet depletion (Figure 3-10), utilizing the two widely used chemotherapeutic agents paclitaxel and doxil (liposomal doxorubicin). To investigate whether the amount of chemotherapeutic agents in the tumor tissue can also be increased by GPVI inhibition, TrampC1- and AT-3-tumor-bearing mice were treated with paclitaxel or doxil, in combination with JAQ1 F(ab')$_2$ or control IgG F(ab')$_2$. Tumors were removed after 2 h (TrampC1 and AT-3 model) or 24 h (AT-3 model) to determine doxil and paclitaxel concentrations (Figure 3-10). Both agents were present at higher concentrations in TrampC1 tumors 2 h after αGPVI treatment compared to the control group. In AT-3 tumors, a tendency towards higher concentrations of the agents, but no statistical significance was observed after 2 h. After 24 h, the amount of chemotherapeutic agent in the tumors of the control group dramatically decreased compared to its value after 2 h, whereas it remained high in AT-3 tumors where platelets had been depleted or GPVI was blocked.
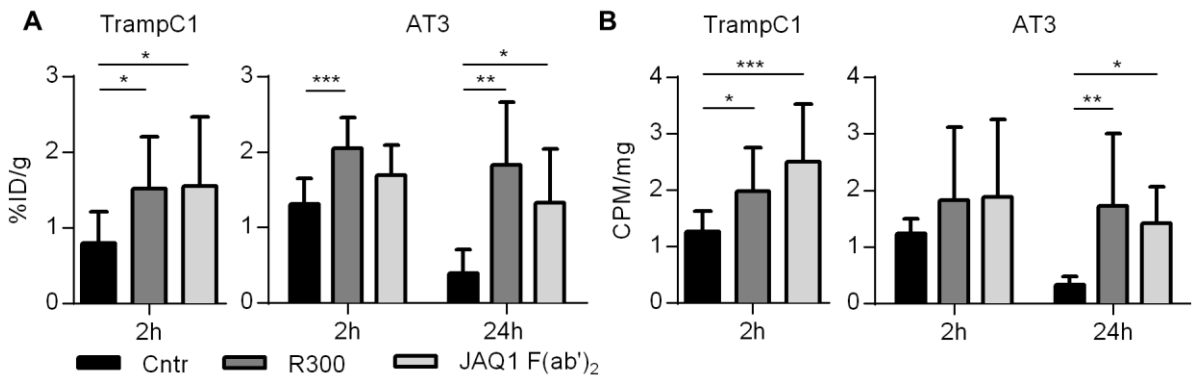
Figure 3-10: GPVI-blockade increases the amount of chemotherapeutic agent in the tumor. TrampC1 and AT-3 tumor-bearing mice were treated with doxil and paclitaxel in combination with IgG control, R300 or JAQ1 F(ab')$_2$. After 2 h/ 24 h the doxil concentration (A) or the paclitaxel concentration (B) within the tumor was measured. mean ± SD. Kruskal-Wallis with Dunn's multiple comparisons test. %ID/g: percent injected dose per g bodyweight; CPM/mg: counts per minute per mg tissue. (Volz *et al. Blood*, 2019)[195]

To confirm the tumor-specificity of this effect, different organs, such as heart, liver, spleen, kidney, intestine and lung from animals of this experiment were also analyzed for their internal doxil concentrations (Figure 3-11).
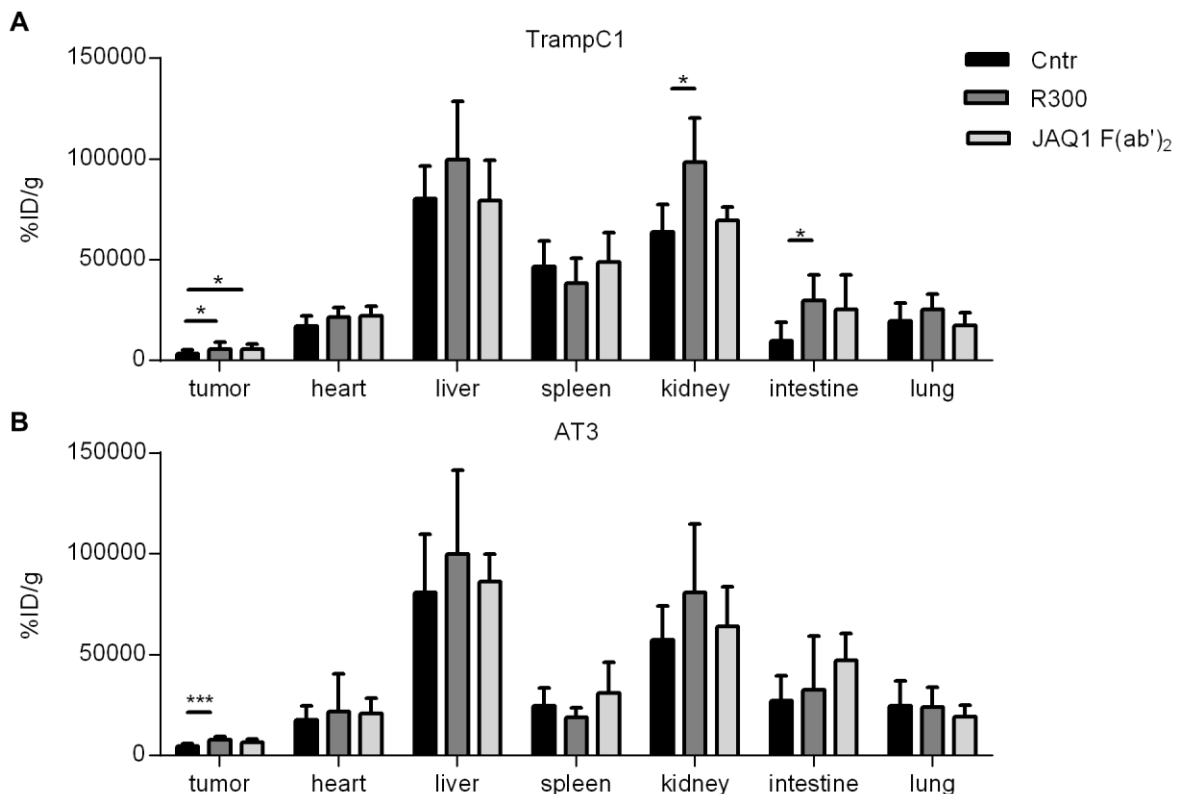

Figure 3-11: No difference in concentration of the chemotherapeutic agent doxil in different organs upon GPVI blockade. (A) TrampC1 and (B) AT-3 tumor-bearing mice were treated with doxil in combination with IgG control, R300 or JAQ1 F(ab')$_2$. After 2 h several organs were taken from the mice and the relative doxil concentration within the organs was detected. mean ± SD is depicted. 1 Way Anova with Dunnett's multiple comparisons test; %ID/g: percent injected dose per g bodyweight. (Volz *et al. Blood*, 2019)[195]

In contrast to the tumor tissue, no significant increase of doxil was detected in any of the tested organs upon JAQ1 F(ab')$_2$ treatment. However, platelet depletion induced a significant increase of doxil in the kidney and the intestine of TrampC1 tumor bearing mice.

These results indicate that inhibition of GPVI profoundly perturbed vascular integrity specifically in tumors. It facilitates the delivery of chemotherapeutic drugs to the tumor site without the side effects triggered by platelet depletion.

3.1.5 Decreased tumor growth upon GPVI inhibition in combination with chemotherapeutic agents

To investigate the effect of GPVI-blockade on tumor growth, TrampC1 and AT-3 tumor-bearing mice were treated with IgG control, R300 or JAQ1 F(ab')$_2$ as soon as the tumors were fully established (average size >50 mm^3). The treatment was repeated after 4 days. Tumor growth was significantly reduced in platelet-depleted and GPVI-inhibited mice compared to the control group in both tested tumor models (Figure 3-12).
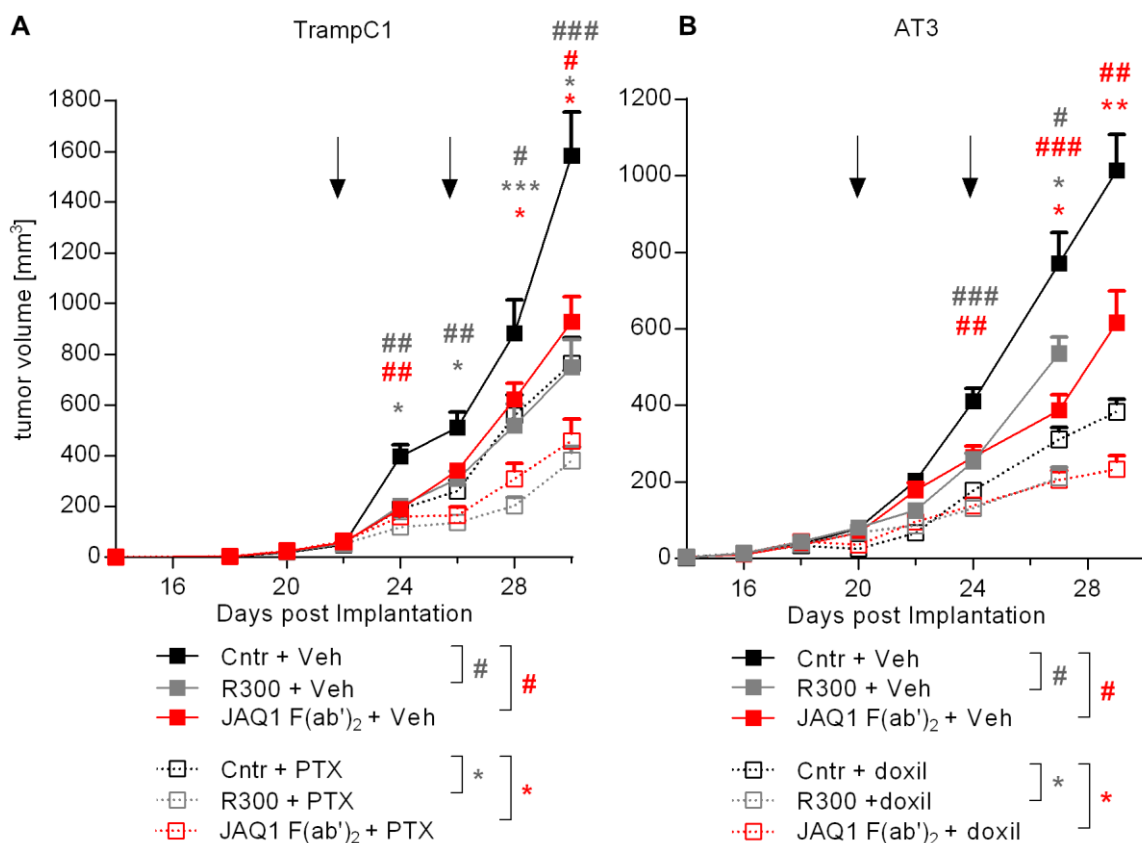

Figure 3-12: Combination of chemotherapeutic agents and GPVI-blockade further decreases tumor growth. (A) TrampC1 and (B) AT-3 tumor-bearing mice were treated with paclitaxel or doxil in combination with IgG control, R300 or JAQ1 F(ab')$_2$ (indicated by arrow) and the tumor volume was measured every second day. mean ± SEM. * indicates the significant differences between the groups treated with the chemotherapeutic agent and # the significant differences between the groups treated with the vehicle in the respective color, Kruskal-Wallis with Dunn's multiple comparisons test. Veh: vehicle; (Volz *et al. Blood*, 2019)[195]

To analyze whether the tumor growth could further be diminished in combination with chemotherapeutic drugs, the antiplatelet treatment was combined with the injection of paclitaxel or doxil in TrampC1 and AT-3 tumor-bearing mice. Treatment of animals with the chemotherapeutic agents in combination with the control IgG decreased the tumor volume by 50-60%, similar to the tumor volume in the group with GPVI blockade. Combination of these drugs with R300 or JAQ1 F(ab')$_2$ reduced tumor volumes by 70-80%, thus demonstrating improved efficacy of a combination treatment (Figure 3-12). These results emphasize the facilitated delivery of doxil and paclitaxel to the tumor site, as shown above, leading to the improvement of their anti-tumor effects.

3.1.6 Neutrophil depletion reverts anti-GPVI-induced intratumoral bleeding and impaired tumor growth

Platelet depletion and anti-GPVI treatment caused bleeding in the tumor, but not in other organs. These results suggested that the altered vasculature in the tumor is more dependent on platelet GPVI function than the intact vasculature in remote organs. Tumor-infiltrating *white blood cells* (WBCs), in particular neutrophils, have been described as a main source of proangiogenic factors, but also as a major cause of tumor vessel damage and intratumoral hemorrhage.[196-198] Indeed, immunofluorescent stainings of tumor sections revealed a coincidence of hemorrhagic spots present almost exclusively in areas where neutrophils accumulate (Figure 3-13).
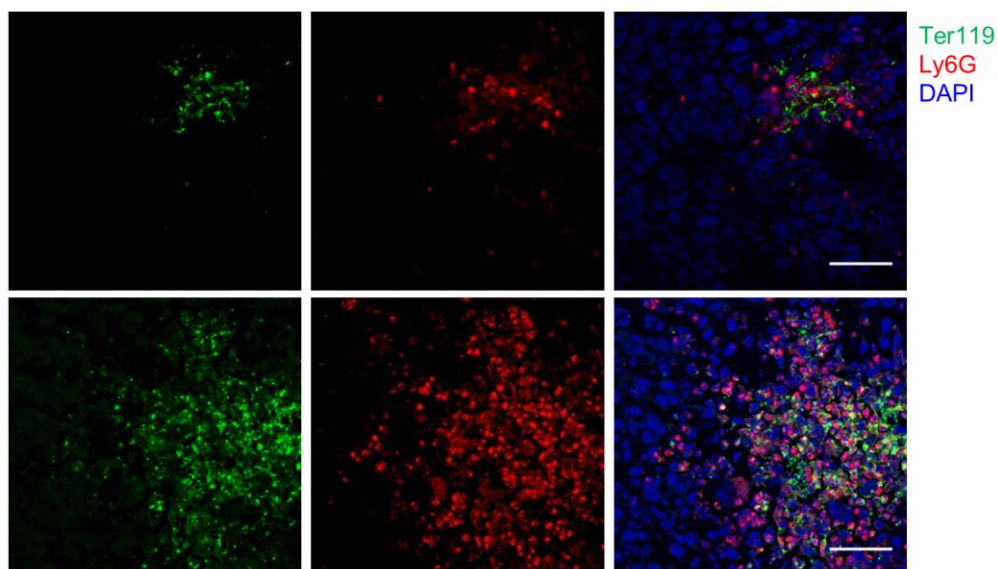

Figure 3-13: Neutrophil accumulation at hemorrhagic tumor sites. Neutrophil infiltration into the hemorrhagic regions of tumors was investigated by confocal microscopy. AT-3 tumor-bearing *WT* mice were treated with JAQ1 F(ab')$_2$. Tumors were harvested and stained for red blood cells (Ter119, green) and neutrophil markers, (Ly6G, red), and counterstained using DAPI (blue). 3 representative hemorrhagic areas are shown. Scale bar: 50 μm. (Volz *et al. Blood*, 2019)[195]

Therefore, we addressed whether the depletion of neutrophils may improve tumor vessel integrity, thereby affecting the intratumoral bleeding phenotype upon GPVI blockade. TrampC1 and AT-3 tumor-bearing mice were treated with the RB6-8C5 antibody to deplete Ly6G$^+$ cells 48 h prior to the treatment with IgG F(ab')$_2$, R300 or JAQ1 F(ab')$_2$, to ensure the absence of neutrophils at the time of the experiment. After 18 h, the hemoglobin concentration in the tumors of these animals was determined (Figure 3-14). Interestingly, Ly6G$^+$ cell depletion by itself had no effect on intratumoral hemorrhage in both tumor models. However, when mice were treated with JAQ1 F(ab')$_2$, Ly6G$^+$ cell depletion protected tumors from bleeding. The hemoglobin concentration of thrombocytopenic mice after Ly6G$^+$ cell depletion was also significantly reduced compared to neutrophil-bearing thrombocytopenic mice, but not to the level of control mice, thus indicating that additional factors contribute to the induction of hemorrhage during thrombocytopenia.
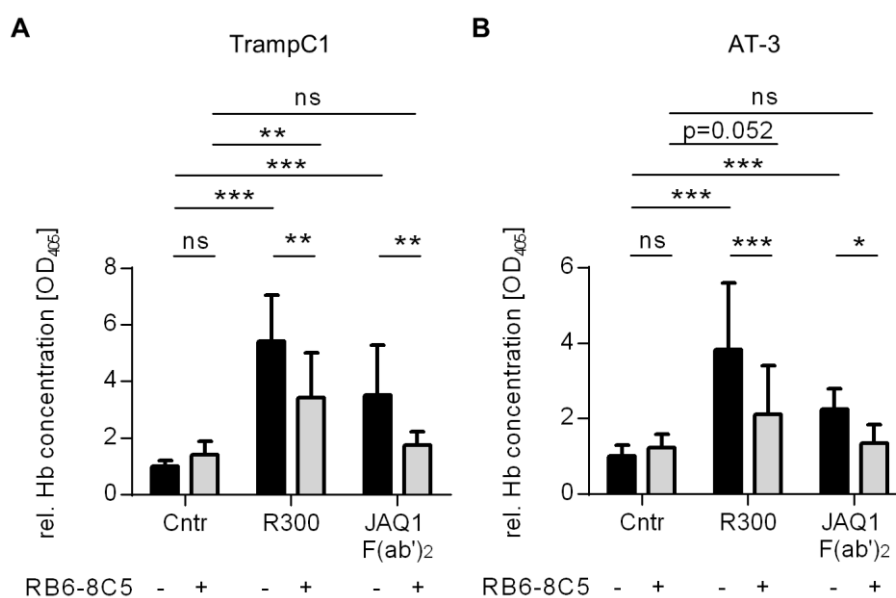

Figure 3-14: Ly6G$^+$ cell depletion reverts the hemorrhagic effect of the GPVI-blockade. (A) TrampC1 and (B) AT-3 tumor-bearing C57BL/6 mice were treated with RB6-8C5 antibody to deplete Ly6G$^+$ cells or with a vehicle control (saline) 48 h prior to the treatment with IgG control, R300 or the GPVI-blocking antibody. After 18 h the relative hemoglobin content of the tumors was measured. n≥10, two-way ANOVA with Tukey's multiple comparison test. (Volz *et al. Blood*, 2019)[195]

To test whether neutrophils also affect the inhibitory effect of platelet depletion and GPVI inhibition on tumor growth, we treated tumor-bearing mice with a combination of RB6-8C5 and R300 or JAQ1 F(ab')$_2$ every 4 days. Depletion of Ly6G$^+$ cells by itself did not affect tumor growth, as demonstrated previously in other models.[199] In line with the absent bleeding, tumor growth was not reduced in Ly6G$^+$ cell-depleted animals upon platelet-depletion or GPVI-inhibition (Figure 3-15).
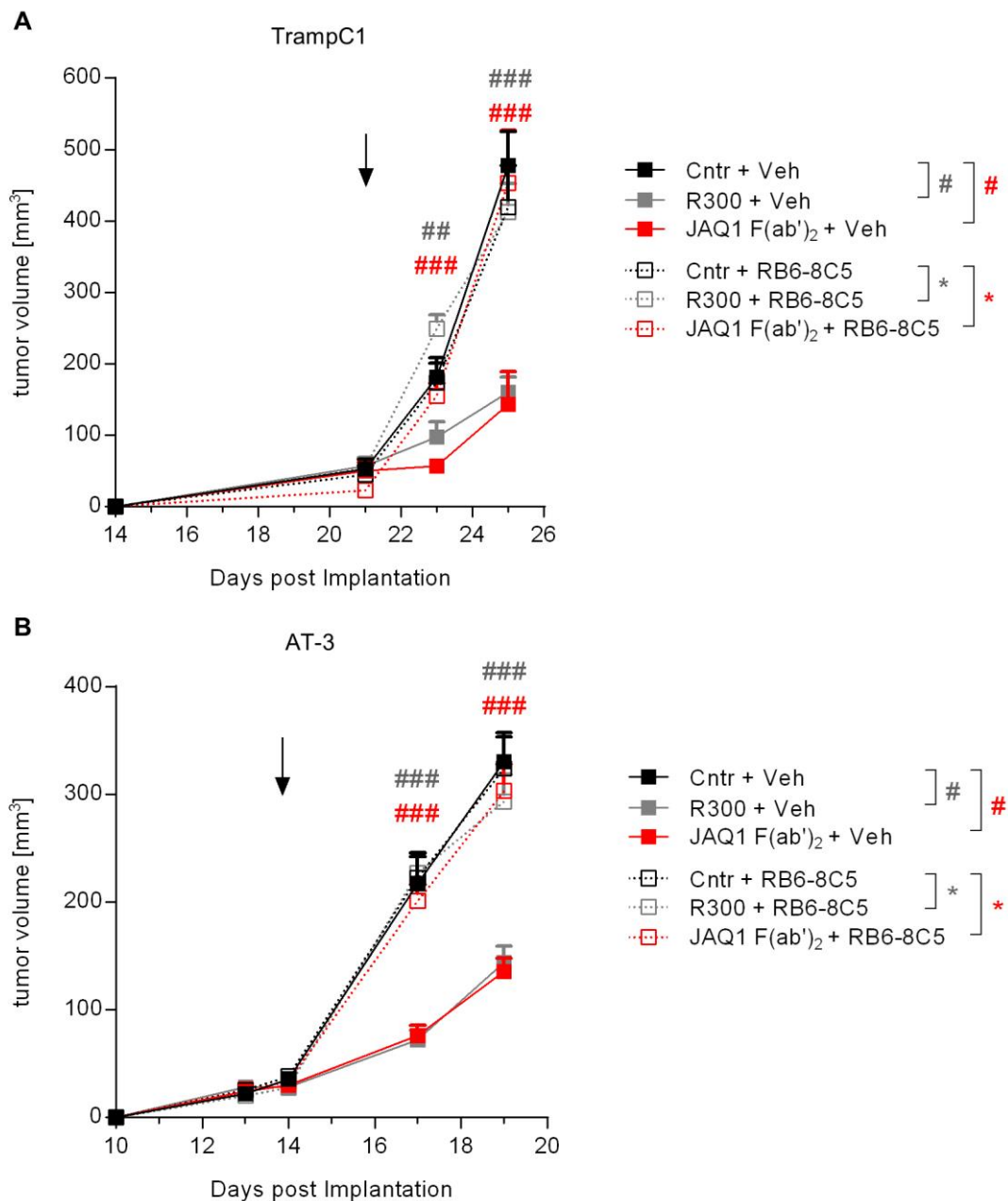
Figure 3-15: Ly6G+ cell-depletion reverts the effect of the GPVI-blockade on tumor growth. (A) TrampC1 and (B) AT-3 tumor-bearing C57BL/6 mice were treated with RB6-8C5 antibody to deplete Ly6G+ cells or with a vehicle control (saline) 48 h before treatment with IgG control, R300 or the GPVI-blocking antibody. The tumor volume was measured every second day. mean ± SEM. * indicates significant differences between the groups treated with the RB6-8C5 and # the significant differences between the groups treated with the vehicle in the respective color; Kruskal-Wallis with Dunn's multiple comparisons test. Veh: vehicle. (Volz *et al. Blood,* 2019)[195]

Given the well described role of platelets in fostering neutrophil infiltration, potential effects of GPVI-inhibition on neutrophil recruitment and infiltration into the tumor tissue was investigated. Therefore, flow cytometric analysis was performed in collaboration with Elmina Mammadova-Bach and Jesus Gil-Pulido in our institute. Comparable frequencies of Ly6G+ intratumoral neutrophils in mice treated with control F(ab')$_2$ and JAQ1 F(ab')$_2$ were detected (Figure 3-16),

suggesting that their recruitment was not dependent on GPVI. Moreover, no difference in the number of neutrophils was observed in peripheral blood or the bone marrow.
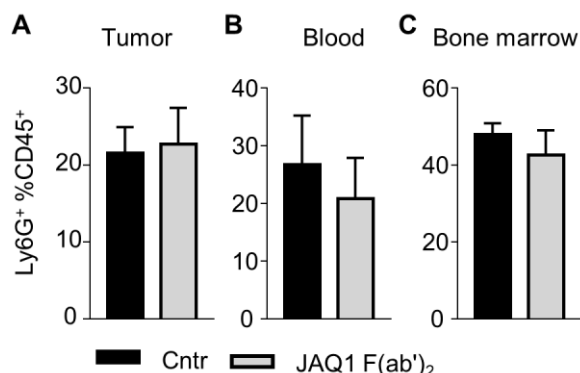

Figure 3-16: No alteration in the number of tumor-infiltrating neutrophils upon GPVI blockade. Collagenase-digested tumors were analyzed by flow cytometry. Total CD45+ leukocytes were gated and dead cells excluded from the analysis. Neutrophils were defined as Ly6G+ cells among living cells. (A) Percentages of tumor-infiltrating Ly6G+ neutrophils in control- or JAQ1 F(ab')₂-treated mice. (B) Percentages of circulating Ly6G+ neutrophils in blood or (C) bone marrow. mean ± SD. This experiment was performed in collaboration with Elmina Mammadova-Bach and Jesus Gil-Pulido. (Volz *et al. Blood*, 2019)[195]

Furthermore, it was assessed whether depletion of Ly6G+ cells leads to a stabilization of the tumor vessel wall. Indeed, treatment with RB6-8C5 decreased tumor vessel density and reduced the enlarged diameter of vessels in AT-3 tumors (Figure 3-17 A-C).
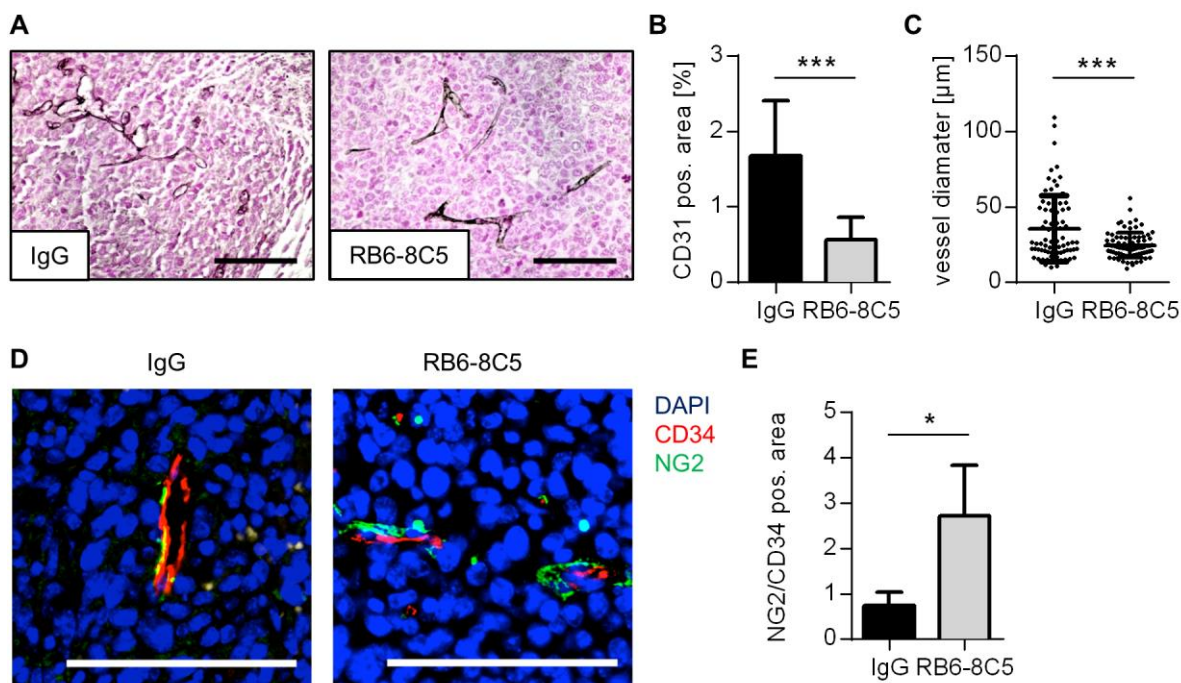

Figure 3-17: Normalization of vessel morphology by Ly6G+ cell depletion. (A) Representative images of AT-3 tumor sections stained for CD31. Scale bar: 100 µm. (B) Vessel density after depletion of Ly6G+ cells. n = 10, mean ± SD. (C) Vessel diameter after depletion of Ly6G+ cells. (D) Tumor sections stained for CD34 and the pericyte marker NG2. Scale bar: 100 µm. (E) Quantification of CD34+/NG2+ areas in tumor sections after depletion of Ly6G+ cells. n=4, mean ± SD. Kruskal-Wallis with Dunn's multiple comparisons test. (Volz *et al. Blood*, 2019)[195]

Moreover, Ly6G+-cell depletion also increased the coverage of blood vessels with NG2+ pericytes, demonstrating improved vessel stabilization and maturation (Figure 3-17 D, E). Thus, the relative specificity of platelet depletion and GPVI-targeting for causing hemorrhage solely in the tumor appears to be based on defects on the tumor vasculature.

3.1.7 Genetic deficiency of GPVI leads to hemorrhages in tumors

To investigate how the tumors develop in the complete absence of GPVI, GPVI-deficient (*Gp6−/−*) mice on a C57BL/6 genetic background and *WT* littermates were implanted with TrampC1 cells or AT-3 cells and the tumor size was evaluated every second day (Figure 3-18 A).
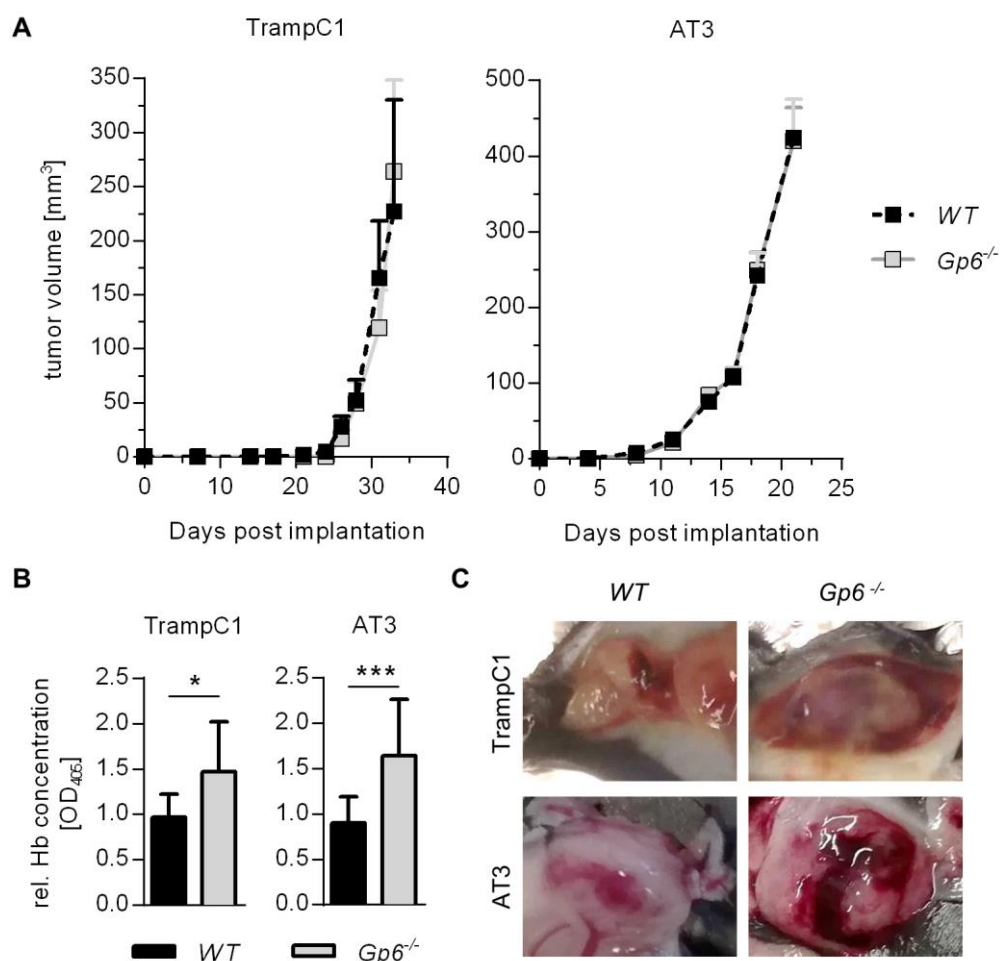
Figure 3-18: Increased bleeding in TrampC1 and AT-3 primary tumors in GPVI-deficient animals. (A) TrampC1 prostate and AT-3 breast cancer tumors were grown in GPVI-deficient (*Gp6−/−*) mice. Tumor growth was measured every second day for 33/21 days post-implantation. n=8, mean ± SEM. (B) 31/21 days post-implantation, the relative hemoglobin content was measured. n=8, mean ± SD. (C) Representative images of the tumors before dissection. (Volz *et al. Blood,* 2019)[195]

Interestingly, genetic GPVI-deficiency did not affect tumor growth. However, hemorrhage was observed in the tumors of *Gp6⁻/⁻* animals, reflected by a 1.5-fold increase in hemoglobin content in the tumor compared to controls (Figure 3-18 B, C). In contrast to the severe hemorrhage observed in GPVI-blocked *WT* animals (Figure 3-1), the bleeding here was less pronounced. To characterize the tumor vasculature in TrampC1 tumors of GPVI-deficient animals, a co-immunofluorescent staining for CD31, laminin α4, as well as collagens I and IV was performed. In contrast to the antibody-mediated blockade of GPVI, the genetic deficiency did not lead to a defective vasculature. No reduction in the number of vessels with lumen was detected (Figure 3-19 A, B) and the distribution of collagen IV and laminin α4 was comparable between tumors from *WT* and *Gp6⁻/⁻* mice.

Figure 3-19: Unaltered tumor vasculature in GPVI-deficient animals. (A) TrampC1 primary tumors from *WT* and *Gp6⁻/⁻* animals stained for CD31 (red), Col I (cyan) and counterstained with DAPI (blue). Scale bar: 100 μm (B) For quantification of the number of vessels with lumen the average of 10 visual fields per mouse was calculated, n>4, mean ± SD (C) TrampC1 primary tumors from *WT* and *Gp6⁻/⁻* animals stained for CD31 (red) Col IV (green, left panel), Lamα4 (green, right panel) and DAPI (blue). Scale bar: 10 μm. (Volz *et al. Blood*, 2019)[195]

Cell viability of TrampC1 tumors grown in $Gp6^{-/-}$ mice was investigated by immunofluorescence staining of cleaved Cas3 and PH3. Even though a tendency towards an increase of apoptotic cells was observed, the statistical analysis showed no significant difference between the two groups (Figure 3-20 A, C). Furthermore, the number of proliferating cells was indistinguishable (Figure 3-20 B, C). Altogether, this indicated that the moderate bleeding observed in tumors of GPVI-deficient mice is insufficient to cause vascular collapse, cell death and therefore does not dampen tumor growth.
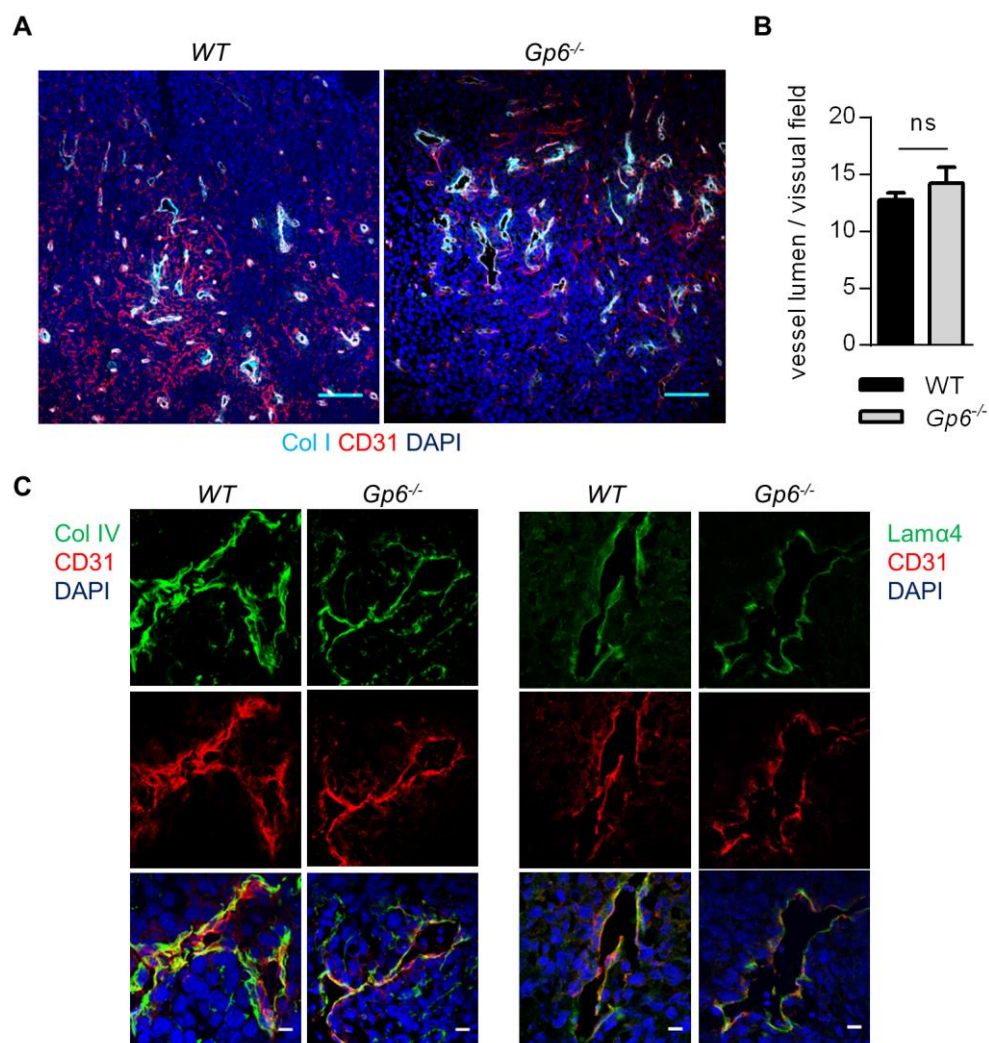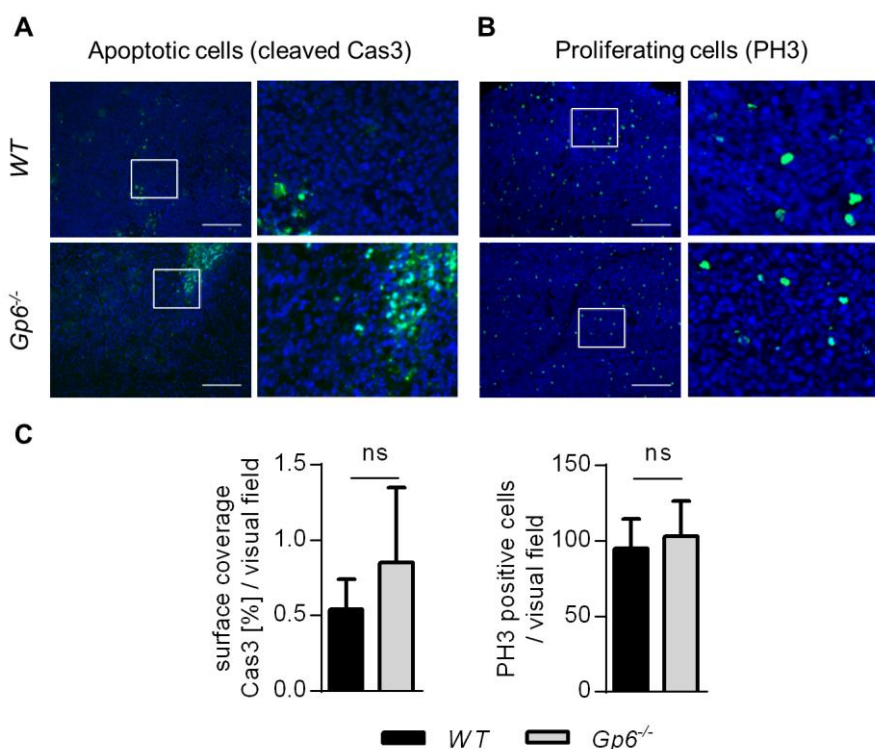

Figure 3-20: Unaltered tumor cell viability in GPVI-deficient animals. TrampC1 primary tumors from *WT* and *Gp6$^{-/-}$* animals stained for (A) *cleaved caspase 3* (Cas3) and (B) *phospho-histone H3* (PH3), Scale bar: 250 µm (C) For quantification the average of 10 visual fields per mouse was calculated, n=4, mean ± SD. (Volz *et al. Blood*, 2019)[195]

3.1.8 Effect of platelet count on intratumoral hemorrhage

Low platelet numbers in the blood stream are still sufficient to maintain their hemostatic and thrombotic function. A study from our lab found that platelet counts between 10% and 2.5% of the normal count in mice are still sufficient to prevent bleeding or to induce thrombus formation.[200] To investigate how many platelets are sufficient to maintain tumor vascular integrity, the R300 antibody was used at lower concentrations to deplete platelets to a range of 10 – 25% or < 5% of the normal platelet count. A platelet count above 5% was sufficient to prevent hemorrhage, whereas a count below 5% resulted in a strong hemorrhagic effect within the tumor (Figure 3-21 A). This demonstrates that only low platelet numbers are required to

maintain tumor vascular integrity, which is line with previous observations in models of thrombosis and hemostasis. The gradual reduction of platelet counts (0.08 µg/g body weight R300 at timepoint 0 h and 9 h) had no influence on the extent of hemorrhage observed after 18 h (Figure 3-21 B).
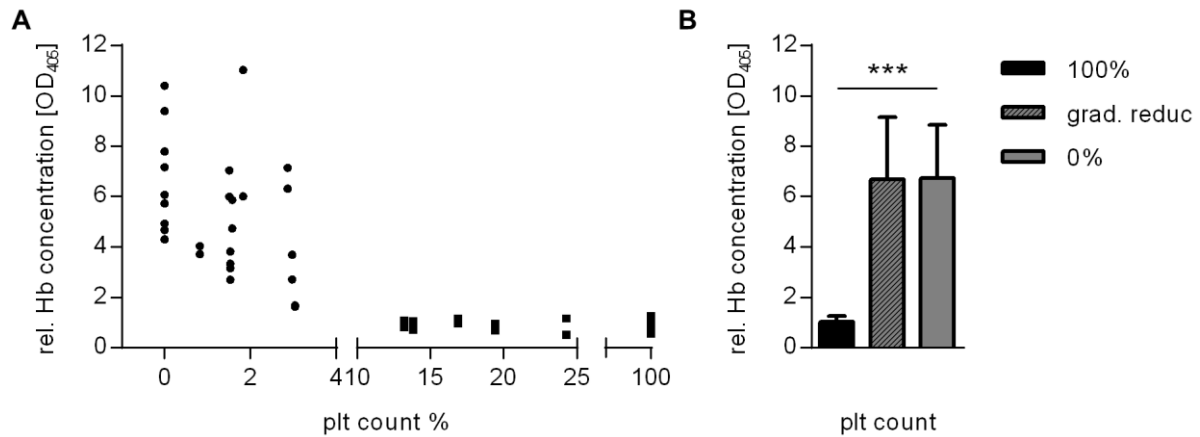

Figure 3-21: Effect of platelet count on intratumoral hemorrhage. (A) AT-3-tumor-bearing *WT* C57BL/6 animals were treated with different concentrations of R300 antibody; 100 µg for complete depletion; 0.12 µg/g body weight to reduce platelet count below 5%; 0.08 µg/g body weight to reduce platelet count to 15-25 % of the initial count. Every dot represents one tumor. Relative hemoglobin concentration was determined 18 h post-depletion. (B) To gradually reduce platelet count, the R300 antibody was injected at time point 0 at a concentration of 0.08 µg/g body weight. To reduce platelet count to maximal level, mice were again treated with R300 antibody after 9 h (0.08 µg/g body weight). Plt: platelet. (Volz *et al. Blood*, 2019)[195]

Using syngeneic mouse models of prostate and breast cancer, the effects of the functional inhibition of GPVI were investigated for the first time in this study. The treatment rapidly induced profound tumor hemorrhage, diminished tumor growth and increased intratumoral accumulation of co-administered chemotherapeutic drugs, resulting in a markedly increased anti-tumor effect.

3.2 BIN2 is a key regulator of platelet calcium signaling

BIN2 was previously discovered by our group as a potential interaction partner of the Ca^{2+}-regulating protein STIM1 in human platelets.[183] To assess the function of BIN2 in mice *in vivo*, a constitutive knockout mouse strain (*Bin2$^{fl/fl,CMV-Cre+/-}$*, referred to as *Bin2$^{-/-}$*) and a platelet/megakaryocyte-specific knockout mouse (*Bin2$^{fl/fl,Pf4Cre+/-}$*) were generated in a mixed genetic background.[183] To eliminate influences of different genetic backgrounds, both mouse lines were backcrossed 10 times into a pure C57BL/6J background and analyzed for their platelet function.

3.2.1 BIN2-deficient mice display unaltered platelet count and size, but slightly altered platelet glycoprotein expression levels

Bin2$^{-/-}$ mice are viable, fertile, born in normal Mendelian ratios and display no obvious signs of impairment. Platelet count and size as well as the basic blood parameters, represented by WBC, RBC and *hematocrit* (HCT) were measured using a blood cell counter. BIN2-deficient animals showed unaltered values in all tested parameters compared to the respective *WT* controls (Table 3-1**)**. This indicated that BIN2 is dispensable for embryonic development. Similar results were obtained with *Bin2$^{fl/fl,Pf4Cre+/-}$* animals, where all tested blood parameter were comparable to their respective *WT* control (Table 3-1).

Table 3-1: Basic blood and platelet parameters of *Bin2$^{-/-}$* and *Bin2$^{fl/fl,Pf4Cre+/-}$* mice. Platelet count, size and basic blood parameters were analyzed using a blood cell counter (ScilVet). n=4, Plt: Platelets; MPV: mean platelet volume; WBC: white blood cells; RBC: red blood cells; HCT: hematocrit; ns: not significant.

	WT	*Bin2$^{-/-}$*	*WT*	*Bin2$^{fl/fl,Pf4Cre+/-}$*
Plt [x103/µl]	928.9 ± 40.01	935.4 ± 96.2	830.2 ± 51.44	821.6 ± 116.48
MPV [fl]	5.72 ± 0.1	6.06 ± 0.39	6.98 ± 0.08	6,8 ± 0.21
WBC [x103/µl]	3.54 ± 1.01	4.08 ± 2.16	8.68 ± 1.73	8,26 ± 2.81
RBC [x106/µl]	9.67 ± 0.27	9.2 ± 1.28	8.032 ± 0.38	8,34 ± 0.71
HCT [%]	46.20 ± 1.48	44.46 ± 3.55	15.24 ± 0.71	15,56 ± 1.02

Transmission electron microscopy was used to investigate the morphology of *Bin2$^{fl/fl,Pf4Cre+/-}$* platelets. In line with the blood cell counter data, no difference in platelet size was detected and the overall morphology was comparable to *WT* platelets (Figure 3-22).
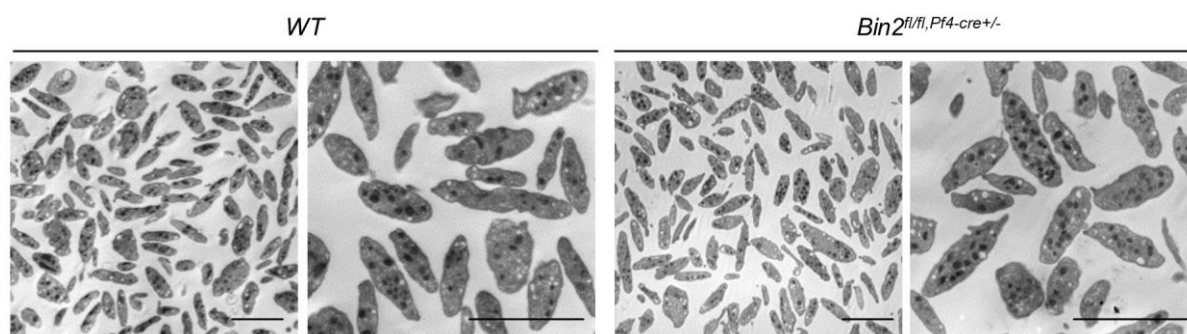
Figure 3-22: Unaltered morphology of BIN2-deficient platelets. Transmission electron microscopy images of *WT* and *Bin2$^{fl/fl,Pf4Cre+/-}$* resting platelets. Scale bar: 5 µm.

To investigate whether glycoproteins expressed on the platelet surface differ between BIN2-deficient and *WT* platelets, a flow cytometric analysis of *Bin2$^{-/-}$* and *Bin2$^{fl/fl,Pf4Cre+/-}$* platelets and the respective *WT* controls was performed. BIN2-deficient platelets from both mouse lines depicted a slight, but significant decrease in GPV, GPVI, CD9 and β1 expression on their surface (Table 3-2).

Table 3-2: Altered glycoprotein expression in BIN2-deficient platelets. Glycoprotein expression on the platelet surface was determined by flow cytometry. MFI ± SD, n=4, one representative of 3 independent experiments. n.d.: not determined

	WT	*Bin2$^{-/-}$*	*WT*	*Bin2$^{fl/fl,Pf4Cre+/-}$*
GPIb	322.7 ± 27.2	296.0 ± 5.6	257.3 ± 16.6	222.6 ± 12.3
GPV	213.0 ± 10.2	184.3 ± 5.5 ***	206.5 ± 8.7	181.0 ± 5.3 **
GPVI	45.3 ± 1.3	35.3 ± 0.6 ***	46.8 ± 1.3	39.2 ± 0.5 ***
GPIX	392.0 ± 12.7	355.7 ± 16.9	396.5 ± 2.1	373.5 ± 13.4
CD9	828.3 ± 30.7	653.7 ± 14.7 ***	857.5 ± 6.9	697.3 ± 12.9 ***
α2	59.8 ± 6.9	53.0 ± 1.0	44.0 ± 0	41.0 ± 2.3
β1	n.d.	n.d.	166.0 ± 3.9	138.7 ± 5.8 ***

3.2.2 Defective Ca^{2+} store release and Ca^{2+} influx in BIN2-deficient platelets

Agonist-induced platelet activation leads to an increase in *cytosolic Ca^{2+} concentrations* ([Ca^{2+}]$_i$) through the release of Ca^{2+} from intracellular stores and subsequent Ca^{2+} entry across the PM through STIM1/Orai1-dependent SOCE. Since BIN2 was previously identified as a potential interaction partner of STIM1 in a mass-spectrometric screening by our group, the role of BIN2 in platelet calcium homeostasis was investigated using the Ca^{2+}-binding fluorophore Fura-2. A comparable Ca^{2+} store content in *Bin2$^{fl/fl,Pf4Cre+/-}$* and *WT* littermate platelets was found by treatment of platelets with the Ca^{2+} ionophore ionomycin in the absence of extracellular Ca^{2+} (Figure 3-23 A).
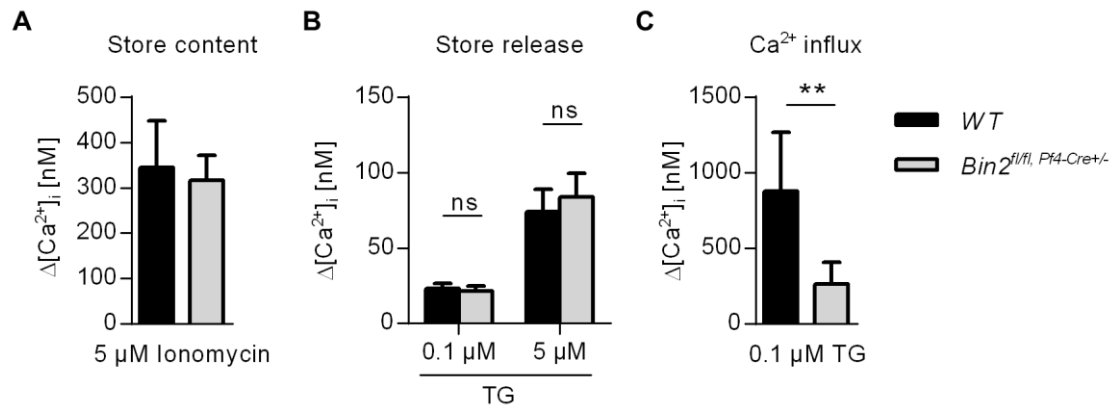
Figure 3-23: Normal Ca²⁺ store content and agonist-independent store release but altered agonist-independent Ca²⁺ influx in BIN2-deficient platelets. Maximum Ca²⁺ changes in the cytoplasm of *Bin2^{fl/fl,Pf4Cre+/-}* or *WT* littermate platelets upon treatment with (A) Ionomycin or (B) thapsigargin in the absence of extracellular Ca²⁺ and (C) thapsigargin in the presence of extracellular Ca²⁺. mean ± SD. n≥8 TG: thapsigargin.

The Ca²⁺ store depletion evoked by the SERCA pump inhibitor TG in the absence of extracellular Ca²⁺ was indistinguishable between both groups (Figure 3-23 B). Remarkably, however, the TG-evoked Ca²⁺ influx in the presence of extracellular Ca²⁺ was markedly diminished in the absence of BIN2 (Figure 3-23 C), pointing towards a defect in the STIM1-mediated opening of CRAC channels in these platelets.

Next, agonist-induced Ca²⁺ responses upon stimulation with the GPCR agonists ADP, thrombin and the stable TxA₂ analogue U46619 were studied. Furthermore, the GPVI agonists CRP and the snake-venom CVX, as well as the snake venom toxin RC, which activates the (hem)ITAM receptor CLEC-2, were used. Ca²⁺ influx in the presence of extracellular Ca²⁺ was markedly diminished in BIN2-deficient platelets in response to all agonists (Figure 3-24 A).
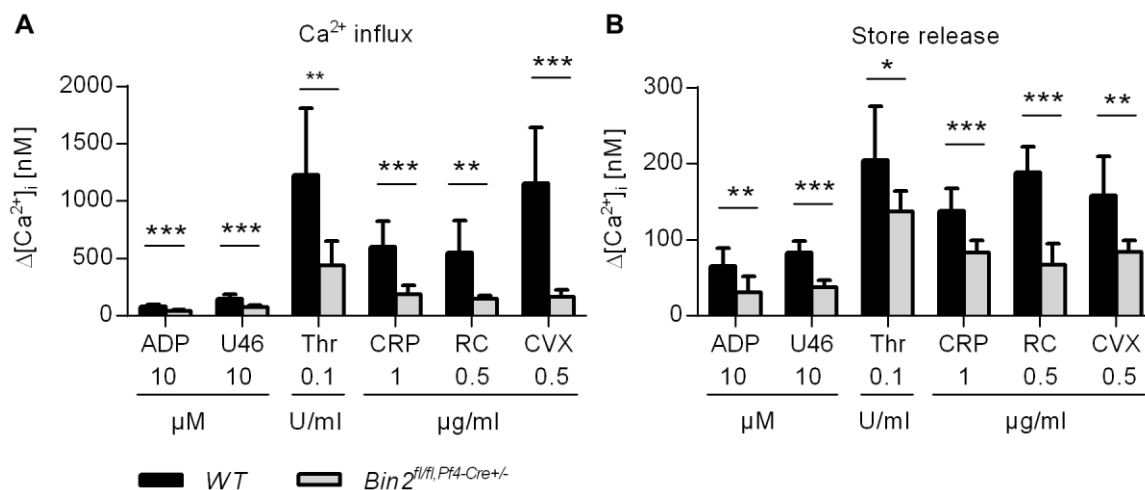
Figure 3-24: Decreased agonist-dependent Ca²⁺ influx and store release in BIN2-deficient platelets. Maximum Ca²⁺ changes in the cytoplasm of *Bin2^{fl/fl,Pf4Cre+/-}* or *WT* littermate platelets upon treatment with the indicated agonists in the (A) presence or (B) absence of extracellular Ca²⁺. mean ± SD, n≥8. ADP: adenosine diphosphate; U46: U46619; Thr: thrombin; CRP: collagen-related peptide; RC: rhodocytin; CVX: convulxin.

Interestingly, despite the normal store content, the Ca^{2+} store release, measured in the absence of extracellular Ca^{2+}, was severely impaired in response to all tested agonists (Figure 3-24 B). Overall, these results clearly demonstrated an essential role of BIN2 in STIM1/Orai1-mediated SOCE, but, surprisingly, also in agonist-induced Ca^{2+} store release.

3.2.3 BIN2 interacts with STIM1 and IP3R

In order to identify the mechanisms underlying the defective agonist-induced Ca^{2+} store release, signal transduction pathways downstream of the (hem)ITAM receptors GPVI and CLEC-2 were investigated. Phosphorylation of the key signaling molecules Syk (Y519/520), LAT (Y191) and PLCγ2 (Y759) was unaltered upon platelet activation with the GPVI-coupled agonist CVX or the CLEC-2-activating agonist RC (Figure 3-25).
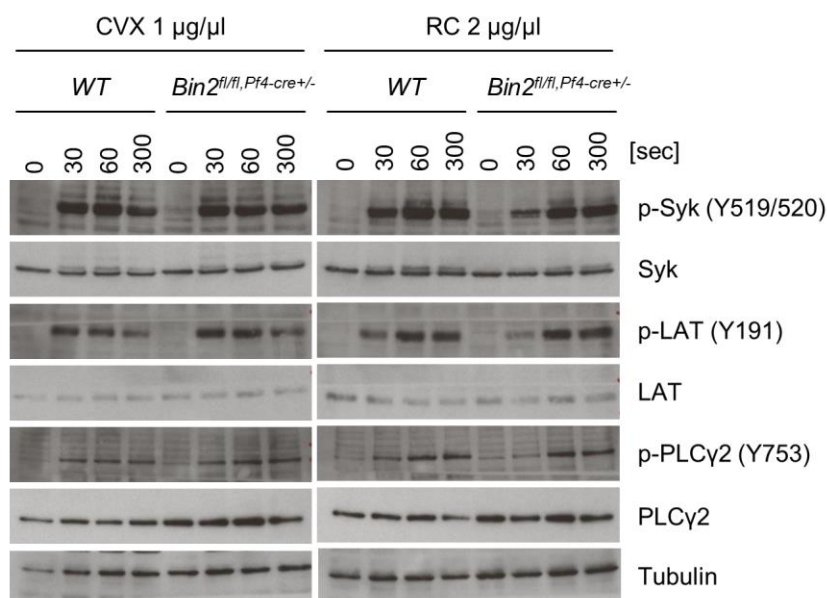
Figure 3-25: Unaltered phosphorylation of proteins downstream of (hem)ITAM-coupled receptors. Washed platelets were stimulated with *convulxin* (CVX) or *rhodocytin* (RC) at the indicated time points, followed by cell lysis and WB analysis using the indicated phospho-specific antibodies. These blots are representative of three independent experiments.

A central downstream pathway of all agonists is the PLC-dependent hydrolysis of PIP_2 into DAG and IP_3. In line with the unaltered (hem)ITAM tyrosine phosphorylation cascade, the amount of IP_3 (determined indirectly by measuring IP_1 levels) produced by $Bin2^{fl/f,Pf4Cre+/-}$ platelets upon activation with CVX and RC, was indistinguishable from *WT* controls (Figure 3-26 A). This was also the case for the GPCR agonist thrombin and indicated that the defect leading to the altered store release is located downstream of IP_3 generation. Therefore, we analyzed IP_3R expression levels in mutant platelets and found no difference to *WT* controls (Figure 3-26 B).

Figure 3-26: Normal IP$_3$ generation and IP$_3$R expression in BIN2-deficient platelets. (A) *WT* and *Bin2*$^{fl/fl,Pf4Cre+/-}$ washed platelets were stimulated with the indicated agonist for 15 min, followed by the detection of produced IP$_1$, an indirect measurement for IP$_3$, in lysed platelets using an IP$_1$-ELISA. One representative out of 3 independent experiments. (B) Determination of IP$_3$R pr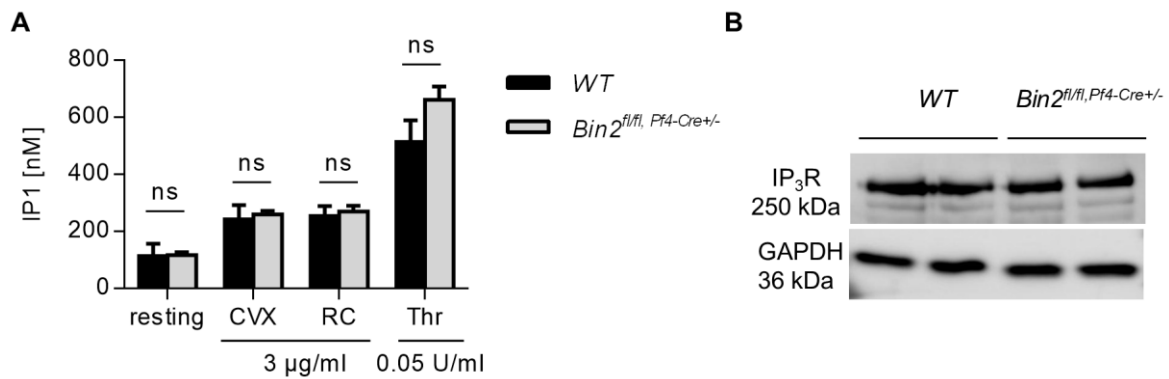otein levels in *WT* and *Bin2*$^{fl/fl,Pf4Cre+/-}$ platelet lysates by immunoblotting. One representative out of 3 independent experiments. mean ± SD, n≥4 Thr: thrombin; RC: rhodocytin; CVX: convulxin.

Since total IP$_3$R expression levels were unaltered, we tested its functionality. To this end, we loaded platelets with inactive, caged IP$_3$, which can be activated with an UV-light pulse during the measurement.[201] Strikingly, both, Ca^{2+} store release as well as SOCE, were markedly reduced in *Bin2*$^{fl/f,Pf4Cre+/-}$ platelets compared to *WT* controls (Figure 3-27), pointing towards a functional defect of the IP$_3$R in the knockout platelets.
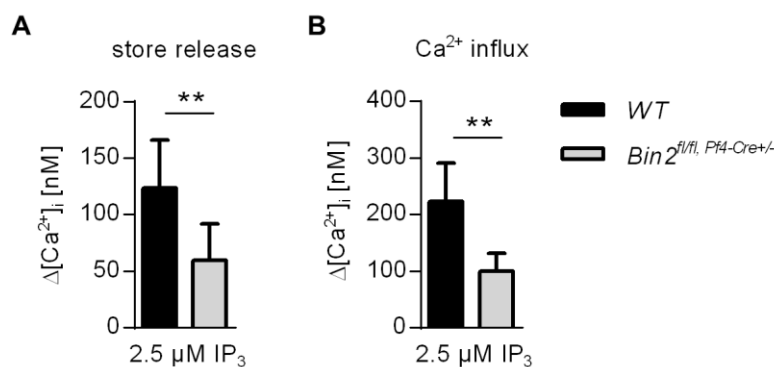
Figure 3-27: Defective IP$_3$R function. (A) Maximum Ca^{2+} changes in the cytoplasm of *WT* or *Bin2*$^{fl/fl,Pf4Cre+/-}$ platelets upon treatment with UV light-activatable IP$_3$ in the (A) absence or (B) presence of extracellular Ca^{2+}. mean ± SD, n≥8.

The results described above indicate that BIN2 may not only interact with STIM1, but possibly also with IP$_3$Rs to regulate Ca^{2+} homeostasis in platelets. To test this hypothesis, a pulldown assay was performed, where *Bin2*$^{fl/f,Pf4Cre+/-}$ platelet lysates were incubated with recombinant HIS-tagged BIN2. Following purification with Ni-NTA beads, the different fractions were eluted and analyzed by immunoblotting. High amounts of BIN2 were detected in the eluate fractions (Figure 3-28), demonstrating the functionality of the pulldown. Furthermore, STIM1 was robustly detected in the eluate fractions (Figure 3-28), confirming previous results obtained

with human platelets.[183] In addition, IP$_3$R was identified in the eluate fraction, demonstrating a robust direct or indirect interaction of BIN2 with both, STIM1 and IP$_3$R in platelets.
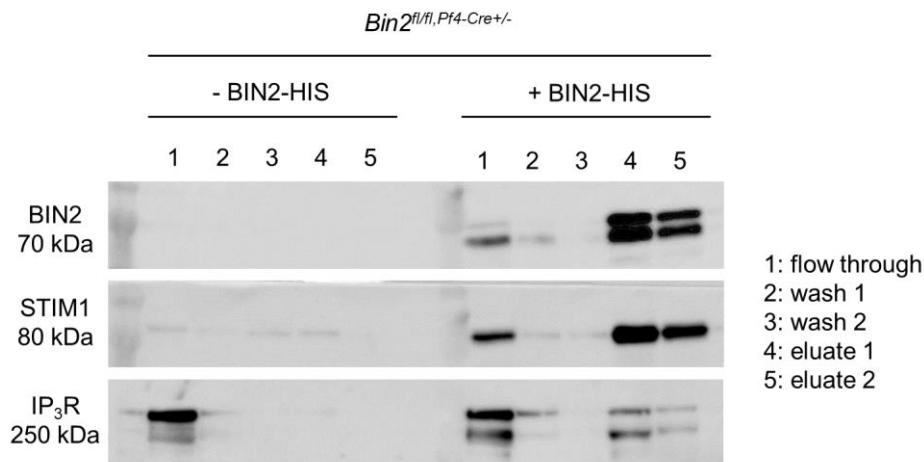
Figure 3-28: BIN2 interacts with STIM1 and IP$_3$R. (A) *Bin2$^{fl/fl,Pf4Cre+/-}$* lysates were incubated with recombinant BIN2-HIS protein, followed by a purification step with Ni-NTA beads. The different fractions were eluted and analyzed by immunoblotting for the presence of STIM1 and IP$_3$R.

3.2.4 Defective platelet activation response upon stimulation of (hem)ITAM receptors upon BIN2 deficiency

To further elucidate the effect of the severe Ca^{2+} signaling defect in *Bin2$^{fl/fl,Pf4Cre+/-}$* platelets, platelet activation was assessed by flow cytometry following stimulation with the GPCR agonists ADP, thrombin and U46619 as well as the (hem)ITAM receptor agonists CRP, CVX and RC. As a measure for platelet activation the activated form of integrin αIIbβ3 was detected using the anti-αIIbβ3 antibody JON/A coupled to PE. To quantify platelet degranulation, P-selectin exposure on the platelet surface was assessed, since P-selectin is stored in α-granules and exposed on the PM upon degranulation. Interestingly, the responses of *Bin2$^{-/-}$* and *Bin2$^{fl/fl,Pf4Cre+/-}$* platelets were unaltered upon activation with all tested GPCR agonists. However, activation of the (hem)ITAM receptors GPVI and CLEC-2 resulted in diminished integrin activation and granule secretion (Figure 3-29). This indicated that the defective Ca^{2+} signaling observed in BIN2-deficient platelets is of particular relevance for (hem)ITAM, but not GPCR signaling.
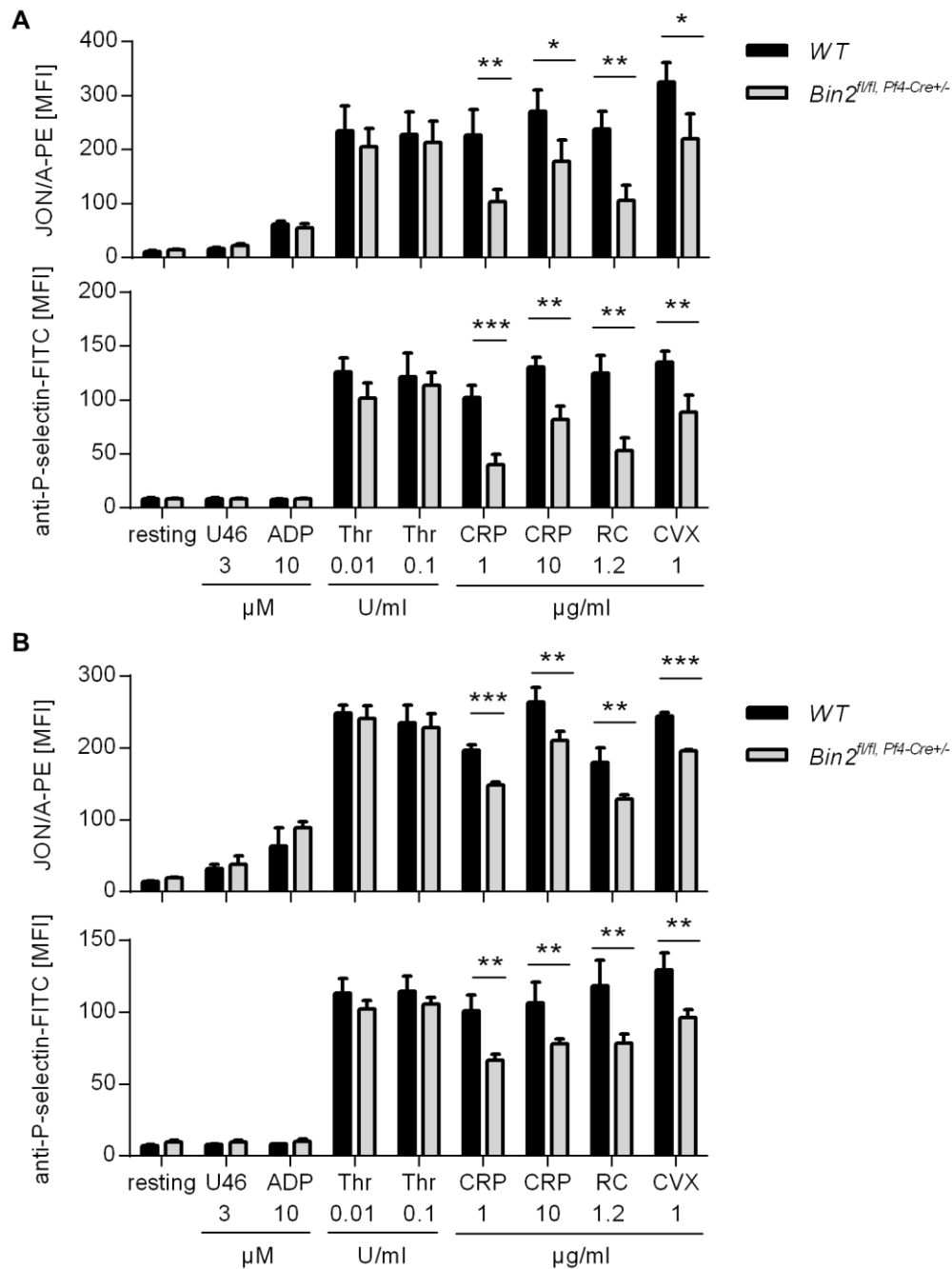
Figure 3-29: Reduced αIIbβ3 integrin activation and degranulation in BIN2-deficient platelets upon stimulation with (hem)ITAM-coupled receptor agonists. Flow cytometric analysis of integrin αIIbβ3 activation and P-selectin exposure in response to the indicated agonists in (A) *Bin2⁻/⁻* and (B) *Bin2fl/fl,Pf4Cre+/-* compared to the respective *WT* animals. This is one representative of three independent experiments. mean ± SD, n≥4 ADP: adenosine diphosphate; U46: U46619; Thr: thrombin; CRP: collagen-related peptide; RC: rhodocytin; CVX: convulxin.

3.2.5 Generation of BIN2-specific antibodies

Direct stochastic optical reconstruction microscopy (*d*STORM) was performed to assess the localization of BIN2 in mouse platelets. However, none of the commercially available BIN2 antibodies showed signal above the levels of the negative control (*Bin2⁻/⁻* platelets). Therefore,

new antibodies directed against BIN2 were generated and characterized. For this purpose, rats were repeatedly immunized with BIN2 inclusion bodies, generated by Dr. Julia Preu in our laboratory. After four to five immunization rounds, animals were sacrificed, the spleen was isolated, a single cell suspension was prepared and fused with mouse myeloma AG14 cells using PEG1500. The generated hybridoma cells were grown in the presence of feeder cells in 96 well plates and the supernatant was tested in a self-made BIN2 ELISA system. Bound antibodies were detected using an HRP-coupled anti-rat IgG antibody (Figure 3-30). A purchased BIN2 antibody from Proteintech (rabbit anti-human BIN2, but also detecting mouse BIN2) was used as a positive control. Unfortunately, from the first two fusions, no clone produced specific anti-BIN2 antibodies. The third fusion generated approximately 1200 clones from which 52 supernatants were tested positive for BIN2 binding in the ELISA system. The 52 positively tested clones were subcloned several times to obtain a monoclonal hybridoma population. During subcloning, the clones were tested for their specificity towards BIN2. Out of the 52 initially positive clones two (clone 2C11 and 12E1) maintained their specificity against BIN2, whereas all others died during the subcloning process or lost the expression of the BIN2-specific antibody.
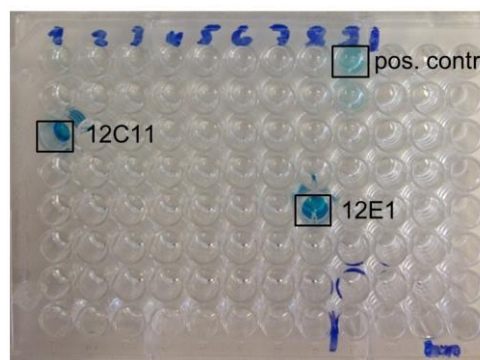
Figure 3-30: BIN2 ELISA to screen for BIN2-specific antibodies. Cell culture supernatants from different hybridoma cell cultures were tested for the presence of antibodies, binding to the coated BIN2 protein. After extensive washing antibodies were detected using an HRP-labeled anti-rat antibody and signals were developed with TMB.

To further characterize the antibodies, a Western blot analyses on mouse platelet lysates were performed under reducing conditions. A single clear band at the size of about 75 kDa was detected with both antibodies in *WT* lysates, corresponding to the molecular weight of mouse BIN2. This band was absent in *Bin2*$^{fl/fl,Pf4Cre+/-}$ lysates, indicating that both tested antibodies were specific for BIN2 (Figure 3-31 A). Interestingly, no band was detected in human platelet lysates for both antibodies, demonstrating that they are specifically detecting mouse BIN2 (Figure 3-31 B). In contrast, the commercially available BIN2 antibody (Proteintech) detected both, mouse and human BIN2 and was used as a control on the same membrane after stripping.
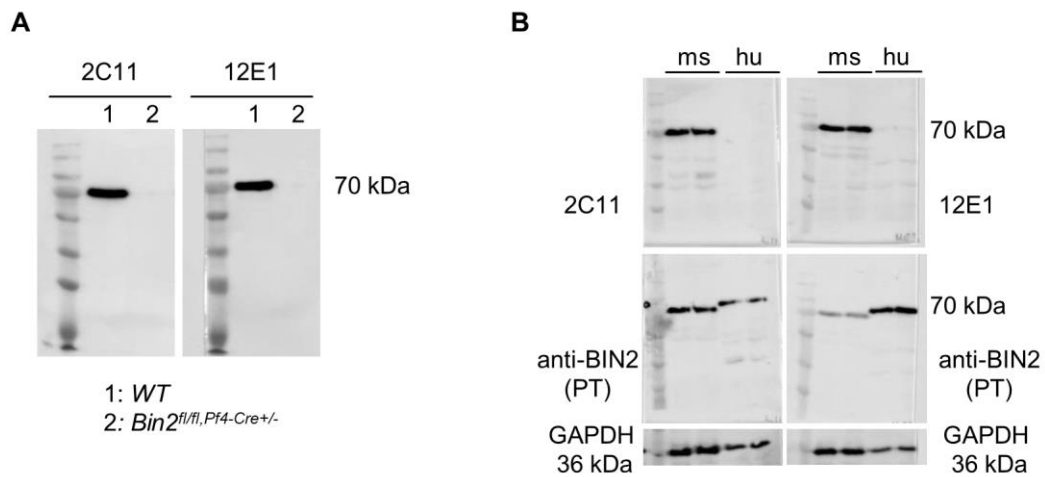
Figure 3-31: Functional BIN2 clones in Western blot analysis. The purified antibodies 2C11 and 12E1 were tested for their ability to detect BIN2 in Western blot analysis using (A) platelet lysates from *WT* or Bin2[fl/fl,Pf4-Cre+/-] mice or (B) human platelet lysates. GADPH served as a loading control PT: Proteintech antibody (commercially available); ms: mouse *WT* platelet lysate; hu: human platelet lysate.

It was previously shown by our lab that BIN2 is cleaved by the calcium-dependent, non-lysosomal cysteine protease, calpain, after platelet treatment with high concentrations of TG.[183] Using a commercially available BIN2 antibody, detecting specifically the N-terminal part of the protein, a 35 kDa band was observed after cleavage, most likely representing the BAR domain (Figure 3-32).
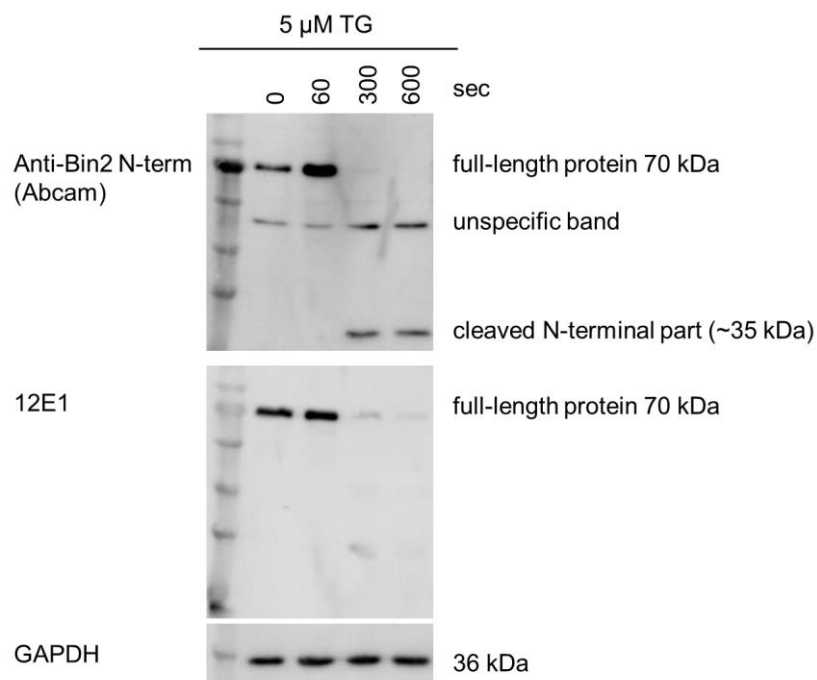
Figure 3-32: The anti-BIN2 antibody 12E1 binds to the C-terminal part of the protein. The purified antibody from the supernatant of the hybridoma cell clone 12E1 was tested for its ability to detect the cleaved N-terminal part of BIN2. To this end, *WT* platelets were treated with TG for the indicated time points and platelet lysates were prepared for Western blot analysis. For comparison, a commercially available antibody which specifically detects the N-terminal part of BIN2 was used in addition on the same membrane.

The unstructured C-terminal part was not detected anymore, indicating a rapid degradation. Interestingly, when 12E1 was used, the band at 75 kDa disappeared upon cleavage, but no band at 35 kDa appeared, suggesting that 12E1 binds to the (degraded) C-terminal part of BIN2 (Figure 3-32).

3.2.6   Visualization of BIN2 in resting and spread platelets

To investigate the localization of BIN2 in murine platelets, we used the newly generated anti-BIN2 antibody (clone 12E1) in dSTORM. Resting platelets were immobilized on glycine, while thrombin-activated platelets were allowed to spread on fibrinogen prior to the staining procedure. An inhomogeneous distribution of BIN2 in the cytoplasm was detected in resting *WT* platelets, whereas no staining was observed in *Bin2*$^{fl/f,Pf4Cre+/-}$ platelets (Figure 3-33 A). In spread *WT* platelets, BIN2 mainly located to the cell center in small clusters (Figure 3-33 B). These results are indicative for an accumulation of BIN2 at internal membranes. However, due to the lack of functional *d*STORM antibodies for STIM1 or IP$_3$R, no co-localization studies could be performed with mouse platelets.

Using a MK/platelet-specific knockout (KO) mouse model, this study demonstrated a key role of BIN2 in Ca^{2+} store release and SOCE in platelets by directly or indirectly interacting with two key molecules in Ca^{2+} homeostasis, IP$_3$R and STIM1. In parallel, Charly Kusch demonstrated the colocalization of BIN2 and STIM1 in human platelets using two-color *d*STORM, emphasizing a potential role of this interaction also in humans.

Figure 3-33: BIN2 localization in resting and spread platelets. (A) Resting *WT* and *Bin2*$^{fl/fl,Pf4Cre+/-}$ platelets immobilized on glycine and (B) thrombin-activated platelets spread on fibrinogen, were permeabil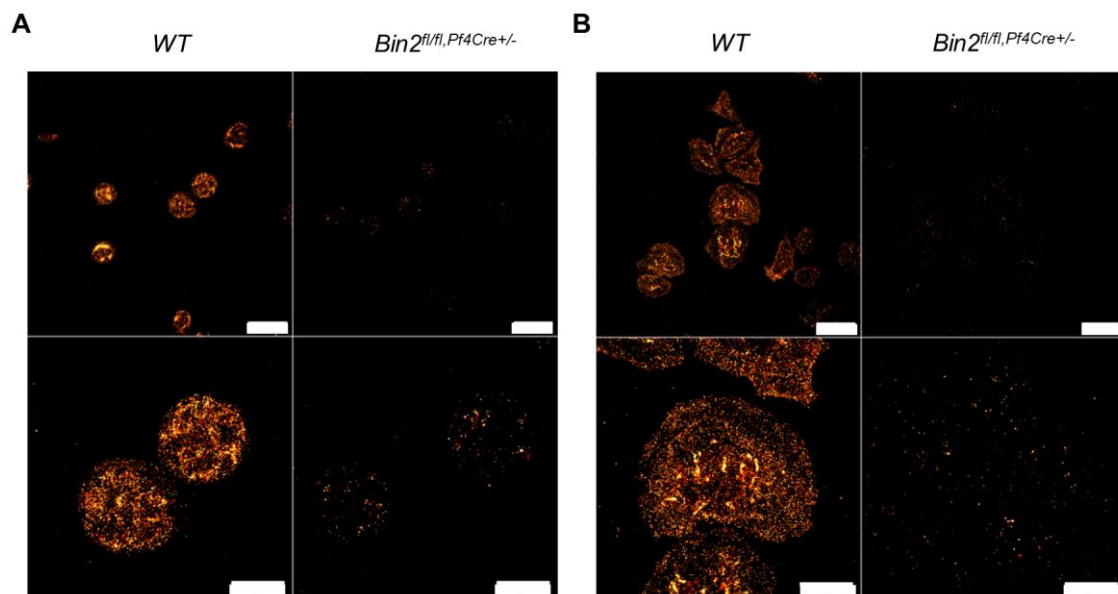ized and stained with the anti-BIN2 antibody 12E1. Scale bar: upper panel: 5 µm, lower panel: 2 µm These experiments were performed in collaboration with Charly Kusch.

3.3 Sema7A promotes platelet aggregate formation under flow

Prof. Peter Rosenberger and Dr. David Köhler (Department of Anesthesiology and Intensive Care Medicine, Tübingen) investigated the role of the *neuronal guidance protein* (NGP) Sema7A on thrombo-inflammation in MIRI.[178] Soluble SEMA7A was found to be elevated in MIRI patient blood. The injection of commercially available recombinant Sema7A (Gln45-Ala646)-mouse IgG$_{2A}$-Fc fusion protein (referred to as rSema7A) into *WT* mice increased the infarct size upon MIRI dramatically, underlining a functional role of Sema7A in MIRI progression. Using different organ specific Sema7A knockout animals, RBCs were identified as mayor source for the soluble Sema7A. Furthermore, PNCs were increased upon rSema7A treatment, indicating a potential effect of Sema7A on platelets and neutrophils.

Therefore, an initial characterization of the effect of rSema7A on platelet function was performed as a collaboration in the framework of this project. Additionally, a 19 amino acid long (KLGFTYVTIRVTYQIRVAG) *Sema7A fragment* (SL4cd), a core structure of the Sema7A-plexinC1 interface[202] was also investigated.

3.3.1 No effect of rSema7A on platelet activation or aggregation *in vitro*

To characterize the effect of rSema7A and the Sema7A peptide SL4cd on platelet activation, flow cytometric analysis of integrin αIIbβ3 activation and degranulation was performed. Platelets were pretreated with two different concentrations of rSema7A, SL4cd or the control IgG$_{2A}$-Fc and subsequently αIIbβ3 activation and P-selectin exposure were measured (Figure 3-34). Interestingly, neither 1 µg/ml nor 10 µg/ml rSema7A or SL4cd induced detectable activation of platelets. Moreover, rSema7A- or SL4cd-pretreated platelets, which were additionally stimulated with ADP, did not display differences in integrin αIIbβ3 activation or degranulation compared to control or IgG$_{2A}$-Fc-pretreated platelets, indicating that rSema7A is not able to potentiate platelet activation in this experimental setup.

In line with the unaltered αIIbβ3 activation and degranulation upon treatment with rSema7A and SL4cd, no aggregation was induced using 2 µg/ml and 6 µg/ml rSema7A or SL4cd (Figure 3-35). To test whether the pretreatment of washed platelets with rSema7A for 5 min can influence the aggregation pattern upon a second stimulus, pretreated platelets were activated using ADP (Figure 3-35).
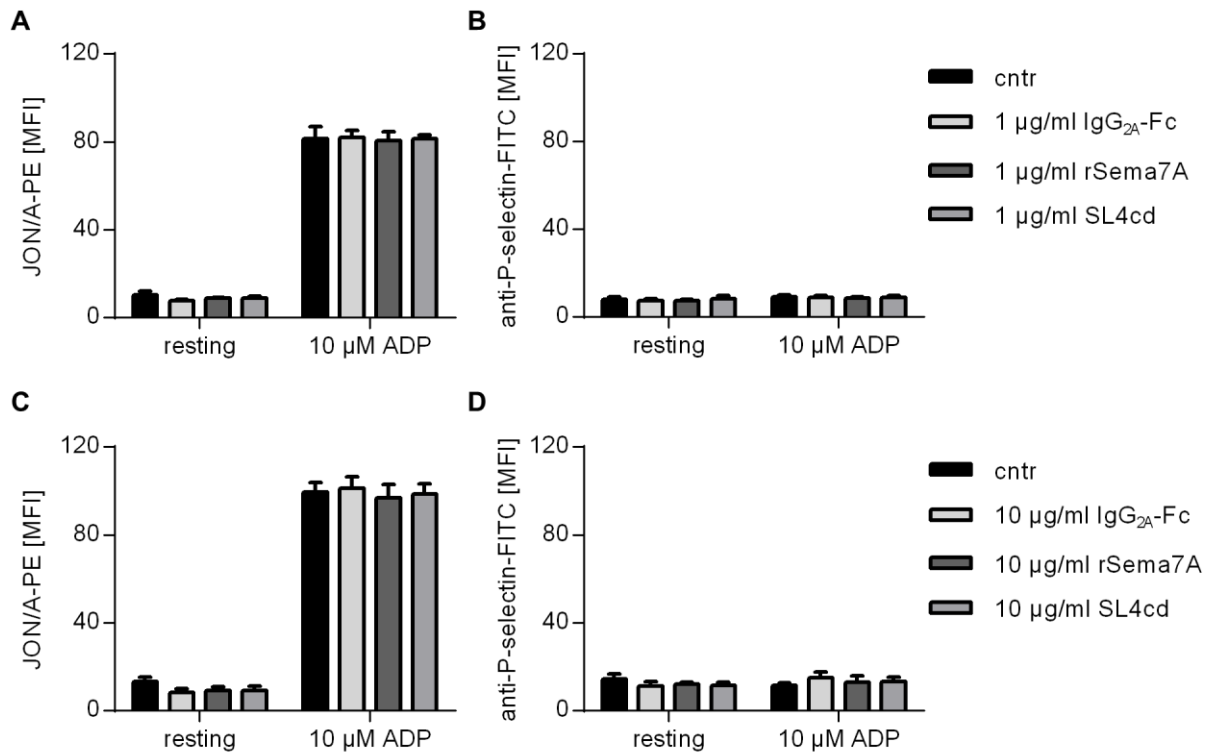
Figure 3-34: No effect of rSema7A and SL4cd on integrin αIIbβ3 integrin activation or degranulation. Flow cytometric analysis of integrin αIIbβ3 activation (JON/A-PE binding) and degranulation (P-selectin exposure) of platelets pretreated with low dose (A,B) or high dose (C,D) of rSema7A, SL4cd or IgG$_{2A}$-Fc without stimulation or in response to 10μM ADP. MFI ±SD. n=4.

However, no difference in aggregation was observed in the presence of rSema7a compared to the untreated samples. These results demonstrate that rSema7A has no effect on platelet activation and aggregation in the tested *in vitro* assays under static as well as stirring conditions.
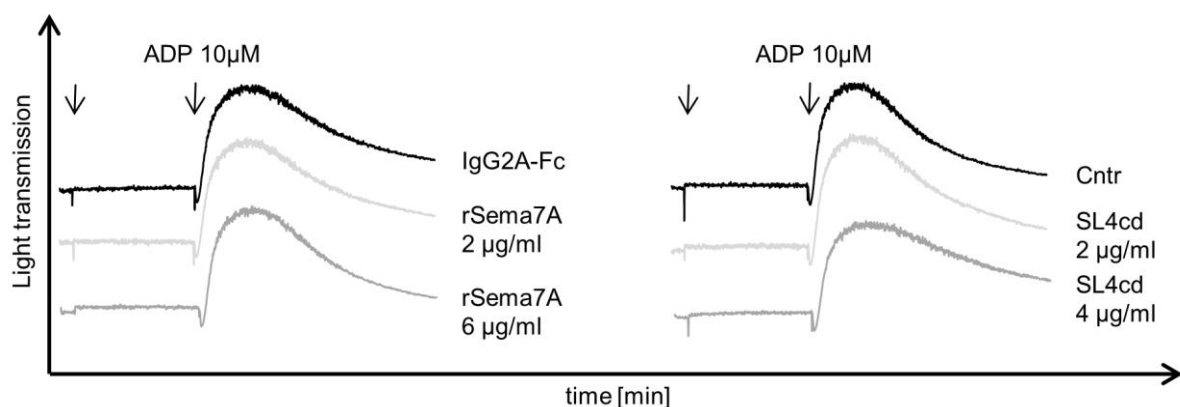
Figure 3-35: Unaltered platelet aggregation upon rSema7A or SL4cd treatment. Platelets were treated with IgG$_{2A}$-Fc, rSema7A or SL4cd and light transmission was recorded using a four channel aggregometer. 5 min post treatment with the indicated proteins aggregation was induced using 10 μM ADP and measured for another 6 min. Representative aggregation curves of 3 independent experiments are shown.

3.3.2 rSema7A increases thrombus volume on collagen under flow

At sites of vascular injury, platelet function is highly dependent on the prevailing shear forces, which vary in different vascular beds. To study the role of Sema7A in a more physiological setup, aggregate formation of platelets under flow conditions was assessed. To this end, anti-coagulated, diluted whole blood was pretreated with rSema7A or SL4cd (1 µg/ml) and perfusion experiments using collagen-coated flow chambers were performed. At an intermediate shear rate of 1000 s^{-1}, reflecting arterial blood flow, platelets rapidly adhered and formed three-dimensional aggregates as quantified by surface coverage and relative thrombus volume. Both parameters were markedly increased when the blood was pretreated with rSema7A compared to the IgG$_{2A}$-Fc control (Figure 3-36 A, B). This was not observed when heat-denatured rSema7A (96°C for 10 min) was used, demonstrating the importance of correct protein folding of rSema7A to exhibit its prothrombotic effect. Interestingly, the Sema7A peptide SL4cd also induced an increase in surface coverage and relative thrombus volume (Figure 3-36 C, D), indicating that these 19 amino acids contain the responsible domain for the observed pro-thrombotic effect of the protein.
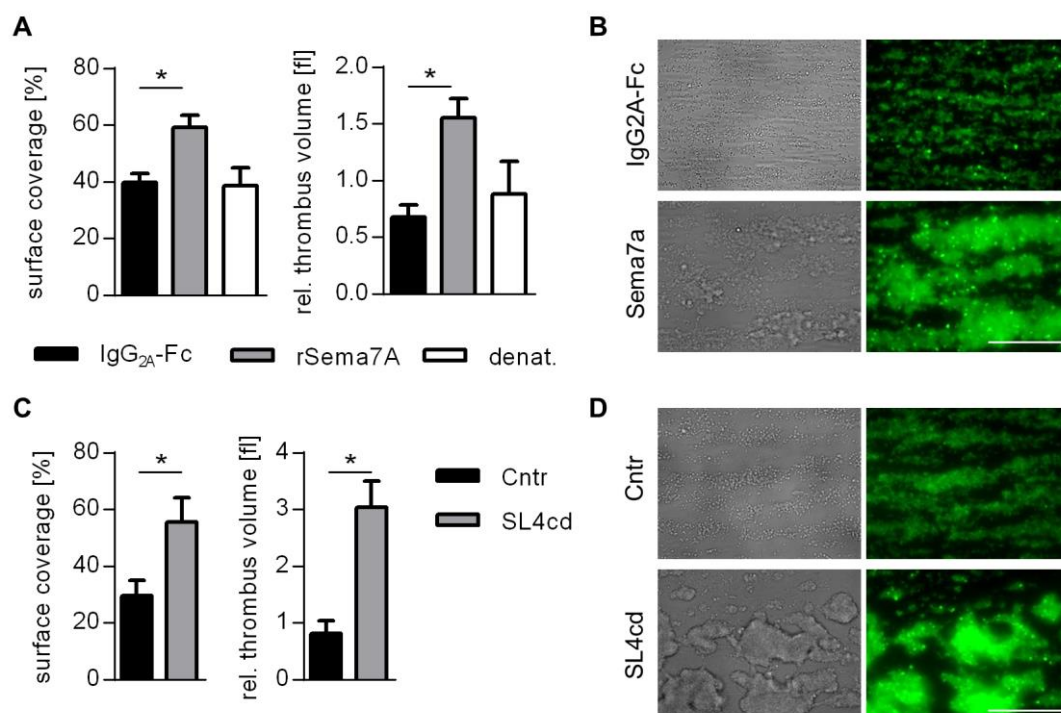
Figure 3-36: Increased thrombus formation on collagen under flow upon rSema7A or SL4cd treatment. Whole blood from *WT* animals, pretreated for 5 min with (A, B) IgG$_{2A}$-Fc control, rSema7A and denatured Sema7A (C, D) or PBS and SL4cd, was perfused over collagen with a shear rate of 1000 s^{-1} and platelet surface coverage and relative thrombus volume is depicted as mean ± SD. Representative bright field and fluorescence images are shown in B and D. One representative of 3 independent experiments, n=4. Scale bar: 50 µm.

3.3.3 The effect of rSema7A is GPIb- and plasma factor-dependent, but vWF-independent

The presence of the prothrombotic rSema7A effect under flow but its absence in the static assays emphasize a flow-dependence and suggest the involvement of a shear-dependent mechanism, as established for GPIb. To test this assumption, the effect of rSema7A treatment in the flow assay on collagen was assessed as described above using blood from GPIbα-hIL-4r-tg mice (Figure 3-37), where the extracellular domain of GPIbα is replaced by the extracellular part of the hIL-4r. As previously published,[2] a reduction of surface coverage and thrombus volume was observed, when GPIbα was absent from the platelet surface. Interestingly, rSema7A treatment did not increase platelet adhesion or the thrombus volume in blood from GPIbα-hIL-4r-tg mice. This supports the assumption of a GPIbα-dependent effect of rSema7A on platelets. Further evidence was provided by the blockade of GPIbα in *WT* blood using Fab fragments of the p0p/B antibody, which also abolished the thrombus increasing effect of rSema7A (Figure 3-37).
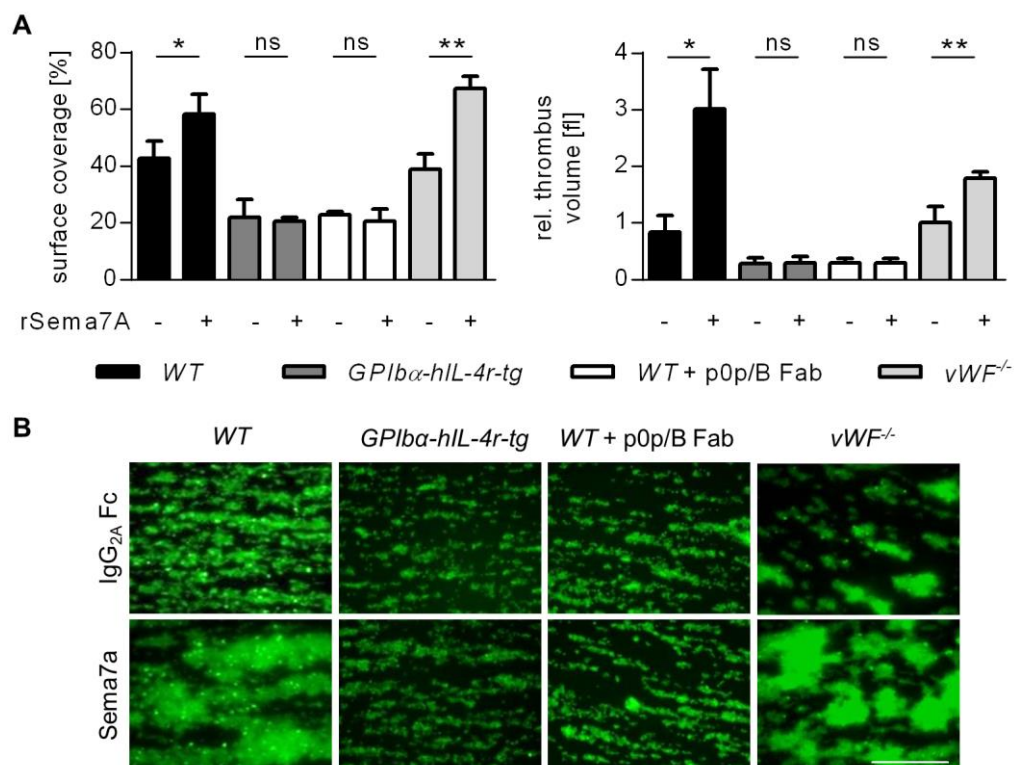
Figure 3-37: No pro-thrombotic effect of rSema7A in GPIbα-hIL-4r-tg or p0p/B Fab-treated *WT* animals. (A) Whole blood from *WT*, *GPIbα-hIL-4r-tg*, p0p/B Fab-treated *WT* or *vWF*^{-/-} animals, pretreated for 5 min with IgG$_{2A}$-Fc control or rSema7A, was perfused over collagen with a shear rate of 1000 s^{-1} and platelet surface coverage and relative thrombus volume are depicted as mean ± SD. (B) Representative fluorescence images. One representative of 3 independent experiments; n=4. Scale bar: 50 μm.

p0p/B is known to block the vWF and thrombin binding site on GPIbα. vWF is one of the most prominent interaction partners of GPIbα, which is present in the plasma and can also be released from platelet granules upon activation. To investigate whether the observed GPIbα-rSema7A effect also depends on vWF, blood from vWF knockout mice (*vWF$^{-/-}$*) was perfused over collagen-coated slides. Interestingly, the increase in surface coverage and thrombus volume was still clearly visible and comparable to *WT* controls, thus strongly suggesting a vWF-independent effect of rSema7A on GPIbα.

Besides vWF, there are many other factors present in blood, which can influence the ability of platelets to form stable thrombi. To analyze if the effect of rSema7A on GPIbα is dependent on plasma factors, a plasma factor-free flow adhesion assay was performed. To this end, RBCs and platelets were washed separately to remove all other blood components and then mixed together and reconstituted with Ca^{2+} and fibrinogen. In the absence of plasma factors, the pretreatment with rSema7A had no effect on platelet adhesion on the collagen-coated surface or the thrombus volume (Figure 3-38), demonstrating the dependence of this interaction on additional factors in the blood.
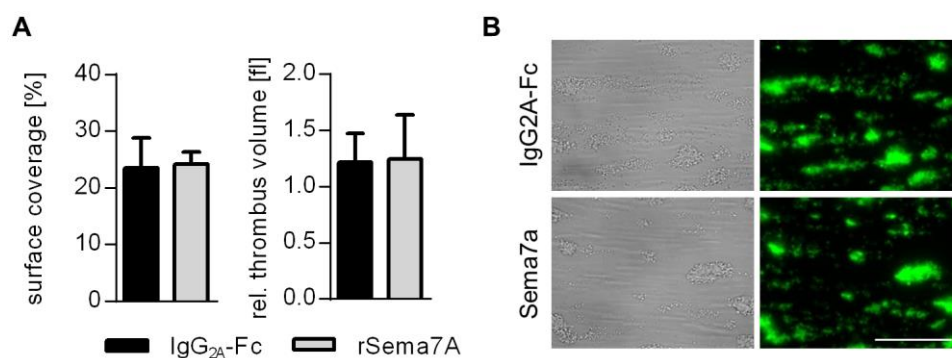
Figure 3-38: No thrombus-promoting effect of rSema7A in the absence of plasma factors. (A) Platelets and RBCs were washed separately to remove all other blood components, followed by mixing and reconstitution with Ca^{2+} and fibrinogen. Afterwards, reconstituted blood was perfused over collagen at a shear rate of 1000 s^{-1} and platelet surface coverage and relative thrombus volume were measured. (B) Representative fluorescence images. One representative of 3 independent experiments; n=4. Scale bar: 50 μm.

Taken together, the flow chamber experiments revealed that the effect of rSema7A on platelets is mediated by GPIbα and is dependent on additional plasma factors. However, the GPIbα ligand vWF is not involved in this process.

4 Discussion

4.1 GPVI is a major regulator of tumor vascular integrity

This thesis establishes the platelet- and megakaryocyte-specific collagen/fibrin receptor GPVI as a key regulator of vascular integrity in solid tumors and proposes its inhibition as a potential new strategy to increase efficacy of anti-tumor chemotherapy.

Systemic therapeutics are a mainstay of cancer therapy and an indispensable instrument especially for the management of progressed, metastatic disease. The treatment effectiveness with systemically applied therapeutics depends on the efficacy of the drug´s delivery into the targeted tissue. The chemotherapeutic agents accumulate at significantly lower doses in solid tumors than in non-target organs, increasing side-effects and thereby the risk of a prematurely terminated treatment.[203-206] However, it is essential that anti-cancer drugs reach tumor cells in concentrations sufficient to exert their therapeutic effect. Thus, development of selective anti-cancer strategies to increase accumulation of drugs within solid tumors represents an important goal in oncology research. One major reason for reduced transport of therapeutics into the tumor is the highly dysfunctional vasculature caused by the chronically inflamed TME and its highly pro-angiogenic profile. Additionally, the abundant, highly condensed ECM including collagens found in solid tumors represent physical barriers impeding effective intratumoral drug transport.[207,208] Improving vascular function has long been discussed as a possibility to increase tumor drug transport.[209] But experimental evidence indicates that the normalization of the vasculature by anti-angiogenic drugs actually further inhibits drug transport by reducing vascular density.[210-213] This would be in line with the intended purpose of these agents to starve the tumor by depriving it of its ability to initiate the growth of new supplying blood vessels.[182,214,215] However, in other reports, a remodeling of the vasculature mediated by inhibition of pathological aspects of tumor angiogenesis increases the accumulation and efficacy of tumor-directed systemic drugs.[216-219] Following the idea to interfere with tumor vascularization, the results of this thesis demonstrate that exploiting the vulnerability of the already damaged tumor vasculature by provoking a complete vascular collapse due to platelet targeting can facilitate the drug delivery to the tumor sites.

Platelets are critical for maintaining a minimum of tumor vascular integrity. Ho-Tin-Noé *et al.* have shown that platelet depletion in mice selectively renders tumor vessels highly permeable. The thrombocytopenia-induced profound bleeding was specifically found at the tumor site, while other organs remained unaffected.[132,136] This effect seems to be largely independent of tumor age, type and affected organ, as it is observed in models of subcutaneous melanoma,

melanoma lung metastasis and mammary carcinoma.[132,134,136] In line with this, acute thrombocytopenia results in decreased tumor growth in a mouse model of ovarian carcinoma.[220] Furthermore, Demers *et al.* have also demonstrated that platelet depletion favors intratumoral accumulation of the chemotherapeutic agent paclitaxel.[134] The accumulation of anti-cancer drugs within the tumor tissue upon platelet depletion could be reproduced in this thesis (Figure 3-10). However, while effective in experimental animals, the induction of acute thrombocytopenia in cancer patients is not a therapeutic option due to severe side effects on hemostasis. Thus, it is imperative to identify the molecular mechanisms how platelets safeguard vascular integrity in tumors in order to develop anti-platelet agents allowing selective destabilization of the tumor vasculature during chemotherapy in patients without triggering unwanted systemic bleeding complications. In the here presented thesis, the inhibition of GPVI on the platelet surface had comparable effects on the tumor vasculature and tumor growth as platelet depletion (Figure 3-1; Figure 3-12). GPVI-inhibition enhanced the anti-tumor effect of the drugs without affecting its overall toxicity or impairing classical hemostasis, thus representing a safer treatment option. Paclitaxel and liposomal doxil, two widely used chemotherapeutic agents with a different mode of action,[221,222] accumulated much longer in treated tumors. Paclitaxel is a microtubule stabilization agent, which blocks the cells in G2/M-phase, whereas doxil intercalates into the DNA and inhibits macromolecular biosynthesis.[221,222] The prolonged accumulation of these drugs was most likely attributed to a flush-out-and-trapping effect (Figure 4-1). Drug levels were already higher immediately after co-administration of platelet-targeted antibodies and cytotoxic drug due to the induced hemorrhage compared to cytotoxic drugs alone. However, the difference in drug concentration was even more evident after 24 h. In control animals, drug levels decreased significantly over 24h, as the agents were secreted. Since this was not possible in the R300 or JAQ1 F(ab')$_2$ treated tumor-bearing mice because the affected compartment was secluded from the bloodstream after treatment-induced vascular collapse, drug levels within the tumor tissue remained high.

In line with previous work,[132,134] strong hemorrhage and subsequent necrosis in the treated tumors was observed, but only in the here presented study, using AT3 breast and TrampC1 prostate cancer models, this resulted in a reduction of tumor growth. In contrast, the Lewis lung carcinoma (LLC) and 4T1 breast cancer models used by Ho-Tin-Noé and Demers *et al.* were unaffected by these detrimental events.[132,134] However, the tumor size at the time of the treatment was much smaller (treatment at day 8 vs treatment at day 20/22 in this study). Moreover, platelet depletion was performed only once and the observation period was noticeably shorter compared to the here presented study (6 days of tumor size measurement

post-treatment vs 9 days). Another explanation could be the presence of other oncogenic factors in these models which may improve vascularization within the developing tumor, but this clearly requires further investigation.
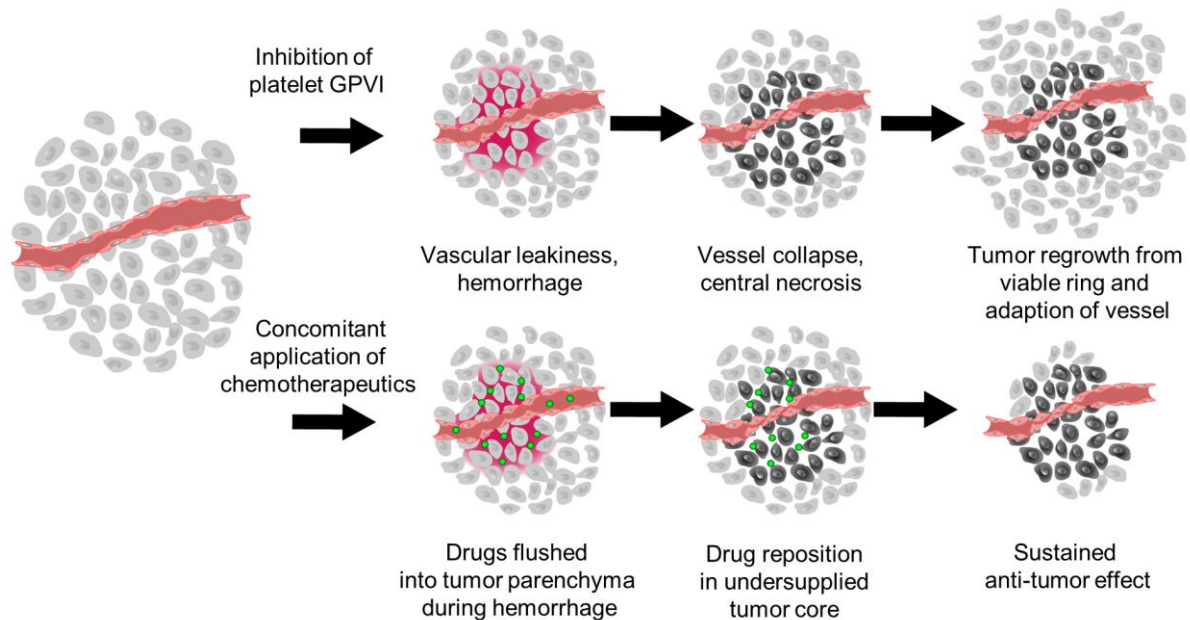
Figure 4-1: Flush-out-and-trapping effect. (Upper panel) Platelet-depletion or inhibition of platelet function by targeting GPVI interferes with the integrity of the defective tumor vasculature. The resulting increase in leakiness and hemorrhage leads to vascular collapse, and an acute undersupply foremost in the central core region of the tumor. However, as the outer rim of the tumor is much less affected, the tumor can rebound. (Lower panel) Concomitantly administered drugs are flushed into the tumor tissue during the hemorrhagic period. As the supplying vasculature collapses, this drug repository is trapped within the necrosis bound central core. Via diffusion it can effectively fight tumor cells in the surrounding, still viable, rim. (Published in Volz *et al. Blood*, 2019)[195]

Although R300 or JAQ1 F(ab')$_2$ treatment lead to an acute undersupply resulting in necrosis of up to 80% of the tumor tissue, a complete stop of tumor growth or a regression was not achieved even with repeated treatments in the absence of chemotherapeutic agents. This is in line with previous observations after anti-angiogenic therapy or treatment with agents, disrupting vascular integrity.[223,224] These vascular intervention therapies mostly affect highly disorganized vessels in the center of the tumor while leaving the margin of the tumor that is supplied by more functional vessels unharmed. From this "viable rim" tumors can recuperate (Figure 4-1).

The here depicted results revealed a key role of GPVI in safeguarding vascular integrity in growing tumors. Besides its critical function in thrombus formation, GPVI is increasingly recognized as a central modulator of thrombo-inflammatory pathologies.[84] In an experimental glomerulonephritis model, GPVI supports platelet adhesion and leukocyte infiltration into the

inflamed tissue.[225,226] Furthermore, in a model of autoimmune rheumatoid arthritis, GPVI mediates the recruitment of platelets to inflamed joints, thereby increasing permeability of the synovial microvasculature and local recruitment of neutrophils.[227] Although it may seem counter-intuitive, as GPVI promotes opening of endothelial junctions and vascular permeability, in distinct inflammatory conditions single platelets seal neutrophil-induced vascular breaches via GPVI.[84] Notably, this is observed in a cutaneous reverse passive Arthus (rpA) inflammation model, in which genetic GPVI deficiency increases bleeding.[84,87] Based on these studies a model has been postulated where platelets may "seal" vascular leakages by adhering to the exposed extracellular matrix (collagens and laminins) in a GPVI-dependent manner.[87,88] This model could, however, not be validated in this thesis for the tumor environment since the number of platelets observed on the vessel wall was indistinguishable in tumors of control and GPVI-inhibited animals (Figure 3-9). Interestingly, $Gp6^{-/-}$ mice challenged in the LPS-induced lung injury model did not display any bleeding phenotype,[87] suggesting that the role of GPVI in maintenance of inflammatory hemostasis is organ and stimulus-dependent.

During cancer progression, innate immune cells, in particular neutrophils, migrate to tumor niches, causing intratumoral hemorrhage and amplifying inflammatory reactions. This in turn results in more aberrant angiogenic signaling and promotion of the defective tumor vessel phenotype.[196-198,228] The data depicted in this thesis provides evidence that the platelet response required to prevent hemorrhage may be similar for cutaneous and tumor inflammation context, emphasizing the role of cancer as an inflammatory disease. In line with this, thrombocytopenia induced bleeding is observed in a variety of tumor types, such as subcutaneous Lewis lung carcinoma, B16F10 melanoma models and 4T1 mammary tumor.[132,134] This suggests that targeting GPVI to improve the efficiency of drug delivery and chemotherapy could be beneficial in a large variety of tumors.

The vasculature disintegrating-effect of GPVI-inhibition was strongly diminished upon depletion of neutrophils (Figure 3-14; Figure 3-15). This is in line with previous studies showing that induction of thrombocytopenia in β2 (CD18) or β3 integrin-deficient mice, which are characterized by a reduction of infiltrating macrophages and neutrophils into the tumor, results in decreased tumor hemorrhage compared to control mice with thrombocytopenia.[136] Together, this emphasizes that neutrophils are to a large extent responsible for the bleeding associated with thrombocytopenia or GPVI-inhibition. Since neutrophil recruitment into the tumors was not GPVI-dependent (Figure 3-16), it appears that GPVI is required to "repair" or limit neutrophil-induced vascular damage. Indeed, major hemorrhagic spots in the tumors were found almost exclusively at sites of neutrophil accumulation (Figure 3-13). However, for a detailed

understanding of the exact mechanisms leading to intratumor bleeding and its prevention by platelets, dynamic imaging of neutrophil-endothelial cell-platelet interactions in the tumor will be required.

Obviously, neutrophils fulfil overall comparable functions in innate immunity in humans and mice. However, there are also potentially relevant species differences, especially with respect to relative leukocyte numbers, certain subpopulations (N1/N2), or attributed granule functions (i.e. defensin expression),[229] making a direct extrapolation of mouse studies to human patients difficult. Neutrophils are rich sources of *reactive oxygen species* (ROS)-generating enzymes, proteases and matrix metalloproteases[228] and platelets have been reported to inhibit (or take up and store) cytotoxic releasates from tumor-inflicting neutrophils, which might contribute to their vessel protective effect.[230-232] A possible role of GPVI in this process has not been studied so far.

Another important finding of this thesis is that pharmacological GPVI inhibition produced a more pronounced tumor hemorrhage than genetic GPVI-deficiency (Figure 3-1; Figure 3-18). The observation that the sudden blockade of a platelet adhesion receptor may have stronger effects than its genetic deficiency is not entirely unexpected as this has previously also been reported for αIIbβ3 in the setting of ischemic stroke. While αIIbβ3 inhibitors provoke massive intracranial hemorrhage in acute stroke in mice[233] and humans,[234,235] this is not seen in mice being genetically deficient for αIIbβ3.[236] Although the exact underlying pathways remain to be identified, these studies strongly suggest that compensatory mechanisms are activated in GPVI- or αIIbβ3-deficient mice (and probably also humans) to minimize hemostatic and/or vascular defects resulting from the genetic deficiency in platelet effector functions.

In the here presented study, antibody-mediated blockade of GPVI or induction of thrombocyto-penia enhanced the accumulation of two different cytotoxic drugs, doxil and paclitaxel, specifically in AT3 and TrampC1 tumors. There are also indications that platelets directly increase resistance against paclitaxel.[237] Platelets increased survival of tumor cells in culture subjected to paclitaxel, even if co-incubated without direct contact to tumor cells across a barrier with 0.4 µm pores. This suggests that platelet secreted factors might have chemopro-tective effects, at least against paclitaxel. Therefore, platelet inhibition might also have a beneficial effect by inhibiting the secretion of chemoprotective factors.

Earlier, other platelet adhesion receptors such as αIIbβ3 and GPIb have also been proposed as anti-tumor targets as they have been implicated in tumor growth and metastasis.[89,238-242] While these receptors are essential for normal hemostasis, their genetic deficiency did not cause major inflammation-induced bleeding in most mouse models in different organ

systems.[88,243] In this thesis, their role in the maintenance of vascular integrity was assessed by antibody-mediated blockade, without observing bleeding in the tumor (Figure 3-1). This indicates that both, αIIbβ3 and GPIb, are dispensable for vascular stabilization in the primary tumor, yet they are indispensable for classical hemostasis, emphasizing the mechanistical differences between these two processes.

Platelets contribute to tumor metastasis, e.g. by shielding circulating tumor cells from the immune system in the blood, as well as by actively enhancing tumor cell migration and extravasation.[114,238,242,244,245] The potential of GPVI-inhibition to reduce the capacity for metastasis formation was demonstrated previously.[246] This indicates multiple beneficial effects of GPVI inhibition by concomitantly decreasing the primary tumor growth, increasing drug deposition, reducing chemoprotection and inhibiting further metastasis.

Of note, GPVI is exclusively expressed on megakaryocyte/platelet lineage, which largely excludes risk of side effects of anti-GPVI agents on other cell types. Due to its role in thrombotic diseases, considerable effort is currently put into the development GPVI inhibitors. Recently, the soluble dimeric GPVI receptor fusion protein, Revacept, has been successfully evaluated in a phase I clinical trial and is currently undergoing a phase II for treatment of a variety of thrombotic pathologies.[82,247] Furthermore, a humanized anti-GPVI antibody (ACT017) was developed and a first clinical trial demonstrated its safety and tolerability.[248,249] In light of these observations and the here presented results, targeting GPVI may represent a seducing approach associating safety to efficacy not only towards thrombotic diseases but also beyond. In our laboratory, several humanized anti-GPVI antibodies have been produced, which reduce the collagen-induced platelet activation in humanized mice and human platelets (Navarro *et al.*, unpublished), thereby also representing promising tools to block GPVI in humans.

In conclusion, this thesis highlights a crucial tumor-supporting role of GPVI and provides a proof of concept that targeting of this platelet receptor could be therapeutically effective against cancer.

4.2 BIN2 is a key regulator of platelet calcium signaling

For the first time, this thesis describes BIN2 as a key regulator of platelet Ca^{2+} signaling. Its deficiency has no influence on Ca^{2+} store content or IP_3 production, but it impairs Ca^{2+} store release as well as Ca^{2+} influx across the plasma membrane. BIN2 was shown to be the first adapter protein that interacts with both, IP_3R and STIM1, thereby connecting Ca^{2+} store release and SOCE function (Figure 4-2).
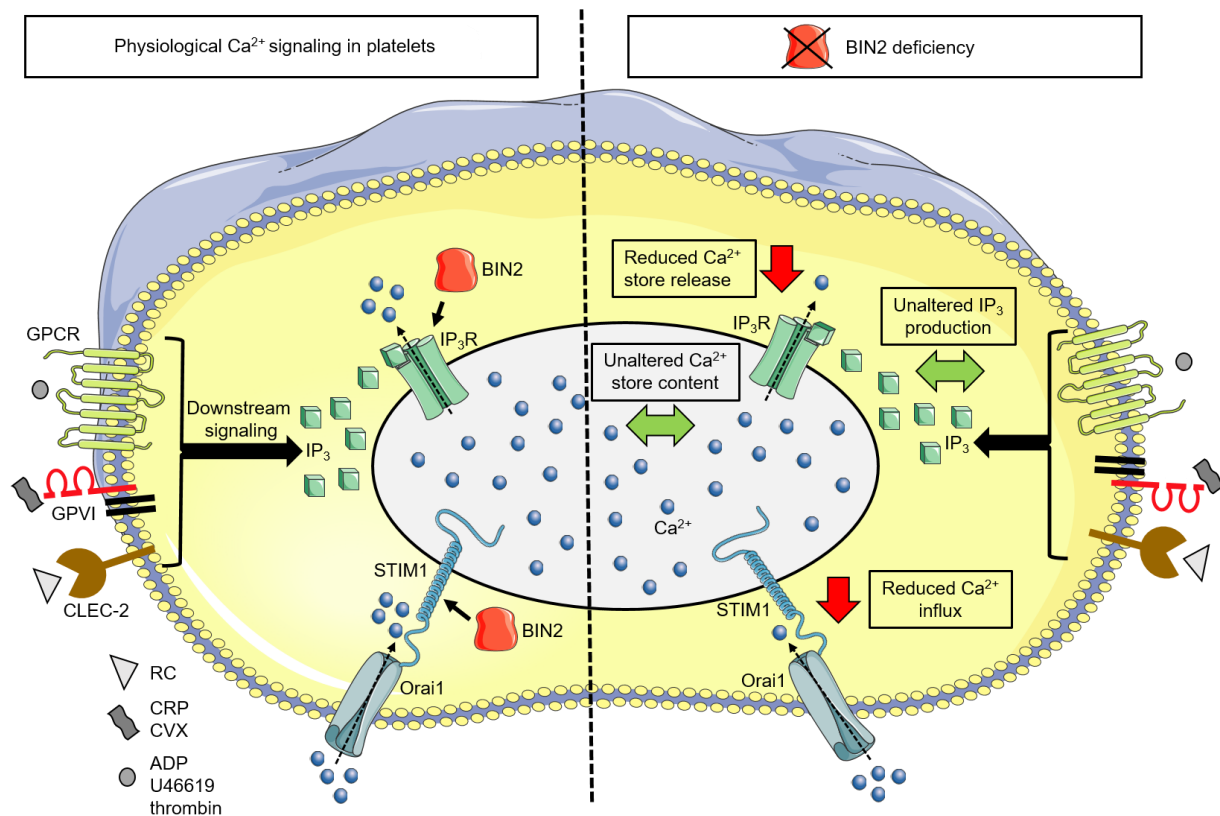
Figure 4-2: Simplified model of physiological Ca^{2+} signaling in platelets and the influence of BIN2 on these processes. Agonist_induced receptor activation leads to the production of *inositol-1,4,5-triphosphate* (IP_3). IP_3 activates its receptor (IP_3R) in the DTS membrane, inducing Ca^{2+} store release. The reduced Ca^{2+} concentration in the store is sensed by *stromal interaction molecule 1* (STIM1), which opens the *Ca^{2+} release-activated Ca^{2+}* (CRAC) channel Orai1 in the plasma membrane, allowing Ca^{2+} influx across the plasma membrane. BIN2 interacts with both, IP_3R and STIM1, and its deficiency dramatically reduces Ca^{2+} release as well as Ca^{2+} influx. (Graphic design: Julia Volz using Servier Medical Art: https://smart.servier.com/)

First evidence that IP_3R can modify Ca^{2+} influx, not only indirectly by releasing Ca^{2+} from the internal store, but also by a direct effect on major regulators of Ca^{2+} entry, was its reported interaction with transient receptor potential (TRP) channels in HEK cells.[250] Conversely, another study revealed a regulating effect of STIM1 on the activity of IP_3R by direct interaction of both proteins in bovine aortic endothelial cells.[251] Also, in STIM1 KO, but not in Orai1 KO platelets a reduced store release was detected in response to all tested agonists.[52,53] However,

the diminished store content in these platelets made a direct conclusion on the functional influence of STIM1 on IP$_3$R difficult. Furthermore, immobile IP$_3$R clusters, responsible for the Ca^{2+} release from the ER, co-localize with STIM1 puncta that form upon activation of SOCE.[59] The association of IP$_3$R to STIM1 has been shown to provide a reduced calcium microenvironment near the STIM1 EF-hand, its calcium sensing part residing inside the Ca^{2+} store, thereby facilitating *puncta* formation and enhancing Orai1 activation and SOCE.[60] Based on the here presented data showing that BIN2 interacts with both, IP$_3$R and STIM1 (Figure 3-28), it is tempting to speculate that BIN2 may be involved in the formation of these IP$_3$R-STIM1 complexes. However, further studies will be required to unravel the exact underlying molecular mechanisms.

Interestingly, BIN1, another member of the BIN protein family, has recently been identified to be a T-tubule anchoring protein, regulating the microtubule-mediated transport and surface expression of the voltage-dependent L-type calcium channel Cav1.2 in cardiomyocytes.[144] Cardiomyocyte-specific loss of BIN1 results in a decreased number of protective membrane folds of T-tubules and alters cation diffusion within the T-tubules, thus increasing the duration of action potentials.[145] Furthermore, Bar domain proteins can bind small GTPases like the Rho GTPases family members Rac1 or Cdc42 controlling the assembly and disassembly of the actin cytoskeleton.[138] Therefore, one might assume that BIN2 may control ion flux and homeostasis by facilitating specific membrane geometries that enable redistribution of IP$_3$R and STIM1, critical for intact store release and SOCE. However, the ultrastructure (Figure 3-22) as well as the ability to change the morphology during spreading is not altered in BIN2-deficient platelets,[183] indicating that BIN2 exerts its effect on Ca^{2+} signaling via a different mechanism.

As previously described for mice lacking STIM1 or Orai1,[52,53] the severe SOCE defect in BIN2-deficient platelets hardly affects their functional responses to GPCR agonists, but impaired cellular activation through (hem)ITAM signaling. The difference in SOCE dependence between these two major activation pathways is currently not understood. It may be related to different kinetics in IP$_3$ production, since the (hem)ITAM/PLCγ2-axis responds slower to a stimulus compared to the GPCR/PLCβ signaling. Another hypothesis to explain the reduced ITAM signaling in BIN2-deficient platelets is related to their slight reduction in GPVI surface expression, maybe dampening the potential of GPVI to cluster upon ligand binding, which is an important mechanism to regulate GPVI signaling.[73,252] However, the GPVI reduction on the platelet surface is relatively minor, making this hypothesis rather unlikely. Furthermore, the defective ITAM signaling in STIM1- and Orai1-deficient platelets, representing normal GPVI levels on their surface, further disproves this hypothesis.

Of note, slightly decreased expression of the surface membrane proteins GPV and CD9 was also observed in BIN2 deficient platelets. However, the alterations are very minor and therefore it is considered very unlikely that they significantly contribute to the observed platelet-related phenotype of BIN2 deficient mice.

Ambily *et al.* previously performed immunoprecipitation of STIM1 protein from thapsigargin-treated human platelet lysates and identified four potential interaction partners, not including BIN2.[253] This might be explained by methodological differences, since here the interaction of BIN2 and STIM1 was found by using resting platelet lysate, whereas Ambily *et al.* used thapsigargin-pretreated platelets.

BIN2 is dispensable for embryonic development, which is in contrast to the perinatally dying STIM1 and Orai1 mutant animals.[51-53,254] Therefore, STIM1 and Orai1 may not be suitable pharmacological targets for long-term treatment of thrombotic diseases, due to undesired effects on different tissues such as immune cells and skeletal muscle, also observed in patients with STIM1 or ORAI1 mutations.[255] The more restricted expression of BIN2 to the hemato-poietic system and its central role in Ca^{2+} signaling in platelets provides proof of principle that the adaptors involved in Ca^{2+} signaling vary between different cell types and might thereby be good targets to selectively inhibit or modulate the Ca^{2+} signaling machinery in a cell type-selective manner. Indeed, previous studies in our laboratory demonstrated that BIN2 defici-ency significantly reduced cerebral infarct growth in a model of acute ischemic stroke without increasing the risk of intracranial hemorrhage.[183] Furthermore, occlusive thrombus formation in the abdominal aorta following mechanical injury of the vessel by compression with a forceps is impaired in BIN2 deficient animals.[183] In contrast, the hemostatic function, assessed by a tail-bleeding assay was not affected,[183] confirming previous findings that even severely impaired Ca^{2+} signaling in platelets does per se not cause a major hemostatic defect. [51-53]

Although BIN2 is an intracellular molecule and therefore might be difficult to target, further studies will be required to assess its potential druggability. Nevertheless, the here depicted findings corroborate the concept that molecules modulating Ca^{2+} homeostasis specifically in platelets may become promising novel targets for the prevention and/or treatment of thrombotic and thrombo-inflammatory diseases with minimal effects on maintaining hemostasis.

4.3 Prothrombotic effect of soluble Sema7A

This thesis establishes soluble Sema7A as a stimulator of platelet thrombus formation via its interaction with platelet GPIbα. Its prothrombotic activity promotes myocardial thrombo-inflammation and contributes to the outcome of myocardial infarction reperfusion injury.

MI belongs to the leading causes of death worldwide. The most effective therapy for this condition is the immediate reperfusion of the myocardium by recanalization of the occluded coronary artery, significantly improving clinical outcome. However, reperfusion of the affected tissue also induces damage and inflammation, accumulating in severe myocardial dysfunction in a large portion of MI patients.[256,257] This mechanism is called *reperfusion injury* (RI) and is also known following recanalization of infarcted regions in other organs, such as the brain and the liver.[258,259] RI is characterized by large numbers of infiltrating immune cells, inducing inflammatory responses.[260-263] Moreover, platelets are also recognized as major players in this pathology in various ways, emphasizing RI to be a thrombo-inflammatory disease process.[258,259,264,265] The formation of PNCs contributes to the severity of the inflammation for example during acid induced lung injury but also in MIRI.[264,266]

Prof. Peter Rosenberger and Dr. David Köhler from the University Hospital in Tübingen (Department of Anesthesiology and Intensive Care Medicine) describe that Sema7A, shed from RBCs upon shear stress and hypoxia, is an important mediator of MIRI.[178] They show that the increase in PNCs is accompanied by an increase in soluble Sema7A in the plasma as early as 1 minute after reperfusion following MI. To gain mechanistical insights into the upregulation of PNC formation, which might be potentially mediated by Sema7A, the effect of soluble Sema7A on platelet function was investigated in this thesis in collaboration with the group of Prof. Rosenberger. Interestingly, no effect of Sema7A on platelet activation or aggregation was found in static *in vitro* assays (Figure 3-34; Figure 3-35) whereas a prominent prothrombotic activity of Sema7A was observed in a collagen flow adhesion assay at a shear rate of 1000 s^{-1} (Figure 3-36). The shear-dependence suggests a possible involvement of vWF-GPIb signaling, which is known to be specifically important for thrombus formation under conditions of high shear, such as 1000 s^{-1} or 1700 s^{-1}.[2,267] Indeed, the involvement of platelet GPIb in the prothrombotic effect of Sema7A was confirmed in this thesis by the use of GPIbα-hIL-4r transgenic mice, lacking GPIbα, as well as by antibody-mediated blockade of GPIbα (Figure 3-37). Furthermore, Köhler *et al.* provided evidence for an interaction of Sema7A and GPIb by immunoprecipitation.[178] The importance of GPIb in platelet-immune cell interactions and thrombo-inflammatory processes is well established,[258,268] making it a potential therapeutic target. For example, GPIb blockade reduces cranial damage in experimental stroke of healthy,

but also aged and comorbid animals.[258,269] Consistently, GPIbα-hIL-4r transgenic mice depicted a reduced infarct size in the animal model of MIRI.[178] However, an antibody-mediated blockade of GPIb, administered shortly after initiation of reperfusion did not reduce infarct size even though it significantly decreased immune cell infiltration,[80] speaking against GPIb-blockade as a potent target in MIRI. Nevertheless, functional blockade of Sema7A before the start of reperfusion clearly decreased infarct size.[178]

GPIb interacts with a variety of immobilized as well as soluble ligands, such as vWF, P-selectin, Mac-1 and different coagulation factors, while exerting a number of essential platelet functions.[2,270-272] In this thesis, the prothrombotic activity of the Sema7A-GPIb interaction was demonstrated to be plasma factor dependent (Figure 3-38). However, in the absence of vWF, a very prominent interaction partner of GPIb, Sema7A could still increase thrombus formation, indicating that vWF is dispensable for this GPIb-dependent process. SL4cd is a 19 amino acid long (KLGFTYVTIRVTYQIRVAG) Sema7A fragment of the core structure of the Sema7A-plexinC1 interface.[202] The use of SL4cd in activation and aggregation studies a well as in the flow adhesion assay on collagen revealed similar prothrombotic effects, implementing that the GPIb interaction site is also in this region of the Sema7A protein.

Hemostasis and other processes, such as vasodilation, are indirectly influenced by RBCs through the delivery of essential molecules, such as ADP, ATP and nitric oxide.[273,274] Moreover, RBCs provide a membrane platform that contributes to thrombin generation.[275] This study adds Sema7A to the list of RBC supplied modulators of thrombo-inflammation. Whether the cleavage of Sema7A directly impacts RBC function is not known.

The formation of PNCs and the transmigration into the myocardium during MIRI aggravates inflammatory tissue injury. The release of ROS, cytokines, growth factors and coagulation factors activates the endothelium, recruits additional immune cells and initiates apoptotic and necrotic cell death pathways.[264,276] This study demonstrated that the absence of either Sema7A or GPIb or the respective antibody-mediated blockade of these molecules significantly decreases platelet activation and thereby PNC formation, mediating a protective effect in MIRI. The developed mechanism by which RBC-derived Sema7A activates platelet activity in a GPIb-dependent manner, followed by PNC formation and thereby contributes to MIRI is depicted in Figure 4-3.

In summary, the here presented results in combination with the data from the collaborators in Tübingen suggest that interfering with the GPIb-Sema7A interaction during MIRI represents a promising strategy to reduce cardiac damage and improve myocardial outcome following MI.

Nevertheless, further studies are necessary to reveal the exact mechanism of interaction and investigate potential risk of its therapeutic inhibition.
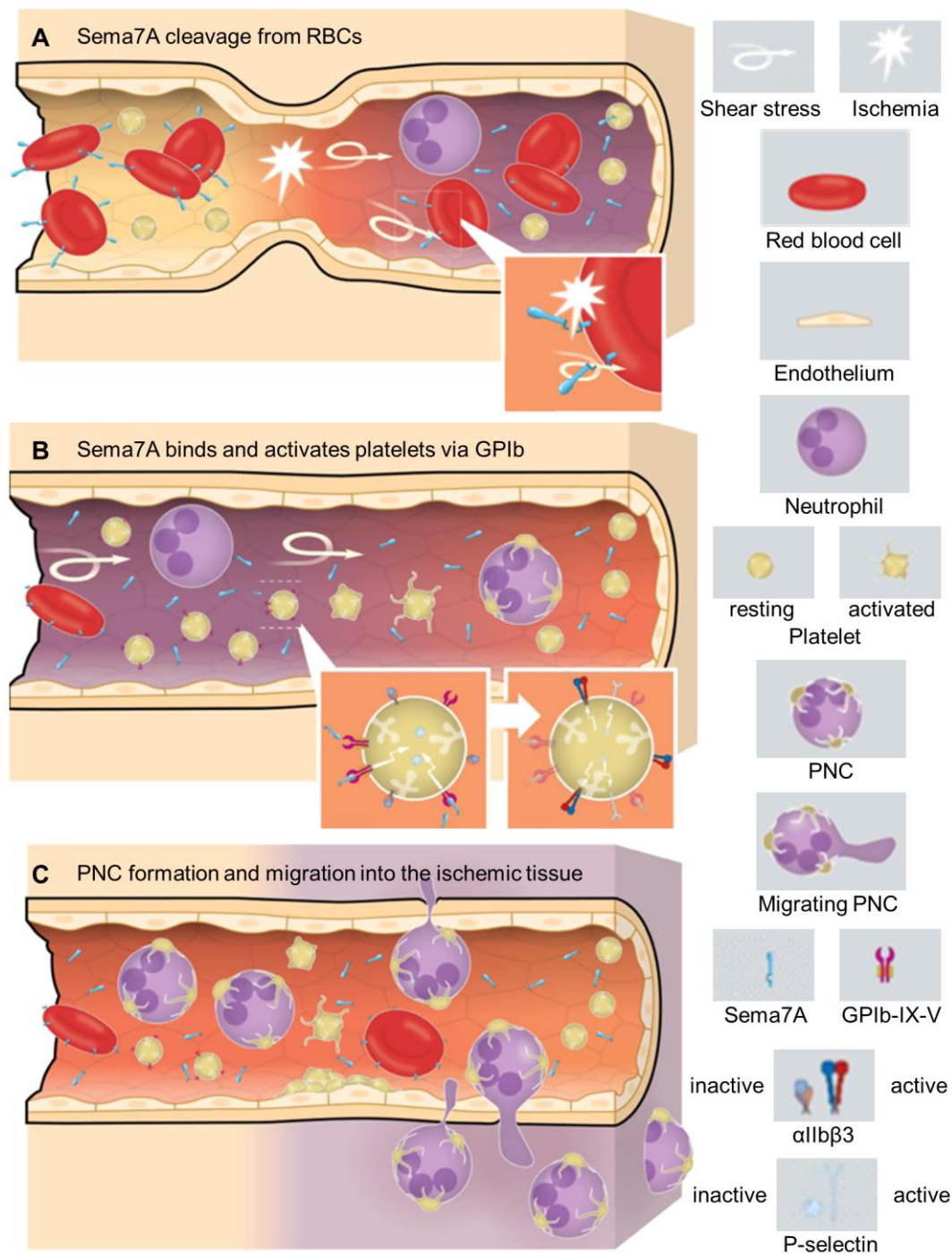
Figure 4-3: Simplified model for the role of Sema7A during MIRI. (A) Shear stress and hypoxia during myocardial ischemia induce Sema7A cleavage from *red blood cells* (RBCs). (B) Soluble Sema7A binds to GPIb on the platelet surface, initiating platelet activation. (C) *Platelet-neutrophil complexes* (PNCs) are formed and transmigrate into the ischemic tissue, resulting in tissue injury and destruction. (Modified from Köhler *et al. Nat. Commun*, 2020)[178]

4.4 Concluding remarks and outlook

In this thesis, the role of GPVI as a major regulator of vascular integrity in tumors was established and its inhibition represents a potential therapeutic strategy to increase the efficacy of chemotherapy without inducing systemic bleeding complications. However, the exact mechanism how GPVI fulfills this function remains to be investigated. To this end, high resolution intravital imaging of the tumor tissue for example by two-photon or confocal microscopy needs to be established to visualize the underlying cellular and molecular processes. Furthermore, it was shown in this thesis that the blockade of GPIb or αIIbβ3 had no significant effect on vascular integrity in tumors. However, the role of the second (hem)ITAM receptor on the platelet surface, CLEC-2 which is involved in maintaining vascular integrity in the course of inflammation in different settings, has not yet been tested in the here presented tumor models. Due to the lack of a CLEC-2 blocking antibody that does not induce thrombocytopenia, the mouse line with a CLEC-2 deficiency and the signaling incompetent CLEC-2 knockin (Y7A KI) mouse line available in our laboratory can be tested in the tumor models to gain insights into the role of CLEC-2 in tumor vascular integrity. Nevertheless, the development of a CLEC-2 blocking antibody or another potent inhibitor which does not interfere with platelet count is mandatory to investigate the potential therapeutic impact of CLEC-2 inhibition.

The discovery of BIN2 as the first Ca^{2+} signaling modulator in platelets that interacts with both IP_3R and STIM1 represents a link between Ca^{2+} store release and SOCE. However, this study could not provide detailed mechanistic insights into these interactions and the molecular mode of action of BIN2. Further biochemical assays may help to reveal the binding domains of the proteins and potential structural changes or modifications (e.g. phosphorylation) upon activation of platelets. Moreover, the expression of BIN2 in the hematopoietic lineage indicates that BIN2 might also be involved in Ca^{2+} signaling in other cell types, such as immune cells. The measurement of intracellular Ca^{2+} levels in immune cells derived from $Bin2^{-/-}$ mice may help to answer this question. Furthermore, the here presented work confirmed that reduced Ca^{2+} signaling has a different impact on (hem)ITAM- versus GPCR-induced platelet activation. This effect was previously also observed in STIM1 and Orai1-deficient animals, but the underlying mechanism remains to be investigated.

This thesis establishes RBC derived soluble Sema7A as a strong promoter of platelet thrombus formation via its interaction with platelet GPIbα. The underlying mechanisms of this interaction, especially the resulting intracellular signaling in platelets remains to be explored. Interestingly, Sema7A is also expressed on platelets and can be cleaved from the cell surface.

However, the role of platelet Sema7A in the process of platelet activation and aggregation remains to be established. Therefore, a platelet specific knockout of Sema7A, investigated in in vitro and ex vivo platelet activity assays, as well as in in vivo hemostasis and thrombosis models may answer these questions.

5 References

1. Brewer DB. Max Schultze (1865), G. Bizzozero (1882) and the discovery of the platelet. *Br J Haematol.* 2006;133(3):251-258.

2. Nieswandt B, Pleines I, Bender M. Platelet adhesion and activation mechanisms in arterial thrombosis and ischaemic stroke. *J Thromb Haemost.* 2011;9 Suppl 1:92-104.

3. Jackson SP. Arterial thrombosis--insidious, unpredictable and deadly. *Nat Med.* 2011;17(11):1423-1436.

4. Ware J, Corken A, Khetpal R. Platelet function beyond hemostasis and thrombosis. *Curr Opin Hematol.* 2013;20(5):451-456.

5. Patzelt J, Langer HF. Platelets in angiogenesis. *Curr Vasc Pharmacol.* 2012;10(5):570-577.

6. Huang HS, Chang HH. Platelets in inflammation and immune modulations: functions beyond hemostasis. *Arch Immunol Ther Exp (Warsz).* 2012;60(6):443-451.

7. Li Z, Yang F, Dunn S, Gross AK, Smyth SS. Platelets as immune mediators: their role in host defense responses and sepsis. *Thromb Res.* 2011;127(3):184-188.

8. Palacios-Acedo AL, Mege D, Crescence L, Dignat-George F, Dubois C, Panicot-Dubois L. Platelets, Thrombo-Inflammation, and Cancer: Collaborating With the Enemy. *Front Immunol.* 2019;10:1805.

9. van der Meijden PEJ, Heemskerk JWM. Platelet biology and functions: new concepts and clinical perspectives. *Nat Rev Cardiol.* 2019;16(3):166-179.

10. Morgenstern E. The formation of compound granules from different types of secretory organelles in human platelets (dense granules and alpha-granules). A cryofixation/-substitution study using serial sections. *Eur J Cell Biol.* 1995;68(2):183-190.

11. J. G. Fox SWB, M. T. Davisson, C. E. Newcomer, F.W. Quimby, and A. L. Smith. The Mouse in Biomedical Research: Academic Press; 2007.

12. Daly ME. Determinants of platelet count in humans. *Haematologica.* 2011;96(1):10-13.

13. Hartwig J, Italiano J, Jr. The birth of the platelet. *J Thromb Haemost.* 2003;1(7):1580-1586.

14. Italiano JJ, Hartwig J. Production and Destruction of Platelets. In: Kerrigan S, Moran N, eds. The Non-Thrombotic Role of Platelets in Health and Disease: IntechOpen; 2015.

15. Machlus KR, Italiano JE, Jr. The incredible journey: From megakaryocyte development to platelet formation. *J Cell Biol.* 2013;201(6):785-796.

16. Semeniak D, Kulawig R, Stegner D, et al. Proplatelet formation is selectively inhibited by collagen type I through Syk-independent GPVI signaling. *J Cell Sci.* 2016;129(18):3473-3484.

17. Gremmel T, Frelinger AL, 3rd, Michelson AD. Platelet Physiology. *Semin Thromb Hemost.* 2016;42(3):191-204.

18. Rendu F, Brohard-Bohn B. The platelet release reaction: granules' constituents, secretion and functions. *Platelets.* 2001;12(5):261-273.

19. Thon JN, Italiano JE. Platelets: production, morphology and ultrastructure. *Handb Exp Pharmacol.* 2012(210):3-22.

20. Lopez AD, Mathers CD, Ezzati M, Jamison DT, Murray CJ. Global and regional burden of disease and risk factors, 2001: systematic analysis of population health data. *Lancet.* 2006;367(9524):1747-1757.

21. Varga-Szabo D, Pleines I, Nieswandt B. Cell adhesion mechanisms in platelets. *Arterioscler Thromb Vasc Biol.* 2008;28(3):403-412.

22. Savage B, Saldivar E, Ruggeri ZM. Initiation of platelet adhesion by arrest onto fibrinogen or translocation on von Willebrand factor. *Cell.* 1996;84(2):289-297.

23. Moroi M, Jung SM, Nomura S, Sekiguchi S, Ordinas A, Diaz-Ricart M. Analysis of the involvement of the von Willebrand factor-glycoprotein Ib interaction in platelet adhesion to a collagen-coated surface under flow conditions. *Blood.* 1997;90(11):4413-4424.

24. Ruggeri ZM. Von Willebrand factor, platelets and endothelial cell interactions. *J Thromb Haemost*. 2003;1(7):1335-1342.

25. Nieswandt B, Brakebusch C, Bergmeier W, et al. Glycoprotein VI but not alpha2beta1 integrin is essential for platelet interaction with collagen. *EMBO J*. 2001;20(9):2120-2130.

26. Nieswandt B, Watson SP. Platelet-collagen interaction: is GPVI the central receptor? *Blood*. 2003;102(2):449-461.

27. Heemskerk JW, Mattheij NJ, Cosemans JM. Platelet-based coagulation: different populations, different functions. *J Thromb Haemost*. 2013;11(1):2-16.

28. Offermanns S. Activation of platelet function through G protein-coupled receptors. *Circ Res*. 2006;99(12):1293-1304.

29. May F, Hagedorn I, Pleines I, et al. CLEC-2 is an essential platelet-activating receptor in hemostasis and thrombosis. *Blood*. 2009;114(16):3464-3472.

30. Shattil SJ, Newman PJ. Integrins: dynamic scaffolds for adhesion and signaling in platelets. *Blood*. 2004;104(6):1606-1615.

31. Ginsberg MH, Partridge A, Shattil SJ. Integrin regulation. *Curr Opin Cell Biol*. 2005;17(5):509-516.

32. Bennett JS. Structure and function of the platelet integrin alphaIIbbeta3. *J Clin Invest*. 2005;115(12):3363-3369.

33. Watson SP, Auger JM, McCarty OJ, Pearce AC. GPVI and integrin alphaIIb beta3 signaling in platelets. *J Thromb Haemost*. 2005;3(8):1752-1762.

34. Stegner D, Nieswandt B. Platelet receptor signaling in thrombus formation. *J Mol Med (Berl)*. 2011;89(2):109-121.

35. Varga-Szabo D, Braun A, Nieswandt B. Calcium signaling in platelets. *J Thromb Haemost*. 2009;7(7):1057-1066.

36. Fox JE. The platelet cytoskeleton. *Thromb Haemost*. 1993;70(6):884-893.

37. Love PE, Hayes SM. ITAM-mediated signaling by the T-cell antigen receptor. *Cold Spring Harb Perspect Biol*. 2010;2(6):a002485.

38. Suzuki-Inoue K, Fuller GL, Garcia A, et al. A novel Syk-dependent mechanism of platelet activation by the C-type lectin receptor CLEC-2. *Blood*. 2006;107(2):542-549.

39. Suzuki-Inoue K, Osada M, Ozaki Y. Physiologic and pathophysiologic roles of interaction between C-type lectin-like receptor 2 and podoplanin: partners from in utero to adulthood. *J Thromb Haemost*. 2017;15(2):219-229.

40. Suzuki-Inoue K, Kato Y, Inoue O, et al. Involvement of the snake toxin receptor CLEC-2, in podoplanin-mediated platelet activation, by cancer cells. *J Biol Chem*. 2007;282(36):25993-26001.

41. Bergmeier W, Stefanini L. Platelet ITAM signaling. *Curr Opin Hematol*. 2013;20(5):445-450.

42. Stegner D, Haining EJ, Nieswandt B. Targeting glycoprotein VI and the immunoreceptor tyrosine-based activation motif signaling pathway. *Arterioscler Thromb Vasc Biol*. 2014;34(8):1615-1620.

43. Watson SP, Herbert JM, Pollitt AY. GPVI and CLEC-2 in hemostasis and vascular integrity. *J Thromb Haemost*. 2010;8(7):1456-1467.

44. Lorenz V, Stegner D, Stritt S, et al. Targeted downregulation of platelet CLEC-2 occurs through Syk-independent internalization. *Blood*. 2015;125(26):4069-4077.

45. Spalton JC, Mori J, Pollitt AY, Hughes CE, Eble JA, Watson SP. The novel Syk inhibitor R406 reveals mechanistic differences in the initiation of GPVI and CLEC-2 signaling in platelets. *J Thromb Haemost*. 2009;7(7):1192-1199.

46. Sanchez-Fernandez G, Cabezudo S, Garcia-Hoz C, et al. Galphaq signalling: the new and the old. *Cell Signal*. 2014;26(5):833-848.

47. Cantley LC. The phosphoinositide 3-kinase pathway. *Science*. 2002;296(5573):1655-1657.

48. Berridge MJ, Bootman MD, Roderick HL. Calcium signalling: dynamics, homeostasis and remodelling. *Nat Rev Mol Cell Biol*. 2003;4(7):517-529.

49. Mammadova-Bach E, Nagy M, Heemskerk JWM, Nieswandt B, Braun A. Store-operated calcium entry in thrombosis and thrombo-inflammation. *Cell Calcium*. 2019;77:39-48.

50. Grosse J, Braun A, Varga-Szabo D, et al. An EF hand mutation in Stim1 causes premature platelet activation and bleeding in mice. *J Clin Invest*. 2007;117(11):3540-3550.

51. Bergmeier W, Oh-Hora M, McCarl CA, Roden RC, Bray PF, Feske S. R93W mutation in Orai1 causes impaired calcium influx in platelets. *Blood*. 2009;113(3):675-678.

52. Varga-Szabo D, Braun A, Kleinschnitz C, et al. The calcium sensor STIM1 is an essential mediator of arterial thrombosis and ischemic brain infarction. *J Exp Med*. 2008;205(7):1583-1591.

53. Braun A, Varga-Szabo D, Kleinschnitz C, et al. Orai1 (CRACM1) is the platelet SOC channel and essential for pathological thrombus formation. *Blood*. 2009;113(9):2056-2063.

54. Liou J, Kim ML, Heo WD, et al. STIM is a Ca2+ sensor essential for Ca2+-store-depletion-triggered Ca2+ influx. *Curr Biol*. 2005;15(13):1235-1241.

55. Luik RM, Wu MM, Buchanan J, Lewis RS. The elementary unit of store-operated Ca2+ entry: local activation of CRAC channels by STIM1 at ER-plasma membrane junctions. *J Cell Biol*. 2006;174(6):815-825.

56. Wu MM, Buchanan J, Luik RM, Lewis RS. Ca2+ store depletion causes STIM1 to accumulate in ER regions closely associated with the plasma membrane. *J Cell Biol*. 2006;174(6):803-813.

57. Zhang SL, Yu Y, Roos J, et al. STIM1 is a Ca2+ sensor that activates CRAC channels and migrates from the Ca2+ store to the plasma membrane. *Nature*. 2005;437(7060):902-905.

58. Xu P, Lu J, Li Z, Yu X, Chen L, Xu T. Aggregation of STIM1 underneath the plasma membrane induces clustering of Orai1. *Biochem Biophys Res Commun*. 2006;350(4):969-976.

59. Thillaiappan NB, Chavda AP, Tovey SC, Prole DL, Taylor CW. Ca(2+) signals initiate at immobile IP3 receptors adjacent to ER-plasma membrane junctions. *Nat Commun*. 2017;8(1):1505.

60. Sampieri A, Santoyo K, Asanov A, Vaca L. Association of the IP3R to STIM1 provides a reduced intraluminal calcium microenvironment, resulting in enhanced store-operated calcium entry. *Sci Rep*. 2018;8(1):13252.

61. Feng JM, Hu YK, Xie LH, et al. Golli protein negatively regulates store depletion-induced calcium influx in T cells. *Immunity*. 2006;24(6):717-727.

62. Palty R, Raveh A, Kaminsky I, Meller R, Reuveny E. SARAF inactivates the store operated calcium entry machinery to prevent excess calcium refilling. *Cell*. 2012;149(2):425-438.

63. Srikanth S, Jew M, Kim KD, Yee MK, Abramson J, Gwack Y. Junctate is a Ca2+-sensing structural component of Orai1 and stromal interaction molecule 1 (STIM1). *Proc Natl Acad Sci U S A*. 2012;109(22):8682-8687.

64. Groschner K, Shrestha N, Fameli N. Non-Orai Partners of STIM Proteins: Role in ER-PM Communication and Ca(2+) Signaling. In: Kozak JA, Putney JW, Jr., eds. Calcium Entry Channels in Non-Excitable Cells. Boca Raton (FL); 2018:177-196.

65. Ramanathan G, Gupta S, Thielmann I, et al. Defective diacylglycerol-induced Ca2+ entry but normal agonist-induced activation responses in TRPC6-deficient mouse platelets. *J Thromb Haemost*. 2012;10(3):419-429.

66. MacKenzie AB, Mahaut-Smith MP, Sage SO. Activation of receptor-operated cation channels via P2X1 not P2T purinoceptors in human platelets. *J Biol Chem*. 1996;271(6):2879-2881.

67. Hechler B, Lenain N, Marchese P, et al. A role of the fast ATP-gated P2X1 cation channel in thrombosis of small arteries in vivo. *J Exp Med*. 2003;198(4):661-667.

68. Clemetson JM, Polgar J, Magnenat E, Wells TN, Clemetson KJ. The platelet collagen receptor glycoprotein VI is a member of the immunoglobulin superfamily closely related to FcalphaR and the natural killer receptors. *J Biol Chem*. 1999;274(41):29019-29024.

69. Jandrot-Perrus M, Lagrue AH, Okuma M, Bon C. Adhesion and activation of human platelets induced by convulxin involve glycoprotein VI and integrin alpha2beta1. *J Biol Chem*. 1997;272(43):27035-27041.

70. Alshehri OM, Hughes CE, Montague S, et al. Fibrin activates GPVI in human and mouse platelets. *Blood*. 2015;126(13):1601-1608.

71. Inoue O, Suzuki-Inoue K, McCarty OJ, et al. Laminin stimulates spreading of platelets through integrin alpha6beta1-dependent activation of GPVI. *Blood*. 2006;107(4):1405-1412.

72. Mammadova-Bach E, Ollivier V, Loyau S, et al. Platelet glycoprotein VI binds to polymerized fibrin and promotes thrombin generation. *Blood*. 2015;126(5):683-691.

73. Poulter NS, Pollitt AY, Owen DM, et al. Clustering of glycoprotein VI (GPVI) dimers upon adhesion to collagen as a mechanism to regulate GPVI signaling in platelets. *J Thromb Haemost*. 2017;15(3):549-564.

74. Gardiner EE, Karunakaran D, Shen Y, Arthur JF, Andrews RK, Berndt MC. Controlled shedding of platelet glycoprotein (GP)VI and GPIb-IX-V by ADAM family metalloproteinases. *J Thromb Haemost*. 2007;5(7):1530-1537.

75. Nieswandt B, Schulte V, Bergmeier W, et al. Long-term antithrombotic protection by in vivo depletion of platelet glycoprotein VI in mice. *J Exp Med*. 2001;193(4):459-469.

76. Schulte V, Rabie T, Prostredna M, Aktas B, Gruner S, Nieswandt B. Targeting of the collagen-binding site on glycoprotein VI is not essential for in vivo depletion of the receptor. *Blood*. 2003;101(10):3948-3952.

77. Stegner D, Popp M, Lorenz V, Wax JK, Gessner JE, Nieswandt B. FcgammaRIIB on liver sinusoidal endothelial cells is essential for antibody-induced GPVI ectodomain shedding in mice. *Blood*. 2016;128(6):862-865.

78. Massberg S, Gawaz M, Gruner S, et al. A crucial role of glycoprotein VI for platelet recruitment to the injured arterial wall in vivo. *J Exp Med*. 2003;197(1):41-49.

79. Bender M, Hagedorn I, Nieswandt B. Genetic and antibody-induced glycoprotein VI deficiency equally protects mice from mechanically and FeCl(3) -induced thrombosis. *J Thromb Haemost*. 2011;9(7):1423-1426.

80. Pachel C, Mathes D, Arias-Loza AP, et al. Inhibition of Platelet GPVI Protects Against Myocardial Ischemia-Reperfusion Injury. *Arterioscler Thromb Vasc Biol*. 2016;36(4):629-635.

81. Vogtle T, Cherpokova D, Bender M, Nieswandt B. Targeting platelet receptors in thrombotic and thrombo-inflammatory disorders. *Hamostaseologie*. 2015;35(3):235-243.

82. Dutting S, Bender M, Nieswandt B. Platelet GPVI: a target for antithrombotic therapy?! *Trends Pharmacol Sci*. 2012;33(11):583-590.

83. Boulaftali Y, Mawhin MA, Jandrot-Perrus M, Ho-Tin-Noe B. Glycoprotein VI in securing vascular integrity in inflamed vessels. *Res Pract Thromb Haemost*. 2018;2(2):228-239.

84. Gros A, Syvannarath V, Lamrani L, et al. Single platelets seal neutrophil-induced vascular breaches via GPVI during immune-complex-mediated inflammation in mice. *Blood*. 2015;126(8):1017-1026.

85. Pierre S, Linke B, Suo J, et al. GPVI and Thromboxane Receptor on Platelets Promote Proinflammatory Macrophage Phenotypes during Cutaneous Inflammation. *J Invest Dermatol*. 2017;137(3):686-695.

86. Boulaftali Y, Hess PR, Getz TM, et al. Platelet ITAM signaling is critical for vascular integrity in inflammation. *J Clin Invest*. 2013;123(2):908-916.

87. Rayes J, Jadoui S, Lax S, et al. The contribution of platelet glycoprotein receptors to inflammatory bleeding prevention is stimulus and organ dependent. *Haematologica*. 2018;103(6):e256-e258.

88. Rayes J, Watson SP, Nieswandt B. Functional significance of the platelet immune receptors GPVI and CLEC-2. *J Clin Invest*. 2019;129(1):12-23.

89. Mammadova-Bach E, Mangin P, Lanza F, Gachet C. Platelets in cancer. From basic research to therapeutic implications. *Hamostaseologie*. 2015;35(4):325-336.

90. Gaertner F, Massberg S. Patrolling the vascular borders: platelets in immunity to infection and cancer. *Nat Rev Immunol.* 2019;19(12):747-760.

91. Dvorak HF. Tumors: wounds that do not heal-redux. *Cancer Immunol Res.* 2015;3(1):1-11.

92. Di Nisio M, Porreca E, Candeloro M, De Tursi M, Russi I, Rutjes AW. Primary prophylaxis for venous thromboembolism in ambulatory cancer patients receiving chemotherapy. *Cochrane Database Syst Rev.* 2016;12:CD008500.

93. Mezouar S, Frere C, Darbousset R, et al. Role of platelets in cancer and cancer-associated thrombosis: Experimental and clinical evidences. *Thromb Res.* 2016;139:65-76.

94. Adesanya MA, Maraveyas A, Madden LA. PO-27 - Thrombin generation in pancreatic cancer and multiple myeloma with use of calibrated automated thrombography. *Thromb Res.* 2016;140 Suppl 1:S186.

95. Menter DG, Tucker SC, Kopetz S, Sood AK, Crissman JD, Honn KV. Platelets and cancer: a casual or causal relationship: revisited. *Cancer Metastasis Rev.* 2014;33(1):231-269.

96. Shao B, Wahrenbrock MG, Yao L, et al. Carcinoma mucins trigger reciprocal activation of platelets and neutrophils in a murine model of Trousseau syndrome. *Blood.* 2011;118(15):4015-4023.

97. Faraday N, Schunke K, Saleem S, et al. Cathepsin G-dependent modulation of platelet thrombus formation in vivo by blood neutrophils. *PLoS One.* 2013;8(8):e71447.

98. Farnsworth RH, Lackmann M, Achen MG, Stacker SA. Vascular remodeling in cancer. *Oncogene.* 2014;33(27):3496-3505.

99. Qi C, Wei B, Zhou W, et al. P-selectin-mediated platelet adhesion promotes tumor growth. *Oncotarget.* 2015;6(9):6584-6596.

100. Brooks PC, Clark RA, Cheresh DA. Requirement of vascular integrin alpha v beta 3 for angiogenesis. *Science.* 1994;264(5158):569-571.

101. Contrino J, Hair G, Kreutzer DL, Rickles FR. In situ detection of tissue factor in vascular endothelial cells: correlation with the malignant phenotype of human breast disease. *Nat Med.* 1996;2(2):209-215.

102. Verheul HM, Hoekman K, Luykx-de Bakker S, et al. Platelet: transporter of vascular endothelial growth factor. *Clin Cancer Res.* 1997;3(12 Pt 1):2187-2190.

103. Pinedo HM, Verheul HM, D'Amato RJ, Folkman J. Involvement of platelets in tumour angiogenesis? *Lancet.* 1998;352(9142):1775-1777.

104. Cross MJ, Claesson-Welsh L. FGF and VEGF function in angiogenesis: signalling pathways, biological responses and therapeutic inhibition. *Trends Pharmacol Sci.* 2001;22(4):201-207.

105. Caine GJ, Lip GY, Blann AD. Platelet-derived VEGF, Flt-1, angiopoietin-1 and P-selectin in breast and prostate cancer: further evidence for a role of platelets in tumour angiogenesis. *Ann Med.* 2004;36(4):273-277.

106. Gresele P, Falcinelli E, Sebastiano M, Momi S. Matrix Metalloproteinases and Platelet Function. *Prog Mol Biol Transl Sci.* 2017;147:133-165.

107. Labelle M, Begum S, Hynes RO. Direct signaling between platelets and cancer cells induces an epithelial-mesenchymal-like transition and promotes metastasis. *Cancer Cell.* 2011;20(5):576-590.

108. Chatterjee M, Huang Z, Zhang W, et al. Distinct platelet packaging, release, and surface expression of proangiogenic and antiangiogenic factors on different platelet stimuli. *Blood.* 2011;117(14):3907-3911.

109. Michael JV, Wurtzel JGT, Mao GF, et al. Platelet microparticles infiltrating solid tumors transfer miRNAs that suppress tumor growth. *Blood.* 2017;130(5):567-580.

110. Meikle CK, Kelly CA, Garg P, Wuescher LM, Ali RA, Worth RG. Cancer and Thrombosis: The Platelet Perspective. *Front Cell Dev Biol.* 2016;4:147.

111. Boucharaba A, Serre CM, Gres S, et al. Platelet-derived lysophosphatidic acid supports the progression of osteolytic bone metastases in breast cancer. *J Clin Invest.* 2004;114(12):1714-1725.

112. Patrignani P, Patrono C. Aspirin and Cancer. *J Am Coll Cardiol.* 2016;68(9):967-976.

113. Egan K, Cooke N, Kenny D. Living in shear: platelets protect cancer cells from shear induced damage. *Clin Exp Metastasis.* 2014;31(6):697-704.

114. Nieswandt B, Hafner M, Echtenacher B, Mannel DN. Lysis of tumor cells by natural killer cells in mice is impeded by platelets. *Cancer Res.* 1999;59(6):1295-1300.

115. Kopp HG, Placke T, Salih HR. Platelet-derived transforming growth factor-beta down-regulates NKG2D thereby inhibiting natural killer cell antitumor reactivity. *Cancer Res.* 2009;69(19):7775-7783.

116. Placke T, Orgel M, Schaller M, et al. Platelet-derived MHC class I confers a pseudonormal phenotype to cancer cells that subverts the antitumor reactivity of natural killer immune cells. *Cancer Res.* 2012;72(2):440-448.

117. Labelle M, Begum S, Hynes RO. Platelets guide the formation of early metastatic niches. *Proc Natl Acad Sci U S A.* 2014;111(30):E3053-3061.

118. Rachidi S, Metelli A, Riesenberg B, et al. Platelets subvert T cell immunity against cancer via GARP-TGFbeta axis. *Sci Immunol.* 2017;2(11).

119. Kolenich JJ, Mansour EG, Flynn A. Haematological effects of aspirin. *Lancet.* 1972;2(7779):714.

120. Gasic GJ, Gasic TB, Galanti N, Johnson T, Murphy S. Platelet-tumor-cell interactions in mice. The role of platelets in the spread of malignant disease. *Int J Cancer.* 1973;11(3):704-718.

121. Franco AT, Corken A, Ware J. Platelets at the interface of thrombosis, inflammation, and cancer. *Blood.* 2015;126(5):582-588.

122. Rothwell PM, Fowkes FG, Belch JF, Ogawa H, Warlow CP, Meade TW. Effect of daily aspirin on long-term risk of death due to cancer: analysis of individual patient data from randomised trials. *Lancet.* 2011;377(9759):31-41.

123. Rothwell PM, Price JF, Fowkes FG, et al. Short-term effects of daily aspirin on cancer incidence, mortality, and non-vascular death: analysis of the time course of risks and benefits in 51 randomised controlled trials. *Lancet.* 2012;379(9826):1602-1612.

124. Rothwell PM, Wilson M, Price JF, Belch JF, Meade TW, Mehta Z. Effect of daily aspirin on risk of cancer metastasis: a study of incident cancers during randomised controlled trials. *Lancet.* 2012;379(9826):1591-1601.

125. Alfonso L, Ai G, Spitale RC, Bhat GJ. Molecular targets of aspirin and cancer prevention. *Br J Cancer.* 2014;111(1):61-67.

126. Mezouar S, Darbousset R, Dignat-George F, Panicot-Dubois L, Dubois C. Inhibition of platelet activation prevents the P-selectin and integrin-dependent accumulation of cancer cell microparticles and reduces tumor growth and metastasis in vivo. *Int J Cancer.* 2015;136(2):462-475.

127. Gebremeskel S, LeVatte T, Liwski RS, Johnston B, Bezuhly M. The reversible P2Y12 inhibitor ticagrelor inhibits metastasis and improves survival in mouse models of cancer. *Int J Cancer.* 2015;136(1):234-240.

128. Su X, Floyd DH, Hughes A, et al. The ADP receptor P2RY12 regulates osteoclast function and pathologic bone remodeling. *J Clin Invest.* 2012;122(10):3579-3592.

129. Rothwell PM, Cook NR, Gaziano JM, et al. Effects of aspirin on risks of vascular events and cancer according to bodyweight and dose: analysis of individual patient data from randomised trials. *Lancet.* 2018;392(10145):387-399.

130. Chung AS, Lee J, Ferrara N. Targeting the tumour vasculature: insights from physiological angiogenesis. *Nat Rev Cancer.* 2010;10(7):505-514.

131. Kisucka J, Butterfield CE, Duda DG, et al. Platelets and platelet adhesion support angiogenesis while preventing excessive hemorrhage. *Proc Natl Acad Sci U S A.* 2006;103(4):855-860.

132. Ho-Tin-Noe B, Goerge T, Cifuni SM, Duerschmied D, Wagner DD. Platelet granule secretion continuously prevents intratumor hemorrhage. *Cancer Res*. 2008;68(16):6851-6858.

133. Manegold PC, Hutter J, Pahernik SA, Messmer K, Dellian M. Platelet-endothelial interaction in tumor angiogenesis and microcirculation. *Blood*. 2003;101(5):1970-1976.

134. Demers M, Ho-Tin-Noe B, Schatzberg D, Yang JJ, Wagner DD. Increased efficacy of breast cancer chemotherapy in thrombocytopenic mice. *Cancer Res*. 2011;71(5):1540-1549.

135. Rayes J, Watson SP. Platelet GPVI repairs its own damage. *Blood*. 2015;126(8):933-934.

136. Ho-Tin-Noe B, Carbo C, Demers M, Cifuni SM, Goerge T, Wagner DD. Innate immune cells induce hemorrhage in tumors during thrombocytopenia. *Am J Pathol*. 2009;175(4):1699-1708.

137. Safari F, Suetsugu S. The BAR Domain Superfamily Proteins from Subcellular Structures to Human Diseases. *Membranes (Basel)*. 2012;2(1):91-117.

138. Suetsugu S. Higher-order assemblies of BAR domain proteins for shaping membranes. *Microscopy (Oxf)*. 2016;65(3):201-210.

139. Stanishneva-Konovalova TB, Derkacheva NI, Polevova SV, Sokolova OS. The Role of BAR Domain Proteins in the Regulation of Membrane Dynamics. *Acta Naturae*. 2016;8(4):60-69.

140. Carman PJ, Dominguez R. BAR domain proteins-a linkage between cellular membranes, signaling pathways, and the actin cytoskeleton. *Biophys Rev*. 2018;10(6):1587-1604.

141. Ren G, Vajjhala P, Lee JS, Winsor B, Munn AL. The BAR domain proteins: molding membranes in fission, fusion, and phagy. *Microbiol Mol Biol Rev*. 2006;70(1):37-120.

142. Sakamuro D, Elliott KJ, Wechsler-Reya R, Prendergast GC. BIN1 is a novel MYC-interacting protein with features of a tumour suppressor. *Nat Genet*. 1996;14(1):69-77.

143. Tan MS, Yu JT, Tan L. Bridging integrator 1 (BIN1): form, function, and Alzheimer's disease. *Trends Mol Med*. 2013;19(10):594-603.

144. Hong TT, Smyth JW, Gao D, et al. BIN1 localizes the L-type calcium channel to cardiac T-tubules. *PLoS Biol*. 2010;8(2):e1000312.

145. Hong T, Yang H, Zhang SS, et al. Cardiac BIN1 folds T-tubule membrane, controlling ion flux and limiting arrhythmia. *Nat Med*. 2014;20(6):624-632.

146. Lundgaard GL, Daniels NE, Pyndiah S, et al. Identification of a novel effector domain of BIN1 for cancer suppression. *J Cell Biochem*. 2011;112(10):2992-3001.

147. Simionescu-Bankston A, Leoni G, Wang Y, et al. The N-BAR domain protein, Bin3, regulates Rac1- and Cdc42-dependent processes in myogenesis. *Dev Biol*. 2013;382(1):160-171.

148. Ge K, Prendergast GC. Bin2, a functionally nonredundant member of the BAR adaptor gene family. *Genomics*. 2000;67(2):210-220.

149. Sanchez-Barrena MJ, Vallis Y, Clatworthy MR, et al. Bin2 is a membrane sculpting N-BAR protein that influences leucocyte podosomes, motility and phagocytosis. *PLoS One*. 2012;7(12):e52401.

150. Luo Y, Raible D, Raper JA. Collapsin: a protein in brain that induces the collapse and paralysis of neuronal growth cones. *Cell*. 1993;75(2):217-227.

151. Kolodkin AL, Matthes DJ, O'Connor TP, et al. Fasciclin IV: sequence, expression, and function during growth cone guidance in the grasshopper embryo. *Neuron*. 1992;9(5):831-845.

152. Kolodkin AL, Matthes DJ, Goodman CS. The semaphorin genes encode a family of transmembrane and secreted growth cone guidance molecules. *Cell*. 1993;75(7):1389-1399.

153. Alto LT, Terman JR. Semaphorins and their Signaling Mechanisms. *Methods Mol Biol*. 2017;1493:1-25.

154. Hota PK, Buck M. Plexin structures are coming: opportunities for multilevel investigations of semaphorin guidance receptors, their cell signaling mechanisms, and functions. *Cell Mol Life Sci*. 2012;69(22):3765-3805.

155. Takamatsu H, Okuno T, Kumanogoh A. Regulation of immune cell responses by semaphorins and their receptors. *Cell Mol Immunol*. 2010;7(2):83-88.

156. Casazza A, Fazzari P, Tamagnone L. Semaphorin signals in cell adhesion and cell migration: functional role and molecular mechanisms. *Adv Exp Med Biol.* 2007;600:90-108.

157. Jongbloets BC, Pasterkamp RJ. Semaphorin signalling during development. *Development.* 2014;141(17):3292-3297.

158. Koncina E, Roth L, Gonthier B, Bagnard D. Role of semaphorins during axon growth and guidance. *Adv Exp Med Biol.* 2007;621:50-64.

159. de Wit J, Verhaagen J. Role of semaphorins in the adult nervous system. *Prog Neurobiol.* 2003;71(2-3):249-267.

160. Potiron V, Nasarre P, Roche J, Healy C, Boumsell L. Semaphorin signaling in the immune system. *Adv Exp Med Biol.* 2007;600:132-144.

161. Epstein JA, Aghajanian H, Singh MK. Semaphorin signaling in cardiovascular development. *Cell Metab.* 2015;21(2):163-173.

162. Kang S, Kumanogoh A. Semaphorins in bone development, homeostasis, and disease. *Semin Cell Dev Biol.* 2013;24(3):163-171.

163. Reidy K, Tufro A. Semaphorins in kidney development and disease: modulators of ureteric bud branching, vascular morphogenesis, and podocyte-endothelial crosstalk. *Pediatr Nephrol.* 2011;26(9):1407-1412.

164. Kagoshima M, Ito T. Diverse gene expression and function of semaphorins in developing lung: positive and negative regulatory roles of semaphorins in lung branching morphogenesis. *Genes Cells.* 2001;6(6):559-571.

165. Gu C, Giraudo E. The role of semaphorins and their receptors in vascular development and cancer. *Exp Cell Res.* 2013;319(9):1306-1316.

166. Tamagnone L. Emerging role of semaphorins as major regulatory signals and potential therapeutic targets in cancer. *Cancer Cell.* 2012;22(2):145-152.

167. Zhu L, Bergmeier W, Wu J, et al. Regulated surface expression and shedding support a dual role for semaphorin 4D in platelet responses to vascular injury. *Proc Natl Acad Sci U S A.* 2007;104(5):1621-1626.

168. Fong KP, Barry C, Tran AN, et al. Deciphering the human platelet sheddome. *Blood.* 2011;117(1):e15-26.

169. Wannemacher KM, Zhu L, Jiang H, et al. Diminished contact-dependent reinforcement of Syk activation underlies impaired thrombus growth in mice lacking Semaphorin 4D. *Blood.* 2010;116(25):5707-5715.

170. Wannemacher KM, Wang L, Zhu L, Brass LF. The role of semaphorins and their receptors in platelets: Lessons learned from neuronal and immune synapses. *Platelets.* 2011;22(6):461-465.

171. Kashiwagi H, Shiraga M, Kato H, et al. Negative regulation of platelet function by a secreted cell repulsive protein, semaphorin 3A. *Blood.* 2005;106(3):913-921.

172. Jaimes Y, Gras C, Goudeva L, et al. Semaphorin 7A inhibits platelet production from CD34+ progenitor cells. *J Thromb Haemost.* 2012;10(6):1100-1108.

173. Morote-Garcia JC, Napiwotzky D, Kohler D, Rosenberger P. Endothelial Semaphorin 7A promotes neutrophil migration during hypoxia. *Proc Natl Acad Sci U S A.* 2012;109(35):14146-14151.

174. Roth JM, Kohler D, Schneider M, Granja TF, Rosenberger P. Semaphorin 7A Aggravates Pulmonary Inflammation during Lung Injury. *PLoS One.* 2016;11(1):e0146930.

175. Suzuki K, Okuno T, Yamamoto M, et al. Semaphorin 7A initiates T-cell-mediated inflammatory responses through alpha1beta1 integrin. *Nature.* 2007;446(7136):680-684.

176. Hu S, Liu Y, You T, et al. Vascular Semaphorin 7A Upregulation by Disturbed Flow Promotes Atherosclerosis Through Endothelial beta1 Integrin. *Arterioscler Thromb Vasc Biol.* 2018;38(2):335-343.

177. You T, Zhu Z, Zheng X, et al. Serum semaphorin 7A is associated with the risk of acute atherothrombotic stroke. *J Cell Mol Med*. 2019;23(4):2901-2906.

178. Kohler D, Granja T, Volz J, et al. Red blood cell-derived semaphorin 7A promotes thrombo-inflammation in myocardial ischemia-reperfusion injury through platelet GPIb. *Nat Commun*. 2020;11(1):1315.

179. Nieswandt B, Bergmeier W, Rackebrandt K, Gessner JE, Zirngibl H. Identification of critical antigen-specific mechanisms in the development of immune thrombocytopenic purpura in mice. *Blood*. 2000;96(7):2520-2527.

180. Bergmeier W, Schulte V, Brockhoff G, Bier U, Zirngibl H, Nieswandt B. Flow cytometric detection of activated mouse integrin alphaIIbbeta3 with a novel monoclonal antibody. *Cytometry*. 2002;48(2):80-86.

181. Nieswandt B, Bergmeier W, Schulte V, Rackebrandt K, Gessner JE, Zirngibl H. Expression and function of the mouse collagen receptor glycoprotein VI is strictly dependent on its association with the FcRgamma chain. *J Biol Chem*. 2000;275(31):23998-24002.

182. Daley JM, Thomay AA, Connolly MD, Reichner JS, Albina JE. Use of Ly6G-specific monoclonal antibody to deplete neutrophils in mice. *J Leukoc Biol*. 2008;83(1):64-70.

183. Popp M. Mechanisms of platelet activation and receptor regulation in genetically modified mice. Department of Experimental Biomedicine – Chair I. Würzburg: Julius-Maximilians-Universität Würzburg; 2016.

184. Ware J, Russell S, Ruggeri ZM. Generation and rescue of a murine model of platelet dysfunction: the Bernard-Soulier syndrome. *Proc Natl Acad Sci U S A*. 2000;97(6):2803-2808.

185. Denis C, Methia N, Frenette PS, et al. A mouse model of severe von Willebrand disease: defects in hemostasis and thrombosis. *Proc Natl Acad Sci U S A*. 1998;95(16):9524-9529.

186. Wolter S, Loschberger A, Holm T, et al. rapidSTORM: accurate, fast open-source software for localization microscopy. *Nat Methods*. 2012;9(11):1040-1041.

187. Aurbach K, Spindler M, Haining EJ, Bender M, Pleines I. Blood collection, platelet isolation and measurement of platelet count and size in mice-a practical guide. *Platelets*. 2018:1-10.

188. Richter KN, Revelo NH, Seitz KJ, et al. Glyoxal as an alternative fixative to formaldehyde in immunostaining and super-resolution microscopy. *EMBO J*. 2018;37(1):139-159.

189. Harrison K, Wagner NH, Jr. Biodistribution of intravenously injected [14C] doxorubicin and [14C] daunorubicin in mice: concise communication. *Journal of nuclear medicine : official publication, Society of Nuclear Medicine*. 1978;19(1):84-86.

190. Laginha KM, Verwoert S, Charrois GJ, Allen TM. Determination of doxorubicin levels in whole tumor and tumor nuclei in murine breast cancer tumors. *Clin Cancer Res*. 2005;11(19 Pt 1):6944-6949.

191. Schuhmann MK, Guthmann J, Stoll G, Nieswandt B, Kraft P, Kleinschnitz C. Blocking of platelet glycoprotein receptor Ib reduces "thrombo-inflammation" in mice with acute ischemic stroke. *J Neuroinflammation*. 2017;14(1):18.

192. Foster BA, Gingrich JR, Kwon ED, Madias C, Greenberg NM. Characterization of prostatic epithelial cell lines derived from transgenic adenocarcinoma of the mouse prostate (TRAMP) model. *Cancer Res*. 1997;57(16):3325-3330.

193. Stewart TJ, Abrams SI. Altered immune function during long-term host-tumor interactions can be modulated to retard autochthonous neoplastic growth. *J Immunol*. 2007;179(5):2851-2859.

194. van Es N, Sturk A, Middeldorp S, Nieuwland R. Effects of cancer on platelets. *Semin Oncol*. 2014;41(3):311-318.

195. Volz J, Mammadova-Bach E, Gil-Pulido J, et al. Inhibition of platelet GPVI induces intratumor hemorrhage and increases efficacy of chemotherapy in mice. *Blood*. 2019;133(25):2696-2706.

196. Rolny C, Mazzone M, Tugues S, et al. HRG inhibits tumor growth and metastasis by inducing macrophage polarization and vessel normalization through downregulation of PlGF. *Cancer cell*. 2011;19(1):31-44.

197. Sprague AH, Khalil RA. Inflammatory cytokines in vascular dysfunction and vascular disease. *Biochem Pharmacol*. 2009;78(6):539-552.

198. Gordon-Weeks AN, Lim SY, Yuzhalin AE, et al. Neutrophils promote hepatic metastasis growth through fibroblast growth factor 2-dependent angiogenesis in mice. *Hepatology*. 2017;65(6):1920-1935.

199. Granot Z, Henke E, Comen EA, King TA, Norton L, Benezra R. Tumor entrained neutrophils inhibit seeding in the premetastatic lung. *Cancer Cell*. 2011;20(3):300-314.

200. Morowski M, Vogtle T, Kraft P, Kleinschnitz C, Stoll G, Nieswandt B. Only severe thrombocytopenia results in bleeding and defective thrombus formation in mice. *Blood*. 2013;121(24):4938-4947.

201. Munzer P, Walker-Allgaier B, Geue S, et al. CK2beta regulates thrombopoiesis and Ca(2+)-triggered platelet activation in arterial thrombosis. *Blood*. 2017;130(25):2774-2785.

202. Konig K, Granja T, Eckle VS, et al. Inhibition of Plexin C1 Protects Against Hepatic Ischemia-Reperfusion Injury. *Crit Care Med*. 2016;44(8):e625-632.

203. Gangloff A, Hsueh WA, Kesner AL, et al. Estimation of paclitaxel biodistribution and uptake in human-derived xenografts in vivo with (18)F-fluoropaclitaxel. *Journal of nuclear medicine : official publication, Society of Nuclear Medicine*. 2005;46(11):1866-1871.

204. Kattel K, Mondal G, Lin F, Kumar V, Mahato RI. Biodistribution of Self-Assembling Polymer-Gemcitabine Conjugate after Systemic Administration into Orthotopic Pancreatic Tumor Bearing Mice. *Mol Pharm*. 2017;14(5):1365-1372.

205. Memon AA, Jakobsen S, Dagnaes-Hansen F, Sorensen BS, Keiding S, Nexo E. Positron emission tomography (PET) imaging with [11C]-labeled erlotinib: a micro-PET study on mice with lung tumor xenografts. *Cancer research*. 2009;69(3):873-878.

206. Glekas AP, Pillarsetty NK, Punzalan B, Khan N, Smith-Jones P, Larson SM. In vivo imaging of Bcr-Abl overexpressing tumors with a radiolabeled imatinib analog as an imaging surrogate for imatinib. *J Nucl Med*. 2011;52(8):1301-1307.

207. Rossow L, Veitl S, Vorlova S, et al. LOX-catalyzed collagen stabilization is a proximal cause for intrinsic resistance to chemotherapy. *Oncogene*. 2018.

208. Senger DR, Connolly DT, Van de Water L, Feder J, Dvorak HF. Purification and NH2-terminal amino acid sequence of guinea pig tumor-secreted vascular permeability factor. *Cancer Res*. 1990;50(6):1774-1778.

209. Jain RK. Normalization of tumor vasculature: an emerging concept in antiangiogenic therapy. *Science*. 2005;307(5706):58-62.

210. Van der Veldt AA, Lubberink M, Bahce I, et al. Rapid decrease in delivery of chemotherapy to tumors after anti-VEGF therapy: implications for scheduling of anti-angiogenic drugs. *Cancer cell*. 2012;21(1):82-91.

211. Rohrig F, Vorlova S, Hoffmann H, et al. VEGF-ablation therapy reduces drug delivery and therapeutic response in ECM-dense tumors. *Oncogene*. 2017;36(1):1-12.

212. Claes A, Wesseling P, Jeuken J, Maass C, Heerschap A, Leenders WP. Antiangiogenic compounds interfere with chemotherapy of brain tumors due to vessel normalization. *Mol Cancer Ther*. 2008;7(1):71-78.

213. Arjaans M, Oude Munnink TH, Oosting SF, et al. Bevacizumab-induced normalization of blood vessels in tumors hampers antibody uptake. *Cancer research*. 2013;73(11):3347-3355.

214. Folkman J. Tumor angiogenesis: therapeutic implications. *N Engl J Med*. 1971;285(21):1182-1186.

215. Folkman J. The role of angiogenesis in tumor growth. *Semin Cancer Biol*. 1992;3(2):65-71.

216. Dickson PV, Hamner JB, Sims TL, et al. Bevacizumab-induced transient remodeling of the vasculature in neuroblastoma xenografts results in improved delivery and efficacy of systemically administered chemotherapy. *Clin Cancer Res*. 2007;13(13):3942-3950.

217. Escorcia FE, Henke E, McDevitt MR, et al. Selective killing of tumor neovasculature paradoxically improves chemotherapy delivery to tumors. *Cancer Res*. 2010;70(22):9277-9286.

218. Henke E, Perk J, Vider J, et al. Peptide-conjugated antisense oligonucleotides for targeted inhibition of a transcriptional regulator in vivo. *Nat Biotechnol*. 2008;26(1):91-100.

219. Yang H, Lee S, Lee S, et al. Sox17 promotes tumor angiogenesis and destabilizes tumor vessels in mice. *J Clin Invest*. 2013;123(1):418-431.

220. Cho MS, Bottsford-Miller J, Vasquez HG, et al. Platelets increase the proliferation of ovarian cancer cells. *Blood*. 2012;120(24):4869-4872.

221. Horwitz SB. Taxol (paclitaxel): mechanisms of action. *Ann Oncol*. 1994;5 Suppl 6:S3-6.

222. Rivankar S. An overview of doxorubicin formulations in cancer therapy. *J Cancer Res Ther*. 2014;10(4):853-858.

223. Shaked Y, Henke E, Roodhart JM, et al. Rapid chemotherapy-induced acute endothelial progenitor cell mobilization: implications for antiangiogenic drugs as chemosensitizing agents. *Cancer Cell*. 2008;14(3):263-273.

224. Shaked Y, Ciarrocchi A, Franco M, et al. Therapy-induced acute recruitment of circulating endothelial progenitor cells to tumors. *Science*. 2006;313(5794):1785-1787.

225. Devi S, Kuligowski MP, Kwan RY, et al. Platelet recruitment to the inflamed glomerulus occurs via an alphaIIbbeta3/GPVI-dependent pathway. *Am J Pathol*. 2010;177(3):1131-1142.

226. Kuligowski MP, Kitching AR, Hickey MJ. Leukocyte recruitment to the inflamed glomerulus: a critical role for platelet-derived P-selectin in the absence of rolling. *J Immunol*. 2006;176(11):6991-6999.

227. Cloutier N, Pare A, Farndale RW, et al. Platelets can enhance vascular permeability. *Blood*. 2012;120(6):1334-1343.

228. Nicolas-Avila JA, Adrover JM, Hidalgo A. Neutrophils in Homeostasis, Immunity, and Cancer. *Immunity*. 2017;46(1):15-28.

229. Eruslanov EB, Singhal S, Albelda SM. Mouse versus Human Neutrophils in Cancer: A Major Knowledge Gap. *Trends Cancer*. 2017;3(2):149-160.

230. Dallegri F, Ballestrero A, Ottonello L, Patrone F. Platelets as scavengers of neutrophil-derived oxidants: a possible defence mechanism at sites of vascular injury. *Thromb Haemost*. 1989;61(3):415-418.

231. Kandler B, Maitz P, Fischer MB, Watzek G, Gruber R. Platelets can neutralize hydrogen peroxide in an acute toxicity model with cells involved in granulation tissue formation. *Bone*. 2005;36(4):671-677.

232. Radomski A, Jurasz P, Sanders EJ, et al. Identification, regulation and role of tissue inhibitor of metalloproteinases-4 (TIMP-4) in human platelets. *Br J Pharmacol*. 2002;137(8):1330-1338.

233. Kleinschnitz C, Pozgajova M, Pham M, Bendszus M, Nieswandt B, Stoll G. Targeting platelets in acute experimental stroke: impact of glycoprotein Ib, VI, and IIb/IIIa blockade on infarct size, functional outcome, and intracranial bleeding. *Circulation*. 2007;115(17):2323-2330.

234. Kellert L, Hametner C, Rohde S, et al. Endovascular stroke therapy: tirofiban is associated with risk of fatal intracerebral hemorrhage and poor outcome. *Stroke*. 2013;44(5):1453-1455.

235. Adams HP, Jr., Effron MB, Torner J, et al. Emergency administration of abciximab for treatment of patients with acute ischemic stroke: results of an international phase III trial: Abciximab in Emergency Treatment of Stroke Trial (AbESTT-II). *Stroke*. 2008;39(1):87-99.

236. Massberg S, Schurzinger K, Lorenz M, et al. Platelet adhesion via glycoprotein IIb integrin is critical for atheroprogression and focal cerebral ischemia: an in vivo study in mice lacking glycoprotein IIb. *Circulation*. 2005;112(8):1180-1188.

237. Bottsford-Miller J, Choi HJ, Dalton HJ, et al. Differential platelet levels affect response to taxane-based therapy in ovarian cancer. *Clin Cancer Res*. 2015;21(3):602-610.

238. Stegner D, Dutting S, Nieswandt B. Mechanistic explanation for platelet contribution to cancer metastasis. *Thromb Res*. 2014;133 Suppl 2:S149-157.

239. Schlesinger M. Role of platelets and platelet receptors in cancer metastasis. *J Hematol Oncol*. 2018;11(1):125.

240. Jurasz P, Alonso-Escolano D, Radomski MW. Platelet--cancer interactions: mechanisms and pharmacology of tumour cell-induced platelet aggregation. *Br J Pharmacol*. 2004;143(7):819-826.

241. Labelle M, Hynes RO. The initial hours of metastasis: the importance of cooperative host-tumor cell interactions during hematogenous dissemination. *Cancer Discov*. 2012;2(12):1091-1099.

242. Xu XR, Yousef GM, Ni H. Cancer and platelet crosstalk: opportunities and challenges for aspirin and other antiplatelet agents. *Blood*. 2018;131(16):1777-1789.

243. Bergmeier W, Stefanini L. Platelets at the Vascular Interface. *Res Pract Thromb Haemost*. 2018;2(1):27-33.

244. Mammadova-Bach E, Zigrino P, Brucker C, et al. Platelet integrin alpha6beta1 controls lung metastasis through direct binding to cancer cell-derived ADAM9. *JCI Insight*. 2016;1(14):e88245.

245. Strilic B, Offermanns S. Intravascular Survival and Extravasation of Tumor Cells. *Cancer Cell*. 2017;32(3):282-293.

246. Jain S, Russell S, Ware J. Platelet glycoprotein VI facilitates experimental lung metastasis in syngenic mouse models. *J Thromb Haemost*. 2009;7(10):1713-1717.

247. Ungerer M, Li Z, Baumgartner C, et al. The GPVI-Fc fusion protein Revacept reduces thrombus formation and improves vascular dysfunction in atherosclerosis without any impact on bleeding times. *PLoS One*. 2013;8(8):e71193.

248. Lebozec K, Jandrot-Perrus M, Avenard G, Favre-Bulle O, Billiald P. Design, development and characterization of ACT017, a humanized Fab that blocks platelet's glycoprotein VI function without causing bleeding risks. *MAbs*. 2017;9(6):945-958.

249. Voors-Pette C, Lebozec K, Dogterom P, et al. Safety and Tolerability, Pharmacokinetics, and Pharmacodynamics of ACT017, an Antiplatelet GPVI (Glycoprotein VI) Fab. *Arterioscler Thromb Vasc Biol*. 2019;39(5):956-964.

250. Boulay G, Brown DM, Qin N, et al. Modulation of Ca(2+) entry by polypeptides of the inositol 1,4,5-trisphosphate receptor (IP3R) that bind transient receptor potential (TRP): evidence for roles of TRP and IP3R in store depletion-activated Ca(2+) entry. *Proc Natl Acad Sci U S A*. 1999;96(26):14955-14960.

251. Beliveau E, Lessard V, Guillemette G. STIM1 positively regulates the Ca2+ release activity of the inositol 1,4,5-trisphosphate receptor in bovine aortic endothelial cells. *PLoS One*. 2014;9(12):e114718.

252. Jiang P, Loyau S, Tchitchinadze M, Ropers J, Jondeau G, Jandrot-Perrus M. Inhibition of Glycoprotein VI Clustering by Collagen as a Mechanism of Inhibiting Collagen-Induced Platelet Responses: The Example of Losartan. *PLoS One*. 2015;10(6):e0128744.

253. Ambily A, Kaiser WJ, Pierro C, et al. The role of plasma membrane STIM1 and Ca(2+)entry in platelet aggregation. STIM1 binds to novel proteins in human platelets. *Cell Signal*. 2014;26(3):502-511.

254. Baba Y, Nishida K, Fujii Y, Hirano T, Hikida M, Kurosaki T. Essential function for the calcium sensor STIM1 in mast cell activation and anaphylactic responses. *Nat Immunol*. 2008;9(1):81-88.

255. Feske S. CRAC channels and disease - From human CRAC channelopathies and animal models to novel drugs. *Cell Calcium*. 2019;80:112-116.

256. Yellon DM, Hausenloy DJ. Myocardial reperfusion injury. *N Engl J Med*. 2007;357(11):1121-1135.

257. Hausenloy DJ, Barrabes JA, Botker HE, et al. Ischaemic conditioning and targeting reperfusion injury: a 30 year voyage of discovery. *Basic Res Cardiol*. 2016;111(6):70.

258. Stegner D, Klaus V, Nieswandt B. Platelets as Modulators of Cerebral Ischemia/Reperfusion Injury. *Front Immunol*. 2019;10:2505.

259. Pak S, Kondo T, Nakano Y, et al. Platelet adhesion in the sinusoid caused hepatic injury by neutrophils after hepatic ischemia reperfusion. *Platelets*. 2010;21(4):282-288.

260. Jolly SR, Kane WJ, Hook BG, Abrams GD, Kunkel SL, Lucchesi BR. Reduction of myocardial infarct size by neutrophil depletion: effect of duration of occlusion. *Am Heart J*. 1986;112(4):682-690.

261. Sisley AC, Desai T, Harig JM, Gewertz BL. Neutrophil depletion attenuates human intestinal reperfusion injury. *J Surg Res*. 1994;57(1):192-196.

262. Schofield ZV, Woodruff TM, Halai R, Wu MC, Cooper MA. Neutrophils--a key component of ischemia-reperfusion injury. *Shock*. 2013;40(6):463-470.

263. Kleinschnitz C, Schwab N, Kraft P, et al. Early detrimental T-cell effects in experimental cerebral ischemia are neither related to adaptive immunity nor thrombus formation. *Blood*. 2010;115(18):3835-3842.

264. Kohler D, Straub A, Weissmuller T, et al. Phosphorylation of vasodilator-stimulated phosphoprotein prevents platelet-neutrophil complex formation and dampens myocardial ischemia-reperfusion injury. *Circulation*. 2011;123(22):2579-2590.

265. Nieswandt B, Kleinschnitz C, Stoll G. Ischaemic stroke: a thrombo-inflammatory disease? *J Physiol*. 2011;589(17):4115-4123.

266. Zarbock A, Singbartl K, Ley K. Complete reversal of acid-induced acute lung injury by blocking of platelet-neutrophil aggregation. *J Clin Invest*. 2006;116(12):3211-3219.

267. Ruggeri ZM, Orje JN, Habermann R, Federici AB, Reininger AJ. Activation-independent platelet adhesion and aggregation under elevated shear stress. *Blood*. 2006;108(6):1903-1910.

268. Rayes J, Bourne JH, Brill A, Watson SP. The dual role of platelet-innate immune cell interactions in thrombo-inflammation. *Res Pract Thromb Haemost*. 2020;4(1):23-35.

269. Kraft P, Schuhmann MK, Fluri F, et al. Efficacy and Safety of Platelet Glycoprotein Receptor Blockade in Aged and Comorbid Mice With Acute Experimental Stroke. *Stroke*. 2015;46(12):3502-3506.

270. Romo GM, Dong JF, Schade AJ, et al. The glycoprotein Ib-IX-V complex is a platelet counterreceptor for P-selectin. *J Exp Med*. 1999;190(6):803-814.

271. Simon DI, Chen Z, Xu H, et al. Platelet glycoprotein ibalpha is a counterreceptor for the leukocyte integrin Mac-1 (CD11b/CD18). *J Exp Med*. 2000;192(2):193-204.

272. Bradford HN, Pixley RA, Colman RW. Human factor XII binding to the glycoprotein Ib-IX-V complex inhibits thrombin-induced platelet aggregation. *J Biol Chem*. 2000;275(30):22756-22763.

273. Helms CC, Gladwin MT, Kim-Shapiro DB. Erythrocytes and Vascular Function: Oxygen and Nitric Oxide. *Front Physiol*. 2018;9:125.

274. Burnstock G. Blood cells: an historical account of the roles of purinergic signalling. *Purinergic Signal*. 2015;11(4):411-434.

275. Whelihan MF, Zachary V, Orfeo T, Mann KG. Prothrombin activation in blood coagulation: the erythrocyte contribution to thrombin generation. *Blood*. 2012;120(18):3837-3845.

276. Lisman T. Platelet-neutrophil interactions as drivers of inflammatory and thrombotic disease. *Cell Tissue Res*. 2018;371(3):567-576.

6 Appendix

6.1 Abbreviations

μg	microgram
μl	microliter
μm	micrometer
μM	micromolar
AB	avidin-biotin
ADAM	a disintegrin and metalloproteinase
ADP	adenosine diphosphate
APS	ammonium persulfate
ATP	adenosine triphosphate
BAR	Bin-Amphiphysin-Rvs
bFGF	basic fibroblast growth factor
BSA	bovine serum albumin
Ca^{2+}	calcium
cAMP	cyclic adenosine monophosphate
Cas3	caspase 3
CLEC-2	C-type lectin-like receptor 2
COX-1	cyclooxygenase-1
CRAC	Ca^{2+} release-activated Ca^{2+}
CRP	collagen related peptide
CVX	convulxin
CXCL	C-X-C motif chemokine ligand
DAG	diacylglycerol
DMS	demarcation membrane system
dSTORM	Direct stochastic optical reconstruction microscopy
DTS	dense tubular system
ECM	extracellular matrix
EDTA	ethylenediaminetetraacetic acid
EGTA	ethylene glycol tetraacetic acid
EMT	epithelial-mesenchymal transition
EPI	epifluorescence

ER	endoplasmic reticulum
FcR	Fc receptor
FCS	fetal calf serum
GARP	glycoprotein A repetition predominant
GEF	guanine nucleotide-exchange factor
GP	glycoprotein
GPCR	G-protein coupled receptor
GPI	glycosylphosphatidylinositol
GPO	glycin-prolin-hydroxyproline
Grb2	growth factor receptor-bound protein 2
h	hours
HBSS	hank's balanced salt solution
HCT	hematocrit
HEPES	N-2-Hydroxyethylpiperazine-N'-2-ethanesulfonic acid
HGPRT	hypoxanthine-guanine phosphoribosyl transferase
i.p.	intraperitoneally
IF	Immune fluorescence
Ig	immunoglobulin
i.v.	intravenously
IP_3	inositol-3,4,5-trisphosphate
ITAM	tyrosine-based activation motif
Lamα4	laminin α4
LAT	linker for activation of T cells
LLC	Lewis lung carcinom
LPA	lysophosphatidic acid
MI	myocardial ischemia
min	minute
MIRI	myocardial ischemia reperfusion injury
MK	megakaryocyte
MLC	myosin light chain
NGP	neuronal guidance protein
NK	natural killer
non-SOCE	non-store-operated calcium entry

o/N	overnight
OCS	open canalicular system
PAR	protease-activated receptor
PBS	dulbecco's phosphate buffered saline
PCR	polymerase chain reaction
PDGF	platelet derived growth factor
PEG	polyethylene glycol
PF4	platelet factor 4
PFA	paraformaldehyde
PGE_2	prostaglandin E2
PGI_2	prostacyclin
PH3	phospho-histone H3
PI-3-K	phosphatidylinositide-3-kinase
PIP_2	phosphatidylinositol-4,5-bisphosphate
PKC	protein kinase C
PLC	phospholipase C
PLP	periodate-lysine- paraformaldehyd
PM	plasma membrane
PMCA	plasma membrane Ca^{2+} ATPase
PNC	platelet-neutrophil complex
PRP	platelet rich plasma
PS	phosphatidylserine
PVDF	polyvinylidene difluoride
RBC	red blood cells
ROCE	receptor-operated calcium entry
ROS	reactive oxygen species
RPMI	roswell Park Memorial Institute
RT	room temperature
SDS	sodium dodecyl sulphate
SERCA	sarcoplasmatic/endoplasmatic reticulum Ca^{2+} ATPase
SFK	Src family kinases
SH2	Src homology 2
SH3	Src-homology 3

SLP-76	SH2 domain-containing leukocyte protein of 76 kDa
SOCE	store-operated Ca^{2+} entry
STIM1	Stromal interaction molecule 1
Syk	spleen tyrosine kinase
TBS	Tris-buffered saline
TCIPA	tumor-cell induced platelet aggregation
TEM	Transmission electron microscopy
TEMED	tetramethylethylendiamine
TF	tissue factor
TG	thapsigargin
TGFβ	transforming growth factor-β
TIRF	total internal reflection fluorescence
TMB	3,3',5,5'-tetramethylbenzidine
TME	tumor microenvironment
TP	TxA_2 receptor
TPO	thrombopoietin
TRP	transient receptor potential
TRPC6	transient receptor potential channel 6
TxA_2	thromboxane A2
VEGF	vascular endothelial growth factor
vWF	von Willebrand factor
WBC	white blood cells
WT	wild-type

6.2 Acknowledgements

The work presented in this thesis was accomplished at the Institute of Experimental Biomedicine Chair I, University Hospital and Rudolf Virchow Center for Experimental Biomedicine, University of Würzburg in the group of Prof. Dr. Bernhard Nieswandt. During my time as Ph.D student from October 2015 to March 2020 many people supported and accompanied me, whom I would like to express special gratitude:

First and foremost, I would like to thank my supervisor and mentor Prof. Dr. Bernhard Nieswandt for the trust and confidence he placed in my abilities to work on the highly relevant projects presented in this thesis and several other interesting collaborations. His enthusiasm, encouragement and the critical and valuable input he provided during scientific discussions were fundamental to achieve my scientific goals.

I thank the members of my thesis committee, Prof. Dr. Süleyman Ergün and Prof. Dr. Guido Stoll for fruitful scientific discussions and for reviewing my thesis.

I am very grateful for the financial support provided by the Graduate School of Life Sciences and the German Excellence Initiative.

Many thanks to Dr. Erik Henke for teaching me everything about tumor models. His expertise and commitment were a valuable support for the tumor project.

I would like to thank all co-workers on the BIN2 project: those who started the project and worked on it long before I joined the lab and all the people who helped finalizing it at the end.

I would like to thank all former and present members of the Institute, who always shared their knowledge, expertise and advise during the seminars, project meetings and valuable discussions. Special thanks to the members of the 'imaging seminar' who helped keeping me on track and were never too tired for trouble-shooting.

I am very grateful for all the external collaboration partners I was able to work with and learn from, and I would like to thank them for the fruitful collaborations. Special thanks to Prof. Dr. Peter Rosenberger and Dr. David Köhler for the interesting Sema7A project discussions.

"*We are only as strong as we are united, as weak as we are divided*" – Albus Dumbledore. The work presented in this thesis would have never been possible without the great support and team spirit of the Ph.D students at the Institute. Special thanks to the members of the former 'Office 3' and the current 'Office 1' for their scientific input and for the nice and cheering working atmosphere. I would like to thank especially Yvonne and Vanessa for the encouragement, the open ear and all the great memories. Furthermore, I thank my desk

neighbor Charly for his support, his patience and all the fun moments. You all did not only celebrate my achievements with me, but also stood by my side whenever it became difficult. Thank you.

A Laboratory would never run without its engines. Therefore, I would like to thank Dr. Dr. Katharina Remer for her help with the mouse business and all the technicians, animal caretakers and secretaries for their constant support and the excellent work they perform.

I would like to thank the GSLS team for the organization of the study program, the valuable scientific courses and their support.

Special thanks to Vanessa, Sarah, Timo, Charly and Isabelle for carefully proofreading this thesis.

Without my family and friends, I would not be where I am now. Therefore, I would like to thank all of you for constant encouragement and everlasting support. Special thanks go to Annika Hain and Sven Barczyk for their help with designing the cover page.

Vielen Dank Mama, ohne deine Unterstützung hätte ich es niemals soweit geschafft.

Last, I would like to thank Steffen for his belief in me, his patience and his love.

6.3 Curriculum vitae

6.4 Publications

6.4.1 Articles

J. Volz, C. Kusch, S. Beck, M. Popp, T. Vögtle, M. Meub, I. Scheller, H. S. Heil, J. Preu, M. K. Schuhmann, T. Premsler, A. Sickmann, K. G. Heinze, D. Stegner, G. Stoll, A. Braun, M. Sauer, B. Nieswandt, BIN2 orchestrates platelet calcium signaling in thrombosis and thrombo-inflammation. Under Revision at *J Clin Invest*

J. Volz, E. Mammadova-Bach, J. Gil-Pulido, R. Nandigama, K. Remer, L. Sorokin, A. Zernecke, S. I. Abrams, S. Ergun, E. Henke, B. Nieswandt, Inhibition of platelet GPVI induces intratumor hemorrhage and increases efficacy of chemotherapy in mice. *Blood* **133**, 2696-2706 (2019).

D. Kohler, T. Granja, **J. Volz**, M. Koeppen, H. F. Langer, G. Hansmann, E. Legchenko, T. Geisler, T. Bakchoul, C. Eggstein, H. A. Haberle, B. Nieswandt, P. Rosenberger, Red blood cell-derived semaphorin 7A promotes thrombo-inflammation in myocardial ischemia-reperfusion injury through platelet GPIb. *Nat Commun* **11**, 1315 (2020).

T. Vogtle, A. A. Baig, **J. Volz**, T. B. Duchow, I. Pleines, S. Dutting, L. Nitschke, S. P. Watson, B. Nieswandt, Critical redundant functions of the adapters Grb2 and Gads in platelet (hem)ITAM signaling in mice. *Platelets*, Doi: 10.1080/09537104.2019.1709633 (2020).

Y. Schurr, A. Sperr, **J. Volz**, S. Beck, L. Reil, C. Kusch, P. Eiring, S. Bryson, M. Sauer, B. Nieswandt, L. Machesky, M. Bender, Platelet lamellipodium formation is not required for thrombus formation and stability. *Blood* **134**, 2318-2329 (2019).

M. Salzmann, W. C. Schrottmaier, J. B. Kral-Pointner, M. Mussbacher, **J. Volz**, B. Hoesel, B. Moser, S. Bleichert, S. Morava, B. Nieswandt, J. A. Schmid, A. Assinger, Genetic platelet depletion is superior in platelet transfusion compared to current models. *Haematologica*, Doi:10.3324/haematol.2019.222448 (2019).

S. Kiran Gotru, J. P. van Geffen, M. Nagy, E. Mammadova-Bach, J. Eilenberger, **J. Volz**, G. Manukjan, H. Schulze, L. Wagner, S. Eber, C. Schambeck, C. Deppermann, S. Brouns, P. Nurden, A. Greinacher, U. Sachs, B. Nieswandt, H. M. Hermanns, J. W. M. Heemskerk, A. Braun, Defective Zn(2+) homeostasis in mouse and human platelets with alpha- and delta-storage pool diseases. *Sci Rep* **9**, 8333 (2019).

M. Bieber, M. K. Schuhmann, **J. Volz**, G. J. Kumar, J. R. Vaidya, B. Nieswandt, M. Pham, G. Stoll, C. Kleinschnitz, P. Kraft, Description of a Novel Phosphodiesterase (PDE)-3 Inhibitor Protecting Mice From Ischemic Stroke Independent From Platelet Function. *Stroke* **50**, 478-486 (2019).

M. Malehmir, D. Pfister, S. Gallage, M. Szydlowska, D. Inverso, E. Kotsiliti, V. Leone, M. Peiseler, B. G. J. Surewaard, D. Rath, A. Ali, M. J. Wolf, H. Drescher, M. E. Healy, D. Dauch, D. Kroy, O. Krenkel, M. Kohlhepp, T. Engleitner, A. Olkus, T. Sijmonsma, **J. Volz**, C. Deppermann, D. Stegner, P. Helbling, C. Nombela-Arrieta, A. Rafiei, M. Hinterleitner, M. Rall, F. Baku, O. Borst, C. L. Wilson, J. Leslie, T. O'Connor, C. J. Weston, D. H. Adams, L. Sheriff, A. Teijeiro, M. Prinz, R. Bogeska, N. Anstee, M. N. Bongers, M. Notohamiprodjo, T. Geisler, D. J. Withers, J. Ware, D. A. Mann, H. G. Augustin, A. Vegiopoulos, M. D. Milsom, A. J. Rose, P. F. Lalor, J. M. Llovet, R. Pinyol, F. Tacke, R. Rad, M. Matter, N. Djouder, P. Kubes, P. A. Knolle, K. Unger, L. Zender, B. Nieswandt, M. Gawaz, A. Weber, M. Heikenwalder, Platelet GPIbalpha is a mediator and potential interventional target for NASH and subsequent liver cancer. *Nat Med* **25**, 641-655 (2019).

C. Deppermann, P. Kraft, **J. Volz**, M. K. Schuhmann, S. Beck, K. Wolf, D. Stegner, G. Stoll, B. Nieswandt, Platelet secretion is crucial to prevent bleeding in the ischemic brain but not in the inflamed skin or lung in mice. *Blood* **129**, 1702-1706 (2017).

6.4.2 Oral presentations

61st American Society of Hematology Annual Meeting, Orlando, USA, December 2019, Invited speaker Friday scientific workshop on the interplay between coagulation and malignancy:
> "Inhibition of platelet GPVI increases chemotherapeutic efficacy".

XXVIIth Congress of the International Society on Thrombosis and Haemostasis, Melbourne, Australia, July 2019, Oral communication session and highlight plenary session:
> "Inhibition of platelet GPVI induces intratumor hemorrhage and increases efficacy of chemotherapy in mice".

IIth European Congress on Thrombosis and Haemostasis, Marseille, France, October 2018, Plenary session:
> "Blockade of platelet glycoprotein VI induces intratumoral hemorrhage and increases efficacy of chemotherapy".

XXVIth Congress of the International Society on Thrombosis and Haemostasis, Berlin, Germany, July 2017, Oral communication session:
> "Defective arterial thrombosis and thrombo-inflammation in mice lacking Bridging Integrator 2 (Bin2)".

6.4.3 Poster presentations

XXVIIth Congress of the International Society on Thrombosis and Haemostasis, Melbourne, Australia, July 2019:
> "Bridging integrator 2 is a key regulator of store-operated calcium entry in platelets"

International Symposium of the Graduate School of Life Science: EUREKA!, Würzburg, Germany, October 2018:
> "Inhibition of platelet GPVI induces intratumor hemorrhage and increases efficacy of chemotherapy in mice"

International Symposium of the Graduate School of Life Science: EUREKA!, Würzburg, Germany, October 2017:
> "Defective arterial thrombosis and thrombo-inflammation in mice lacking Bridging Integrator 2"

Joint Symposium of the Collaborative Research Center 688 and the Comprehensive Heart Failure Center Würzburg, Germany, October 2017:
> "Defective arterial thrombosis and thrombo-inflammation in mice lacking Bridging Integrator 2"

6.5 Affidavit

I hereby confirm that my thesis entitled "Studies on the influence of platelets on vascular integrity in primary tumors and the role of BIN2 in platelet calcium signaling" is the result of my own work. I did not receive any help or support from commercial consultants. All sources and/or materials applied are listed and specified in the thesis.

Furthermore, I confirm that this thesis has not yet been submitted as part of another examination process neither in identical nor in similar form.

Würzburg,   May 2020   _____

                                              Julia Volz

6.6 Eidesstattliche Erklärung

Hiermit erkläre ich an Eides statt, die Dissertation „Studien zum Einfluss von Thrombozyten auf die Gefäßintegrität im Primärtumor und zur Rolle von BIN2 im Calcium-Signalweg von Thrombozyten" eigenständig, d.h. insbesondere selbstständig und ohne Hilfe eines kommerziellen Promotionsberaters, angefertigt und keine anderen als die von mir angegebenen Quellen und Hilfsmittel verwendet zu haben.

Ich erkläre außerdem, dass die Dissertation weder in gleicher noch in ähnlicher Form bereits in einem anderen Prüfungsverfahren vorgelegen hat.

Würzburg,   Mai 2020   _____

                                              Julia Volz